

**Blue biotechnology to fight the plastic problem:  
Exploring microbes and enzymes for biodegradation**

Inaugural-Dissertation

zur Erlangung des Doktorgrades  
der Mathematisch-Naturwissenschaftlichen Fakultät  
der Heinrich-Heine-Universität Düsseldorf

vorgelegt von

**Rebecka Molitor**

aus Köln

Düsseldorf, Januar 2024

aus dem Institut für Molekulare Enzymtechnologie  
der Heinrich-Heine-Universität Düsseldorf

Gedruckt mit der Genehmigung der  
Mathematisch-Naturwissenschaftlichen Fakultät der  
Heinrich-Heine-Universität Düsseldorf

Berichtersteller:

1. Prof. Dr. Karl-Erich Jäger

2. Prof. Dr. Jörg Pietruszka

Tag der mündlichen Prüfung: 09.09.2024

## Zusammenfassung

Seit Beginn des 20. Jahrhunderts hat die Produktion von Plastik stetig zugenommen. Über die Jahre hinweg wurden Millionen metrische Tonnen hergestellt und aufgrund einer unzureichenden Abfallbewirtschaftung gelangte ein erheblicher Teil davon in die Umwelt. Verschiedene Methoden zur Abfallbewirtschaftung wurden im Laufe der Jahre erprobt, aber dennoch gelangt immer noch viel Plastik in die Natur. Daher sind innovative Methoden zur Behandlung von Plastikabfällen wie Polyethylenterephthalat-Flaschen nötig, die in Abfallentsorgung und -recycling integriert werden. Seit 2016 wurden zahlreiche Enzyme entdeckt, die PET abbauen können und die dazu beitragen könnten, die Belastung durch Plastikabfälle in unserer Welt zu verringern, z.B. die Cutinase LCC, *ISPETase* oder die PE-H von *Halopseudomonas aestusnigri* (*Haes*\_PE-H).

Ziel dieser Arbeit war, das Wissen um Polyester aktive Enzyme durch Finden neuer Enzyme, Charakterisierung und Mutagenese zu erweitern und die Mechanismen des enzymatischen Plastikabbaus besser zu verstehen.

Während einer Expedition auf dem BMBF-Forschungsschiff „Sonne“ wurde Tiefseesediment aus der Plastikakkumulationszone des Nordatlantischen Strudels gesammelt und die mikrobielle Gemeinschaft nach neuen Polyester-abbauenden Mikroorganismen gescreent. Anreicherungskulturen und funktionale Screenings mit Polyestern führten zu der Entdeckung mehrerer Polyesterhydrolasen verschiedenen Typs. Ein Set aus sieben zu *Haes*\_PE-H homologen *Halopseudomonas* Polyester abbauenden Enzymen wurde aus Sequenz Daten ermittelt, rekombinant in *E. coli* produziert, gereinigt und vergleichend charakterisiert mittels verschiedener Polyester Substrate. Trotz der hohen Sequenzhomologie der Enzyme konnten Unterschiede in der Expression, Substratpräferenz, Schmelztemperatur (von bis zu 10°C) und Ionen-Abhängigkeit festgestellt werden, die später noch durch das Lösen der Kristallstruktur von *Hsab*\_PE-H analysiert wurden.

Die besten neuen Enzyme, *Hfor*\_PE-H und *Hoce*\_PE-H wurden für Mutagenesestudien mit besonderem Augenmerk auf einer besonders wichtigen Position neben dem katalytisch aktiven Histidin ausgesucht. Für beide Enzyme was es möglich, verbesserte Varianten, mit einer effektiveren Degradation von Polyestern bei Umgebungstemperatur zu ermitteln. Eine Sättigungsmutagenese an dieser Stelle führte bei *Hoce*\_PE-H zusammen mit der

biochemischen Charakterisierung und *in silico* Rigiditäts-Analyse zu der Annahme, dass nicht nur die Größe der Aminosäure wichtig ist, sondern auch ihre Ladung.

Zusammenfassend trägt die vorgelegte Dissertation zur Vertiefung des Verständnisses der Verbreitung und molekularen Eigenschaften von polyesterabbauenden Hydrolasen bei, was zur biotechnologischen Anwendung solcher Enzyme beitragen kann.



**Abstract**

Since the beginning of the 20th century, plastic production has steadily increased. Over the years, millions of metric tons have been manufactured, and a significant portion has ended up in the environment due to inadequate waste management. Various waste management methods have been attempted over the years. However, a substantial amount of plastic still finds its way into nature. Innovative strategies for treating plastic waste, such as PET bottles, need to be found, that can be integrated into waste disposal and recycling systems. Since 2016, numerous enzymes have been discovered that are capable of degrading PET including LCC cutinase, *ISPETase* and *Halopseudomonas aestusnigri* PE-H. These enzymes have been proposed to be a viable option to help reduce the burden of plastic waste in our world.

This work aimed to expand knowledge on polyester-active enzymes by characterizing new enzymes with particular emphasis on marine source organisms and conducting mutagenesis to better understand the mechanisms of enzymatic polyester degradation.

During a research cruise with the BMBF research vessel “Sonne”, deep sea sediment samples were collected from the plastic accumulation zone of the North Atlantic Gyre to analyze the present microbial communities and search for novel polyester-degrading microorganisms. Enrichment cultivation and functional screening with polyesters led to the discovery of several polyester hydrolases of two distinct types.

Complementary, a set of the seven *Haes*\_PE-H homologous *Halopseudomonas* polyester degrading enzymes were retrieved from sequence databases for recombinant expression, purification, and comparative characterization with different polyester substrates. Despite the high similarity of the enzymes, pronounced differences in expression yields, substrate preference, melting temperature (up to ca. 10°C) and ion dependency were found, of which the latter could be explained by features of the *Hsab*\_PE-H crystal structure solved here.

The best new enzymes, *Hfor*\_PE-H and *Hoce*\_PE-H, were chosen for mutagenesis studies with particular emphasis on the apparently crucial position next to the catalytic histidine residue. For both, improved variants able to effectively degrade polyester at ambient temperatures were obtained; saturation mutagenesis of this position in *Hoce*\_PE-H together with biochemical characterization and *in silico* rigidity analysis yielded hints that not (only) the residue size is crucial but a lack of charge.

In conclusion, the presented thesis contributes to deepening the understanding of the distribution and molecular characteristics of polyester-degrading hydrolases, which may support their biotechnological application.

## Publications published during this work

### Paper:

Molitor, R., Bollinger, A., Kubicki, S., Loeschcke, A., Jaeger, K., & Thies, S. (2020). Agar plate-based screening methods for the identification of polyester hydrolysis by *Pseudomonas* species. *Microbial Biotechnology*, (634486), 1751-7915.13418. <https://doi.org/10.1111/1751-7915.13418>

Bollinger, A., Molitor, R., Thies, S., Koch, R., Coscolín, C., Ferrer, M., & Jaeger, K.-E. (2020). Organic Solvent-Tolerant Carboxylic Ester Hydrolases for Organic Synthesis. *Applied and Environmental Microbiology*, 86(9), 1–15. <https://doi.org/10.1128/AEM.00106-20>

Caliskan, M., Poschmann, G., Gudzuhn, M., Waldera-Lupa, D., Molitor, R., Strunk, C.H., Streit, W.R., Jaeger, K.-E., Stühler, K., Kovacic, F. (2023) *Pseudomonas aeruginosa* responds to altered membrane phospholipid composition by adjusting the production of two-component systems, proteases and iron uptake proteins, *Biochimica et Biophysica Acta (BBA) - Molecular and Cell Biology of Lipids*, 1868(6) 6,2023,159317, <https://doi.org/10.1016/j.bbalip.2023.159317>

Perez-Garcia, P., Chow, J., Costanzi, E. Gurschke, M., Dittrich, J., Dierkes, R.F., Molitor, R., Applegate, V., Feuerriegel, G., Tete, P., Danso, D., Thies, S., Schumacher, J., Pfleger, C., Jaeger, K.-E., Gohlke, H., Smits, S.H.J., Schmitz, R.A., Streit, W.R. (2023). An archaeal lid-containing feruloyl esterase degrades polyethylene terephthalate. *Commun Chem* 6, 193 <https://doi.org/10.1038/s42004-023-00998-z>

de Witt, J., Molitor, R., Gätgens, J., Ortmann de Percin Northumberland, C., Kruse, L., Polen, T. et al. (2023) Biodegradation of poly(ester-urethane) coatings by *Halopseudomonas formosensis*. *Microbial Biotechnology*, 00, 1–15. <https://doi.org/10.1111/1751-7915.14362>

### Podcast:

Bakterien im Meer - fressen sie unseren Plastikmüll? Interview mit Wissenschaftlerin Rebecka Molitor, Ozeankind. Der Umwelt Podcast, March 11, 2021, <https://anchor.fm/ozeankind/episodes/Bakterien-im-Meer---fressen-sie-unseren-Plastikmüll-Interview-mit-Wissenschaftlerin-Rebecka-Molitor-es6jop>

Plastik-News-Update: Faktencheck aus der Forschung mit Rebecka Molitor, Ozeankind. Der Umwelt Podcast, September 15, 2022, <https://podcasters.spotify.com/pod/show/ozeankind/episodes/Plastik-News-Update-Faktencheck-aus-der-Forschung-mit-Rebecka-Molitor-e1npdmu/a-a8h6fei>

### Blogpost:

SO279 – It all started with the dinosaurs, JPIOceans project HOTMIC – Transport and Fate of Marine Microplastic Blog, December 31, 2020, <https://www.oceanblogs.org/hotmic/2020/12/31/so279-it-all-started-with-the-dinosaurs/>

Blaue Biotechnologie – Eine Expedition zum Nordatlantischen Müllstrudel, IBG-1 Biotechnologie, Bioökonomie Blog, March 1, 2021, <https://blogs.fz-juelich.de/biooekonomie/2021/03/01/blaue-biotechnologie-eine-expedition-zum-nordatlantischen-muellstrudel/>

#### **Poster:**

Molitor, R., Bollinger, A., Thies, S., Jaeger, K.-E. (2021) Identification of novel polyester hydrolases from the North Atlantic Garbage Patch deep sea floor; AcES Aachen Protein Engineering Symposium 2021, Online

Molitor, R., Königshausen, N., Dierkes, R., Bollinger, A., Horbach, T., Thies, S., Streit, W., Jaeger, K.-E. (2022) Novel polyester hydrolases from marine Halopseudomonas - A comparative study of a naturally evolved variant library of PET-active biocatalysts; 10th International Congress on Biocatalysis 2022 (BioCat), Hamburg, Germany

Horbach, T., Molitor, R., Perez-Garcia, P., Thies, S., Golyshin, P., Coscolin, C., Ferrer, M., Streit, W.R., Jaeger, K.-E. (2023) Identification of polyester-degrading esterases from deep-sea samples. Annual Conference 2023 of the Association for General and Applied Microbiology (VAAM). Göttingen/D, 2023-09-10-13

Horbach, T., Molitor, R., Perez-Garcia, P., Thies, S., Golyshin, P., Streit, W.R., Jaeger, K.-E. (2023). Activity- and sequence-based screening for polyester-degrading enzymes from Deep-Sea sediments. 5. European Summer School on Industrial Biotechnology (ESSIB), Hamburg/D, 2023-07-03-07.

#### **Oral presentation:**

Molitor, R., Bollinger, A., Dierkes, R., Streit, W., Thies, S., Jaeger, K.-E. (2022) Polluted marine habitats as prolific sources for polyester degrading enzymes; Annual Meeting 2022 of the Association for General and Applied Microbiology (VAAM), Online,

Molitor, R., Königshausen, N., Dierkes, R., Bollinger, A., Horbach, T., Thies, S., Streit, W., Jaeger, K.-E. (2022) Marine resources for polyester degrading enzymes; Biocatalysis for the Biological Transformation of Polymer Science (efb) 2022, Cologne, Germany

Caliskan, M., Poschmann, G., Waldera-Lupa, D., Molitor, R., Jaeger, K.-E., Stühler, K., Kovacic, F. (2023) *Pseudomonas aeruginosa* responds to altered membrane phospholipid composition by adjusting the production of two-component systems, proteases, and iron uptake proteins; Annual Conference 2023 of the Association for General and Applied Microbiology (VAAM). Göttingen/D

#### **Awards:**

VAAM2022 Presentation Price

[https://vaam.de/media/posterpreise\\_talks\\_2022gesamt.pdf](https://vaam.de/media/posterpreise_talks_2022gesamt.pdf)

# Contents

<b>ZUSAMMENFASSUNG</b>	<b>I</b>
<b>ABSTRACT</b>	<b>III</b>
<b>PUBLICATIONS PUBLISHED DURING THIS WORK</b>	<b>V</b>
<b>LIST OF TABLES</b>	<b>X</b>
<b>LIST OF FIGURES</b>	<b>X</b>
<b>ABBREVIATIONS</b>	<b>XIII</b>
<b>1. INTRODUCTION</b>	<b>1</b>
<b>1.1. Plastic waste handling</b>	<b>2</b>
1.1.1. Plastics in the ocean	4
<b>1.2. Polyester</b>	<b>6</b>
1.2.1. Polyester degrading enzymes	7
1.2.2. Polyester degradation mechanism exemplified for PET	9
1.2.3. Characteristics of PET degrading enzymes	11
<b>1.3. How to find novel enzymes for biotechnological application</b>	<b>13</b>
1.3.1. The ( <i>Halo-</i> ) <i>Pseudomonas pertucinogena</i> lineage	15
<b>1.4. Aim</b>	<b>17</b>
<b>2. MATERIAL AND METHODS</b>	<b>19</b>
<b>2.1. Working with bioinformatics</b>	<b>19</b>
2.1.1. Online Databases and tools	19
2.1.2. Alignment Tools	19
2.1.3. UCSF ChimeraX	19
2.1.4. Python	19
2.1.5. CloneManager9	20
	vii

---

<b>2.2.</b>	<b>Working with DNA</b>	<b>20</b>
2.2.1.	Preparation of primer	20
2.2.2.	Polymerase chain reaction (PCR)	20
2.2.2.1.	Quick-Change PCR	21
2.2.3.	Cloning	23
2.2.3.1.	Restriction and ligation cloning	23
2.2.3.2.	One-step sequence- and ligation-independent cloning (SLIC)	23
2.2.4.	Agarose gel electrophoresis	24
2.2.5.	Isolation of circular plasmid DNA from bacterial cells	24
2.2.6.	Isolation of metagenomic DNA from sediment	25
2.2.7.	Analysis of metagenomic DNA	25
<b>2.3.</b>	<b>Working with bacterial cells</b>	<b>25</b>
2.3.1.	Preparation and transformation of chemical competent cells	25
2.3.2.	Sampling of bacterial cells from Deep-Sea sediment	26
2.3.3.	Enrichment cultures	26
2.3.4.	Production of proteins	27
<b>2.4.</b>	<b>Working with proteins</b>	<b>28</b>
2.4.1.	Purification of Proteins using an IMAC	28
2.4.2.	SDS-PAGE	29
2.4.3.	Esterase activity assay	29
2.4.4.	Measurement of thermic stability	30
2.4.5.	Detection of polyester degradation	30
2.4.5.1.	Ultra-performance liquid chromatography (UPLC)	30
2.4.5.2.	Polyester-polyurethane optical density assay	31
2.4.5.3.	pH activity optimum determination using polyester-polyurethane	32
2.4.5.4.	Fluorescein pH sensitive assay	32
2.4.5.5.	Impranil DLN-SD assay plates	32
<b>3.</b>	<b>RESULTS AND DISCUSSION</b>	<b>33</b>
<b>3.1.</b>	<b>Activity-based uncovering of novel polyesterases from marine samples</b>	<b>34</b>
3.1.1.	Analysis of environmental DNA from deep-sea sediment	34
3.1.2.	Enrichment culturing on polyester substrates as sole carbon source	40
<b>3.2.</b>	<b>Sequence-based compiling of a set of homologous polyester hydrolases for a comparative characterization</b>	<b>44</b>
3.2.1.	Expression and purification of <i>Halopseudomonas</i> PE-Hs	47

---

3.2.2.	Concentration dependent inhibition of polyester hydrolases	49
3.2.3.	Ion dependency of PE-H activity	50
3.2.4.	Thermal stability	56
3.2.5.	Temperature dependent activity	58
3.2.6.	pH dependent activity	61
3.2.7.	Analysis of polyester degradation	62
<b>3.3.</b>	<b>Rational mutagenesis of PE-Hs to improve polyester conversion</b>	<b>69</b>
3.3.1.	Addition of a second active site	69
3.3.2.	Mutagenesis between the active site histidine and disulfide bridge forming cysteine	72
3.3.3.	Saturation mutagenesis of <i>Hoce</i> _PE-H position Y265	75
<b>3.4.</b>	<b>Summarizing evaluation</b>	<b>83</b>
3.4.1.	Insights from comparisons of wild typical <i>Halopseudomonas</i> PE-H	83
3.4.2.	Insights from mutagenesis experiments	85
<b>4.</b>	<b>CONCLUSION AND OUTLOOK</b>	<b>88</b>
<b>REFERENCES</b>		<b>91</b>
<b>APPENDIX</b>		<b>109</b>
<b>ACKNOWLEDGMENTS</b>		<b>111</b>
<b>ERKLÄRUNG</b>		<b>113</b>

## List of Tables

Table 1: Parameters important to consider for the industrial usage of PETases. ....	12
Table 2: PCR ingredients and volumes. ....	20
Table 3: Quick-Change PCR mixture ingredients for 25 µl reaction mixture in total per primer. ....	21
Table 4: Sampling points from the cruise SO279. ....	26
Table 5: List of expression conditions to obtain the characterized enzymes. ....	27
Table 6: List of all enzymes compared in this thesis with PDB numbers, NCBI accession numbers and first publication. ....	45
Table 7: <i>Haes</i> _PE-H variants predicted by the Barcelona Supercomputing Center to have a second active site specific for MHET degradation. ....	70
Table 8: Ranking of the different characteristics for the radar diagrams. ....	83
Table 9: List of all used primers in this work. ....	109

## List of Figures

Figure 1: Synthetic polymers produced globally in 2022 in million metric tons.....	1
Figure 2: Primary plastic production and plastic waste fate from 1950 until 2015 with predictions up until 2050.....	4
Figure 3: Modelled concentration of plastic particles at the ocean surface.....	5
Figure 4: PET degradation by PETase and MHETase .....	9
Figure 5: Docking model of <i>ISPETase</i> with the reaction intermediate 2-HE(MHET) <sub>4</sub> . ....	10
Figure 6: Amino-acid sequence alignment of the key positions of the PETase groups. ....	10
Figure 7: PCR cycle temperature and time.....	21
Figure 8: Quick-Change PCR cycle temperature and time graph .....	22
Figure 9: (A) Map of the planned sampling stations of the research cruise SO279.....	35
Figure 10: Relative abundance of bacterial phyla at the different stations in the marine sediment and the principal component analysis (PCA) of their class relationship.....	36
Figure 11: (A) Phylogenetic tree of all currently known and characterized PETases.....	39
Figure 12: Impranil DLN-SD agar plates with halo formation of the enrichment cultures. ....	41
Figure 13: Organism identified by Horbach (2023) .....	42



Figure 14: (A) Neighbor-joining tree with distances indicated as percentage and (B) percent identity matrix for the <i>Halopseudomonas</i> PE-H homologues.....	45
Figure 15: Distributional map of the <i>Halopseudomonas</i> clade.....	46
Figure 16: (A) Coomassie Blue stained SDS-gel of all expressed enzymes with measured concentrations after purification from the soluble fraction of the <i>E. coli</i> cell lysate. ....	48
Figure 17: Relationship of enzyme concentration and enzyme activity. ....	49
Figure 18: pNPB assay of the enzymes <i>Hsab</i> _PE-H and <i>Hoce</i> _PE-H in the presence of 10 mM EDTA or puffer with average conditions of sea salt. ....	51
Figure 19: Calcium dependency of <i>Hsab</i> _PE-H .....	52
Figure 20: Comparison of the crystal structure of Cut190 with <i>Hsab</i> _PE-H and <i>Haes</i> _PE-H. ....	54
Figure 21: Comparison of the environment of Cut190 position N133 in Ca <sup>2+</sup> bound state with the homologue regions of <i>Haes</i> _PE-H_Y250S and <i>Haes</i> _PE-H based on the crystal structures.....	55
Figure 22: Melting temperatures of the investigated homologous PE-H from <i>Halopseudomonas</i> spp. ....	57
Figure 23: Temperature-dependent activity of the investigated homologous PE-H from <i>Halopseudomonas</i> spp. ....	59
Figure 24: pH optimum for the enzyme set. ....	61
Figure 25: Polyester degradation activities of the enzyme set.....	64
Figure 26: Comparison of adipic acid release [μmol/h] A and general acid release (Loss of fluorescence [AU/min]) B from the degradation of PU-foam.....	67
Figure 27: Crystal structure of <i>Haes</i> _PE-H (6SBN) with the Plurizyme positions marked by colored squares. ....	70
Figure 28: Melting temperatures of the investigated Plurizymes.....	72
Figure 29: Relative activity of the <i>Hfor</i> _PE-H mutants and thermal stability. ....	74
Figure 30: Sequence alignment of all PE-H homologues with the <i>ISPETase</i> .....	76
Figure 31: Temperature stability and activity of the <i>Hoce</i> _PE-H mutations.....	78
Figure 32: pH optimum of the <i>Hoce</i> _PE-H variants. ....	80
Figure 33: Released adipic acid from PU-foam of the variants relative to the released adipic acid of the wild type. ....	81
Figure 34: Radar diagrams of the enzyme set in relation to <i>ISPETase</i> .....	84

---

Figure 35: Radar diagram of the <i>Hfor</i> _PE-H mutants.....	85
Figure 36: Radar diagrams of the <i>Hoce</i> _PE-H mutants. ....	86
Figure 37: By Biosynth in <i>Pichia pastoris</i> produced and lyophilized enzymes from the set. .....	90
Figure 38: Relationship of enzyme concentration and enzyme activity. ....	110
Figure 39: Enzymatic activity of 1500 nM enzyme solution on amorphous PET-film over 96 h of incubation at 30°C. ....	110

## Abbreviations

### B

BHET

Bis(2-Hydroxyethyl) terephthalate

### C

CV

Column volume

### D

ddH<sub>2</sub>O

Double distilled water, Millipore water

DMSO

Dimethyl sulfoxide

dNTP

Deoxy nucleoside triphosphate

### E

EDTA

Ethylenediaminetetraacetic acid

EG

ethylene glycol

### G

GC-ToF-MS

Gas chromatography time-of-flight mass  
spectrometry

### H

HMM

Hidden Markov Model

### I

IMAC

Immobilized metal ion affinity chromatography

### M

M

mol/l

MD

Molecular docking simulation

MHET

2-Hydroxyethyl terephthalic acid

MWCO

Molecular Weight Cut-Off

### N

NCBI

National Center for Biotechnology Information

### O

OD<sub>580nm</sub>

Optical Density at a wavelength of 580 nm

ORF

open reading frame

### P

PBT

polybutylene terephthalate

PCA

Principal Component Analysis

PCL

polycaprolactone

PCR

Polymerase chain reaction

PEF

polyethylene 2,5-furandicarboxylate

PELE

Protein energy landscaping exploration

PET

polyethylene terephthalate

PFAS

per- and polyfluoroalkyl

PHA

polyhydroxyalkanoates

PLA

polylactic acids

*p*NPB

4-nitrophenyl-butyrate

*p*NPH

4-nitrophenyl-hexanoate

PTFE

polytetrafluoroethylene

PVC

polyvinyl chloride

## R

RPM

rounds per minute

## T

TPA

terephthalic acid

## U

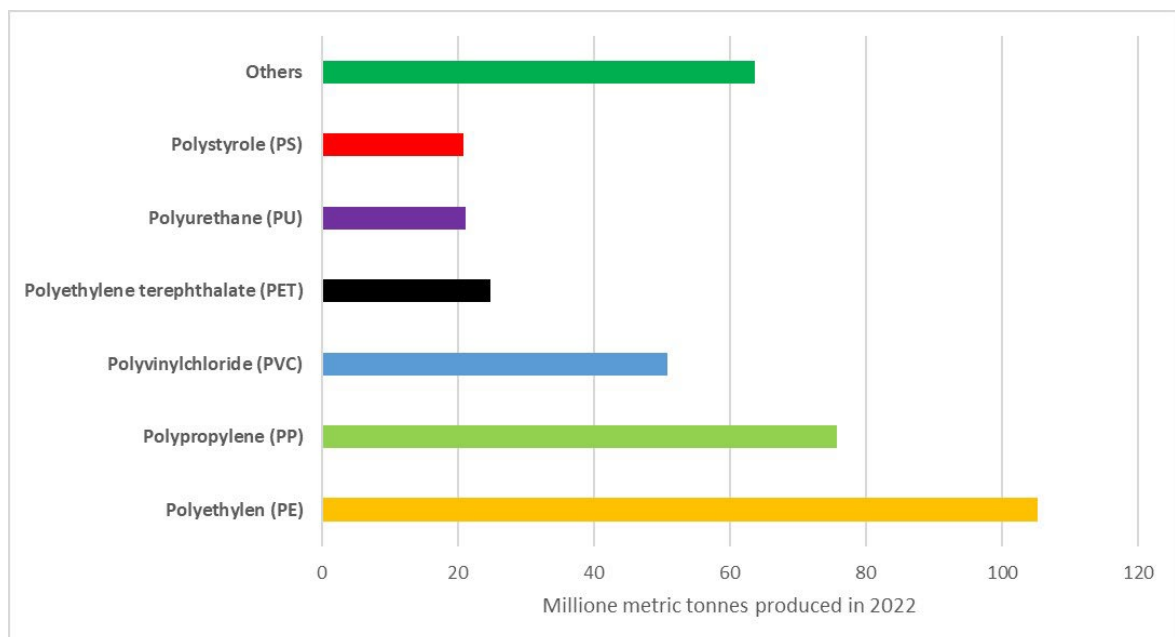
UPLC

Ultra-performance liquid chromatography

## 1. Introduction

For thousands of years, humans have employed natural polymers for various applications. Examples include the use of wood (lignin) in construction, cellulose for paper and cotton, or proteins in the form of wool or silk for diverse purposes. Despite their versatility, natural polymers have limitations, particularly in aqueous environments. To overcome these limitations and enhance their properties, the concept of improving natural polymers emerged. One early example of such an enhanced polymer is cellophane which was invented in 1985 (Cowley, 1985). Cellophane, a precursor to artificial polymers made from cellulose (Cowley, 1985) proved particularly valuable for packaging food due to its waterproof and transparent nature. Since the 1900s, techniques have been developed to synthesize completely artificial polymers, with inventors aiming to tailor polymers for specific purposes. To this date, a wide range of artificial polymers, commonly known as plastics, have been developed with specific applications in mind. Plastics are nowadays used for virtually anything, ranging from packing material to house construction, electronics, as well as clothing.

The basic structure of plastics is always based on either one unit (a monomer) or multiple units that repeat N times forming long chains (polymers). Generally, modern plastics can be long aliphatic chains like polyethylene or have aromatic parts like polystyrene (Figure 1).



**Figure 1: Synthetic polymers produced globally in 2022 in million metric tons** The monomers of the polymers are shown around next to the column (data according to Plastics Europe – Plastics- the fast Facts 2023)

Furthermore, plastics can consist of carbon bonds only (polyolefins) like polyethylene and polystyrene or contain heteroatoms like oxygen in polyester polyurethanes (e.g., polyethylene terephthalate (PET)), polyether, polycarbonates, silicone as in silicone polymers, or nitrogen as in polyamides and polyurethanes. The polymer backbones may be decorated with carboxyl esters (polyacrylates) or halogens (polyvinyl chloride (PVC), polytetrafluoroethylene (PTFE)). Different kinds of polymers can be mixed to form hybrid or composite polymers, such as for example polyester-polyurethane. Polyester-polyurethane is a mix between ester units and urethane units giving the resulting plastic benefits from both plastic types. Depending on the crystallinity and the interlinkage of the chains, plastics can have different characteristics. Plastics with wider interlinkage tends to be more elastic. Crystalline plastic is more glass like and rigid (Li *et al.*, 2022).

Plastics are versatile, cheap, and easy to manufacture. Compared to the production of glass or cotton, plastics are less energy and resource intensive. Typically, plastics is manufactured from petroleum-based feedstock due to its cost advantage. However, it is possible to produce plastics from renewable resources. This can make the production more environmentally friendly, while plastics retains its favorable properties (Atiweh *et al.*, 2021).

### **1.1. Plastic waste handling**

The amount of plastic waste has steadily risen together with the increased amount of produced plastic. With most consumer plastic being single use items, plastic waste treatment has become a problem for most countries. From the primary produced plastic in the years of 1950-2015, 30 % of the plastic is currently in-use (for example in the form of building materials in construction), and 59 % has been discarded into either long-term sanitary landfills, or into uncontained open dumps through which the plastic might eventually enter the natural environment (Geyer *et al.*, 2017; Li *et al.*, 2022). Only 7 % of produced plastic has been recycled, and around 10 % of plastic has been incinerated (Geyer *et al.*, 2017). Therefore, to date most countries are not yet able to treat their plastic waste in a sustainable and circular way.

Many plastics on the market are combinations of the actual polymer with additional materials (Li *et al.*, 2022). Due to additives like plasticizers and pigments, or due to printing on packaging, a lot of plastic cannot be properly recycled and ends up in landfills or gets

incinerated. Plastic that is suitable for recycling, especially PET, often faces limitations in being reused in the same way as virgin (newly produced) plastic, primarily due to the presence of coloring (Li *et al.*, 2022). Thermoplastics can sometimes be heated to a liquid state and be remodeled to some extent. However, not all plastics are thermoplastics and retain their properties while heated. To reuse those types of plastic, other ways of recycling need to be implemented. One way is thermal decomposition in an oxygen-deficient atmosphere, called pyrolysis (Li *et al.*, 2022; Moharir & Kumar, 2019). Pyrolysis uses very high temperatures around 350-700°C to break the polymer chains (Li *et al.*, 2022). The resulting products are oils, waxes, gases, and char that can be used to build new plastic. The advantages of this method are less emission and loss of carbon compared to incineration of the plastic, as well as the possibility to recycle more heterogeneous plastics than is currently possible with mechanical recycling (Li *et al.*, 2022).

Another often-used approach is the dissolution of plastics in solvents. For this the plastic is dissolved in the appropriate solvent at a certain temperature, then filtered, and separated (Li *et al.*, 2022; Nisticò, 2020). The advantages of this technique are, like pyrolysis, that the plastics to be recycled can be less pure, as any impurities can be filtered out during the process. In addition, the purity of the end-product is higher compared to mechanical recycling (Li *et al.*, 2022).

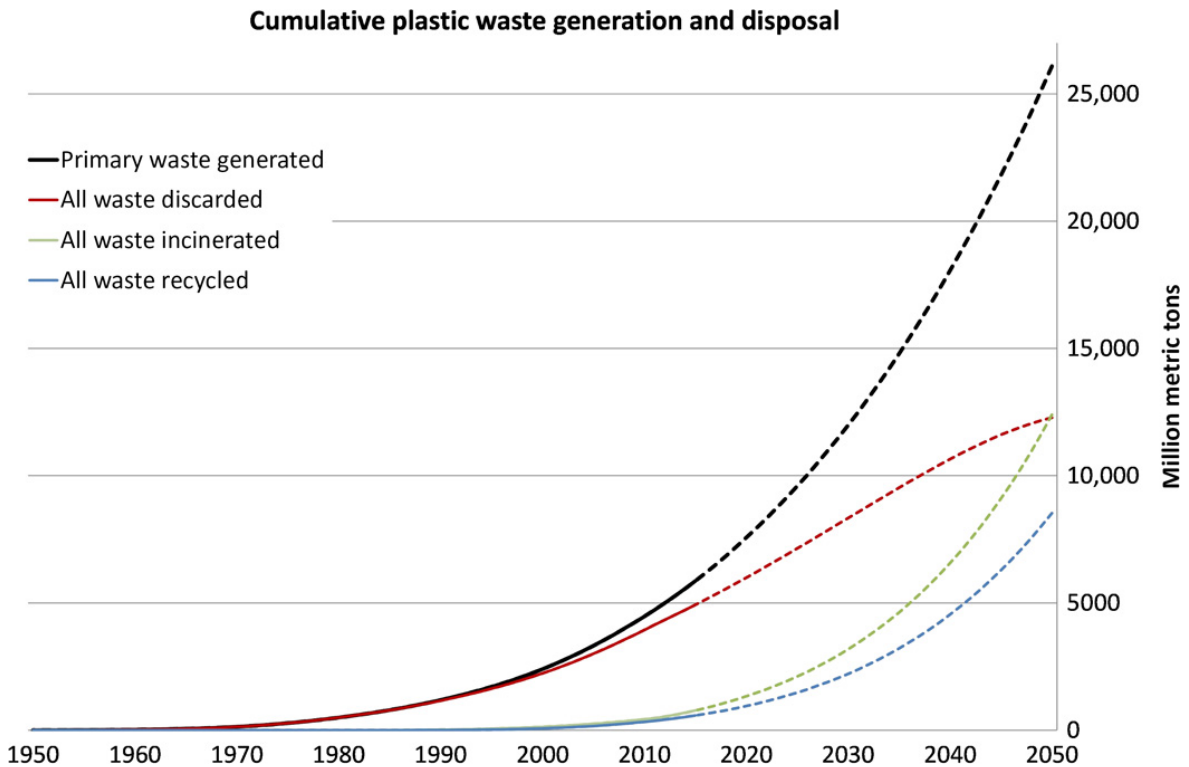
The last pathway for especially PET degradation is hydrolysis. It degrades the polymer chain into its monomers in the presence of a trans-esterification catalyst like ethylene glycol (Fukushima *et al.*, 2011; Sheel & Pant, 2019). It is considered to be an environmentally friendly process if no metallic catalysts, but rather organic catalysts are used (Xin *et al.*, 2021).

However, all these techniques require a lot of energy and are therefore most of the time not cost-effective enough. With prices of the plastic feedstock being very low, virgin plastic is so far preferred over recycled plastic.

Another not yet established option is the biological depolymerization into individual building blocks. Enzymes can break up the chemical bonds between the polymers, creating usable building blocks under ambient temperatures without the need for harsh chemicals or excessive energy usage (Li *et al.*, 2022; Nisticò, 2020).

### 1.1.1. Plastics in the ocean

Due to high demand, the production of plastic has reached new heights in the past years. Figure 2 shows the plastic production from the 1950s up until 2015 with the production of plastic growing exponentially. In the year 2015 a cumulative 8300 million metric tons of plastic have been produced, and 5800 million metric tons of plastic waste has been generated.



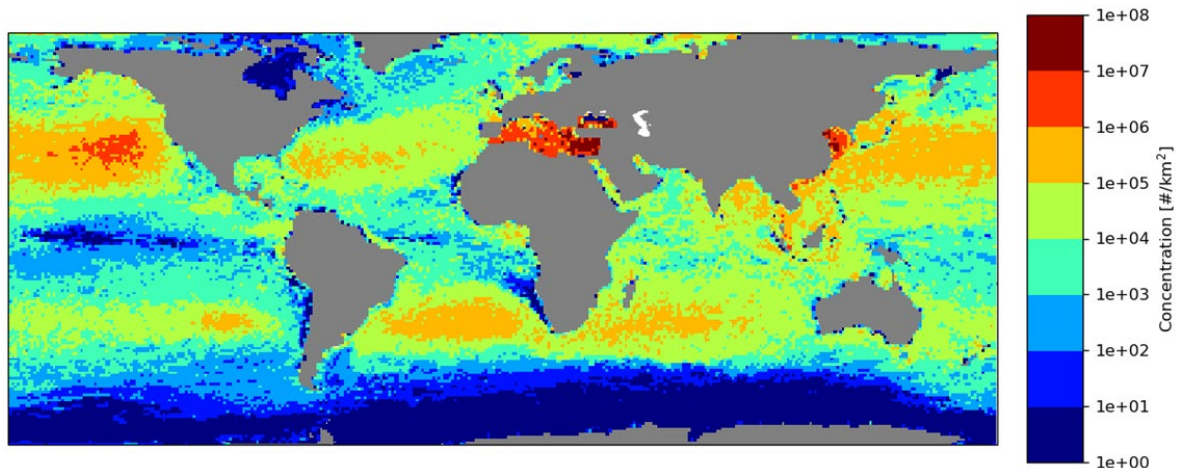
**Figure 2: Primary plastic production and plastic waste fate from 1950 until 2015 with predictions up until 2050** (Geyer *et al.* (2017) published under creative commons license CC BY-NC).

The large amount of mismanaged plastic waste together with a lack of effective recycling concepts has resulted in more and more plastics finding its way into the natural environment.

Kaandorp *et al.* (2023) have recently reevaluated the plastic intake as well as the plastic amount present in the global ocean. They estimated that 3,146 kilotons of plastic are floating on the ocean surface, as well as 54 kilotons of plastic being found on the coastlines. They specified the intake of plastic into the ocean to about 63 kilotons from riverine input, 203 kilotons from coastal input and 239 kilotons intake from fishing activity each year. They estimated that 3 kilotons of plastic are removed from the beach every year (due to e.g. degradation and cleanup of the plastics) and estimated that 73 kilotons are lost to fragmentation and 220 kilotons are sinking to the ocean floor every year (Kaandorp *et al.*,



2023). Most of the floating plastic accumulates in large-scale circular currents in the middle of the oceans called gyres (Figure 3). The North Atlantic Ocean garbage accumulation zone is one of those gyres (Cozar *et al.*, 2014; van Sebille *et al.*, 2020). In Figure 3 these accumulation zones are visible as areas of high plastic concentrations in red and orange.



**Figure 3: Modelled concentration of plastic particles at the ocean surface.** Modified by Kaandorp data from van Sebille *et al.* (2015) published under creative commons license CC BY. The concentration of plastic pieces (#) per km<sup>2</sup> is shown in a range from blue to red indicating more plastic pieces (red) or less plastic pieces (blue) per km<sup>2</sup>.

Due to different factors like biofouling and varying plastic densities, a lot of plastic particles in the gyres and on the way there sink to the ocean floor (Martin *et al.*, 2022). Due to abiotic factors (e.g. UV-radiation, waves, salinity), big plastic objects eventually disintegrate and break down into smaller plastic particles (Thompson *et al.*, 2004). This process can break down plastic objects into microplastics (<5 mm) and even smaller nanoplastics. However, microplastics are also intentionally produced by different industries for cosmetic and other uses. In addition, abrasion of car tires continuously releases microplastic particles into the environment, which might eventually end up in the rivers and oceans.

Plastic poses a threat to many species in the marine and terrestrial ecosystem. The most obvious threat which is widely shown in the media is the ingestion and entanglement of marine species in plastic debris (Bergmann *et al.*, 2015). Many pictures have been shown of dolphins or seals drowning in so-called ghost nets (Butterworth & Sayer, 2017), or sea birds and whales dying of starvation due to congestions of their intestines caused by plastic particles (Caldwell *et al.*, 2019). Sea turtles can mistake clear plastic bags for jellyfish and subsequently die due to malnourishment (Avio *et al.*, 2017; Wilcox *et al.*, 2018).

A less obvious problem regarding plastic pollution is the adsorption of organic compounds, which is especially the case for microplastics due to their relatively large surface area (Mato

*et al.*, 2001). Due to their hydrophobicity, most plastics attract organic compounds in saltwater. Over time, compounds like the highly persistent per- and polyfluoroalkyl (PFAS) accumulate on the plastic surface, after which they can be ingested by marine wildlife (Costigan *et al.*, 2022; Lynch *et al.*, 2022). Besides the accumulation of environmental pollutants, some plastic are enriched with additives that are meant to change its properties (Hermabessiere *et al.*, 2017; Routti *et al.*, 2019). These plastic additives, as well as adsorbed organic compounds, can leach into the organism after ingestion and accumulate in fat tissue in particular (Hermabessiere *et al.*, 2017; Hernandez-Milian *et al.*, 2023). Due to the consumption of marine animals like fish, the chemicals can be passed on to humans, possibly leading to health issues (Koelmans *et al.*, 2014; Rodrigues *et al.*, 2019).

## **1.2. Polyester**

Polyesters, invented in 1929 by Carothers, have revolutionized modern society (Gubbels *et al.*, 2018; Penczek *et al.*, 2005). Characterized by ester bonds, polyesters have been used as coating material and especially packaging material. Polyesters can be characterized into four categories: (I) high molecular mass linear polymers, (II) and (III) low molecular mass polyesters characterized by different aliphatic and aromatic compounds and the involved alcohol compounds, and (IV) unsaturated polyesters (Gubbels *et al.*, 2018). The most commonly used polyesters are, among others, PET, polybutylene terephthalate (PBT), polyethylene 2,5-furandicarboxylate (PEF), and a variety of special polyesters like polycaprolactone (PCL) and polylactic acids (PLA) (Gubbels *et al.*, 2018). All these polyesters have different thermal stabilities and usage, depending on the base materials and copolymers used (Penczek *et al.*, 2005). Polyesters are synthesized by polycondensation of various monomers and cross-linked by peroxides or photochemically initiated radical polymerization (Penczek *et al.*, 2005).

Most polyesters are produced from fossil-based raw materials. However, some members of this group also occur naturally like polyhydroxyalkanoates (PHA) (Nisticò, 2020). Other naturally occurring polyesters are the plant materials cutin and suberin (Kolattukudy, 1980; Nawrath & Poirier, 2008). Both substances have the function of making the plant surfaces water impermeable.

Especially the polyester PET, mostly used for single use consumer packaging, is of special importance. It was the fourth most produced plastic type in 2016 (Figure 1) and

monopolizes the market for drinking bottles (Nisticò, 2020). Around 33 million metric tons of PET were produced in 2016 (Danso *et al.*, 2019; Geyer *et al.*, 2017) with most of it being single use.

PET is produced by polymerization of terephthalic acid and ethylene glycol (Ravindranath & Mashelkar, 1986; Sin & Tueen, 2023). It is semi-crystalline and has crystalline and amorphous parts in varying degrees depending on the manufacturing process (Barnard *et al.*, 2021). By using heat or additives, PET can become more crystalline. However, PET always starts out amorphous (Sinha *et al.*, 2008). Its glass-transition temperature is at 72°C where it changes from a rigid to a rubber-like state (Sinha *et al.*, 2008). This glass transition temperature is mainly a property of the amorphous parts of the PET, giving the polymer chain energy for enhanced movement. This leads to a more rubbery state of the PET, with polymer chains being able to shift around, and eventually transitioning into a liquid state (Li *et al.*, 2022). The melting temperature is a property mainly defined by the crystalline regions. (Li *et al.*, 2022). The crystalline regions are usually less affected by the glass transition temperature.

PET can be produced with different molecular weights depending on its specific target use. High molecular weight is achieved by a second polymerization step removing impurities, making the PET more stiff and resistant to bursting under pressure (Sinha *et al.*, 2008).

### **1.2.1. Polyester degrading enzymes**

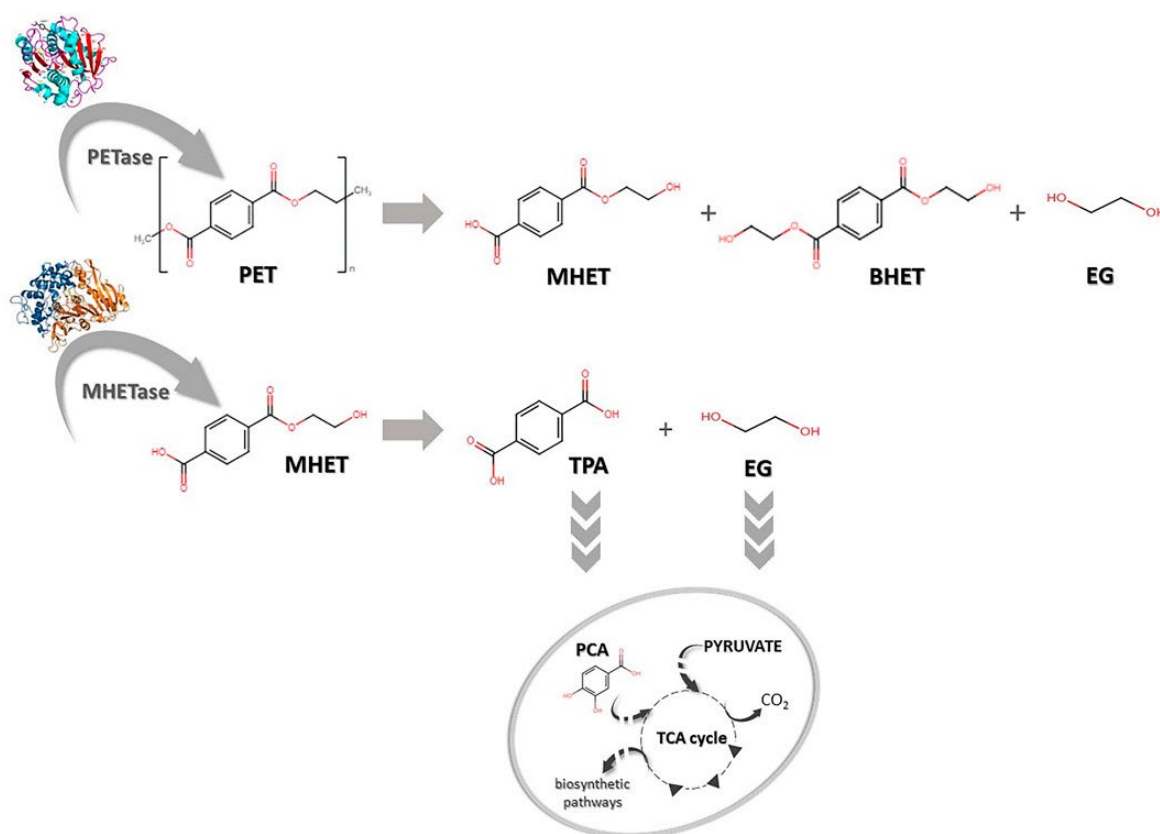
Because of more media attention, as well as the direct visibility of garbage in the environment, the plastic waste problem has found its way into the collective consciousness. New ways of dealing with plastic waste need to be found. A promising tool for dealing with this issue could be the usage of enzymes. Ester bonds are ubiquitous around the world. Due to its frequent occurrence, a lot of microorganisms possess enzymes to degrade these ester bonds. It is reasonable to assume that these enzymes, especially when they are promiscuous, might be able to degrade polyesters (Nikolaivits *et al.*, 2018). Scientists around the world have tried to find organisms and subsequently the responsible enzymes that are able to degrade polyesters.

Several enzymes have been identified that are able to degrade PET, such as lipases, esterases, carboxylases, and cutinases (Duan *et al.*, 2023) mainly belonging to the class of carboxyl ester hydrolases (EC 3.1.1.). Tournier *et al.* (2023) reported, that previously 853

putative PET hydrolase genes were identified in databases and metagenomes, with 108 from marine origin and 25 from terrestrial origin, showing an overrepresentation of marine environments.

All these enzymes have in common that they belong to the  $\alpha/\beta$ -hydrolase superfamily, with a serine hydrolase motif and a highly conserved catalytic triad consisting of serine, histidine, and aspartate (Joo *et al.*, 2018; Richter *et al.*, 2023). The PAZy database (Buchholz *et al.*, 2022), dedicated to collecting all enzymes active on plastic, lists to date (accessed 28.11.2023) 94 biochemically characterized wild type enzymes acting on PET and other polyesters. Most of these PET active enzymes are found in the family of proteobacteria and actinobacteria. However, some enzymes were found in archaea and eukarya, as well as in the families of bacillota, bacteroidota, chloroflexota, deinococcata, and derived from metagenomes.

Every enzyme able to degrade PET belongs to the PETase family. Enzymes within the PETase family significantly differ in PET-hydrolytic activity as well as in thermal stability (Richter *et al.*, 2023). The family of PETases was divided into two groups (Joo *et al.*, 2018). The type I includes well known cutinases like the leave compost cutinase (LCC). Type II PETases contains enzymes like the PE-H (Bollinger *et al.*, 2020c), PHL7 (Richter *et al.*, 2023), and the most prominent example of PETases, the enzyme *ISPETase* from the bacterium *Ideonella sakaiensis* (Yoshida *et al.*, 2016). The latter was first discovered at a PET recycling facility and can use PET as its sole carbon source.



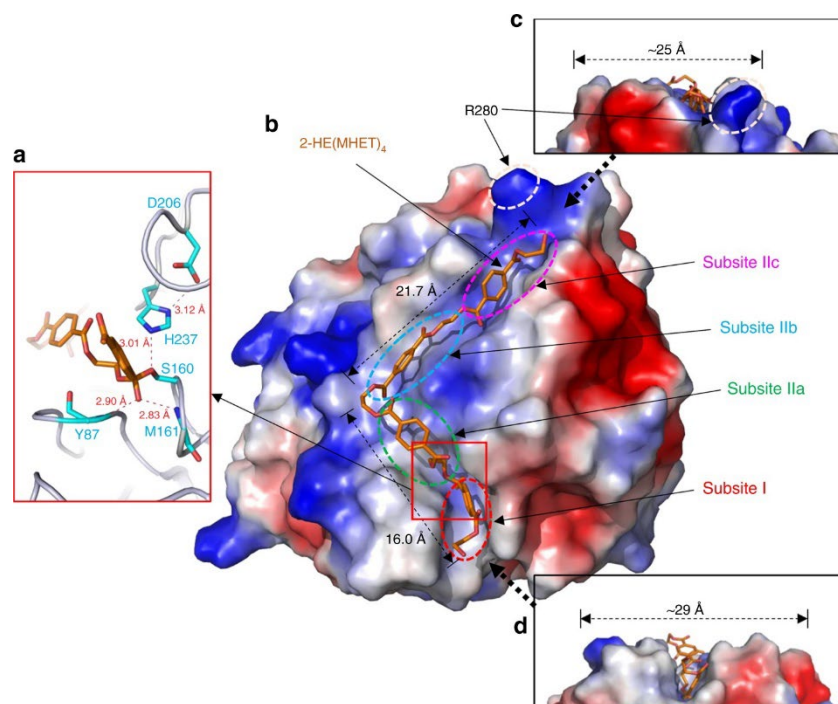
**Figure 4: PET degradation by PETase and MHETase** (Urbanek *et al.* (2021) published under creative commons license CC BY). The plastic degradation pathway using the enzymes PETase and MHETase from *Ideonella sakaiensis* is shown including the use of the building blocks terephthalic acid (TPA) and ethylene glycol (EG) in the tricarboxylic acid cycle (TCA-cycle). Also shown is the monomer mono-(2-hydroxyethyl)terephthalic acid (MHET) and the dimer bis-(2-hydroxyethyl)terephthalate (BHET).

*I. sakaiensis* has two enzymes, namely *ISPETase* and *ISMHETase*, which work hand in hand to fully degrade long chain PET into its basic components ethylene glycol (EG) and terephthalic acid (TPA), seen in Figure 4 (Duan *et al.*, 2023; Yoshida *et al.*, 2021).

### 1.2.2. Polyester degradation mechanism exemplified for PET

For understanding the structural features of the PETase family, we look at the most famous member of it, the *ISPETase* and structural relatives like PHL7. Comparing the structure of *ISPETase* as a type II PETase to type I PETases, one of the most important differences seems to be the formation of two disulfide bridges, compared to only one (Duan *et al.*, 2023). This second disulfide bridge additionally connects to the catalytic triad area. This area is the active center of most  $\alpha/\beta$ -hydrolases and is where substrate conversion takes place. Here the second disulfide bridge stabilizes the active center and enhances the substrate conversion (Duan *et al.*, 2023).

All PETase enzymes seem to have a highly conserved subsite I where the initial binding of the PET monomer, MHET moiety takes place, see Figure 5 (Joo *et al.*, 2018).



**Figure 5: Docking model of *ISPETase* with the reaction intermediate 2-HE(MHET)<sub>4</sub>.** Modified according to Joo *et al.* (2018) published under creative commons license CC BY (<http://creativecommons.org/licenses/by/4.0/>). Visible in **a** is the catalytic triad with the reaction intermediate 2-HE(MHET)<sub>4</sub>. **b** shows the structure model of the *ISPETase* with electrostatic surface potential from negative (red) to positive (blue) with the reaction intermediate in the different subsites. **c** and **d** show different binding modes.

The main differences between type I and II PETases seem to be in subsite II and the extended loop area (Figure 6). Based on this area, type II enzymes were subdivided into two subgroups called IIa and IIb.

Residues in <i>ISPETase</i>	Enzyme catalysis			Subsite I				Subsite II				Extended loop					Additional disulfide bond			
	S160	H237	D206	Y87	Q119	M161	W185	T88	A89	W159	S238	N241	S242	G243	N244	S245	N246	Q247	C203	C239
Type I	S	H	D	Y <sub>F</sub>	Q <sub>Y</sub>	M	W	TL	A <sub>G</sub>	H	F	N <sub>Q</sub>	TS <sub>LMF</sub>	SP <sub>VTIAE</sub>	N <sub>D</sub>	—	—	—	GA	FA
Type IIa	S	H	D	Y <sub>F</sub>	Q	M	W	VL	S <sub>L</sub>	W	FY	N	G <sub>TSD</sub>	G <sub>D</sub>	Y <sub>GNS</sub>	FT <sub>IFLA</sub>	N <sub>YIS</sub>	NED <sub>G</sub>	C	C
Type IIb	S	H	D	Y <sub>F</sub>	Q	M	W	T	A	W	S <sub>T</sub>	N	S <sub>T</sub>	G	N	S	N	Q <sub>A</sub>	C	C

**Figure 6: Amino-acid sequence alignment of the key positions of the PETase groups.** Modified according to Joo *et al.* (2018) published under creative commons license CC BY (<http://creativecommons.org/licenses/by/4.0/>). Visible are the key amino acid residue involved in the enzyme catalysis aligned. Amino acids that are highly conserved are seen bigger than amino acids that are less conserved. Amino acids with lower probability are seen in subscript.

Type I PETases do not have the extended loop area and have different amino acids in subsite II. However, subsite II also varies between type IIa and IIb PETases. Despite being

quite variable between the different PETase types, subsite II seems to be important for PET degradation. Especially the serine at position 238 in *ISPETase* seems to be important in the degradation of PET (Bollinger *et al.*, 2020c; Joo *et al.*, 2018). A serine at this position is only present in type IIb PETases and PET degradation is higher in type IIb enzymes compared to type IIa. Mutation of this amino acid leads to much lower PET degradation in type IIb PETase but much higher PET degradation in type IIa PETases (Austin *et al.*, 2018; Avilan *et al.*, 2023; Bollinger *et al.*, 2020c; Charupanit *et al.*, 2022; Cui *et al.*, 2021; Guo *et al.*, 2022; Joho *et al.*, 2023; Joo *et al.*, 2018; Richter *et al.*, 2023; Sevilla *et al.*, 2023). Since PET polymers and oligomers are relatively long and therefore have sterical hindrance, a wider active site cleft aids in accommodating these long molecules. This was also detected by other authors in the LCC for example. They tried to improve MHET substrate binding by targeted mutagenesis and found the amino acid position to be crucial at the homologue position as it was reported for the PE-H (Bollinger *et al.*, 2020c; Tournier *et al.*, 2020).






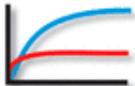
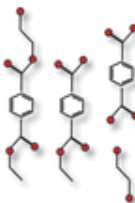

The second favorable feature for PET degradation seems to be the extended loop area. This elongated loop in more active type IIa and type IIb PETases increases the flexibility of the area close to the catalytic triad, compromising its integrity (Richter *et al.*, 2023). The second disulfide bridge of type II PETases restricts this flexibility making this whole area more accessible for bulky PET substrates (Richter *et al.*, 2023).

### 1.2.3. Characteristics of PET degrading enzymes

Despite being part of one family, the biochemical characteristics of PETases can vary greatly. Furthermore, due to individual laboratory conditions and methods, comparing the biochemical properties between publications can be difficult. Arnal *et al.* (2023) attempted to collect some important factors that should be compared to select the best candidates for industrial use. Even though some enzymes might look promising in small-scale laboratory experiments, their usage in big industrial settings might not work. The most important parameters to consider according to Arnal *et al.* (2023) are listed in Table 1.



**Table 1: Parameters important to consider for the industrial usage of PETases.** Table by Arnal *et al.* (2023) published under creative commons license CC BY.

	Parameter	Critical constraint	Proposed solutions
	<b>PET crystallinity</b>	Recalcitrance of highly crystalline PET regions to enzymatic hydrolysis.	Use of amorphized PET samples (Goodfellow PET film and pre-treated post-consumer waste amorphized by extrusion).
	<b>Surface of exchange</b>	Low enzyme performance with large PET substrate pieces due to limited reaction surface.	Micronization (< 500 µm) of substrate to increase the reaction surface and to enable high efficiency of the depolymerization.
	<b>Temperature</b>	At temperatures largely below $T_g$ of PET, the availability of productive substrate conformations (dihedral angles around the ester bond) is limited.	According to Arrhenius' law and substrate peculiarities, maximal enzyme performance is reached when PET depolymerization is performed at temperatures close to the $T_g$ of PET.  Enzyme thermostability must be high enough.
	<b>Enzyme efficiency vs PET crystallization</b>	Re-crystallization phenomena of PET when incubated at temperatures close or higher than the $T_g$ .	A highly efficient enzyme is required to overcome the kinetic of PET re-crystallization.
	<b>PET concentration</b>	Commonly used concentrations of PET are far below the requirement for a high-productivity process.	Initial PET waste load to maximize the productivity per batch without loss of TPA needs to be assessed according to running operation conditions.
	<b>Yield of depolymerization</b>	Initial rate of the reaction is not the only parameter to consider. Enzyme activity deteriorates during the reaction either due to instability or product inhibition.	Enzyme efficiency should allow near 100% PET conversion to maximize productivity per batch. Enzyme stability in highly concentrated PET solution upon completion of depolymerization is mandatory.
	<b>Composition of the products</b>	Yield and productivity of an enzyme-based PET depolymerization process is negatively affected by the presence of MHET or soluble oligomers that might be lost during the purification scheme.	Final product composition should be thoroughly determined (e.g., by HPLC) to assess the purity of the products (e.g. TPA and MEG) of the PET depolymerization.  Enzyme performance must ensure a complete hydrolysis of PET into TPA and MEG.
	<b>Availability of the enzyme</b>	Instability, aggregation and low expression rates of soluble protein may limit an upscaling of the reaction to reach industrial scales.	The availability of the enzyme in large quantities has to be explored early on.  Industrial expression hosts are required to obtain sufficient enzyme quantities for large scale reactions

Parameters to consider in PET degradation are mostly related to the chemistry of PET and the biochemistry of the PETases.

First, the crystallinity of PET should be considered. Due to the different crystallinities of PET and a preference of PETases for the mobile amorphous parts, the enzymes need to be either temperature stable, to heat PET up to its glass transition temperature, or the PET



needs to be pretreated (Thapa *et al.*, 2019). A problem with heating the PET to its glass transition temperature is the PET re-crystallization when heated and the whole process therefore not leading to products. Pretreatment of PET might be important considering the preference of PETases for higher surface area. The smaller the PET particles, the higher the total surface area, and the easier the enzymes can attach to the PET surface.

Secondly, some enzymes could be made more thermostable by adding ions like  $\text{Ca}^{2+}$ , which are shown to improve the degradation performance of PETases at high temperatures by stabilizing the active site (Wei *et al.*, 2022).

Third, regarding the biochemistry of enzymes, the composition of the products is important. It has been observed that certain products like MHET can lead to product inhibition stopping the degradation process.

Next up is the general stability of the enzymes in the treatment solution over time. If the enzymes do not get inhibited by the product they might deteriorate and stop working after some time.

In addition, the amount of enzyme that is expressible plays an important role in using them for industrial processes. If the enzyme is poorly expressible and not easy to handle the costs of production outrun the use of the enzyme (Arnal *et al.*, 2023).

Due to the nature of the PET degradation process, acidic compounds are released. Therefore, ideally, PETases should be able to work in acidic conditions (Carniel *et al.*, 2021; Thapa *et al.*, 2019).

Lastly, the availability of enzymes is an important factor. If the enzyme is only expressible in low quantities, even the best performing enzymes have no use for large scale applications. Enzymes that are easy to express and in high quantities are therefore necessary.

### **1.3. How to find novel enzymes for biotechnological application**

The vastness of the oceans compared to land cause a wide diversity of ecosystems that make the ocean a perfect breeding ground for novel microorganism and enzymes for biotechnological applications (Khambhaty, 2023). This has led to the formation of the biotechnological field using marine-derived bioresources named “blue biotechnology” (Blasiak *et al.*, 2023). Especially deep-sea environments are of special interest (Khambhaty, 2023). They are difficult to access and are therefore mostly undisturbed. Also, extreme

pressures, salinity and general conditions may lead to organisms with extraordinary abilities (Khambhaty, 2023). Over the past decades, plastic has found its way into the deep-sea (Harris *et al.*, 2023; Sonke *et al.*, 2022). Due to the lack of nutrients and other sources of energy in this environment, it is reasonable to assume that the microorganism might have found ways to harvest this valuable carbon source. This has already been observed in other less extreme environments like PET recycling facilities (Yoshida *et al.*, 2016). There are different ways of harvesting these naturally developed resources for biotechnological applications.

First, one of the more traditional ways of finding new enzymes, is to screen for homologue enzymes of families that have proven to be useful in databases like the NCBI (Sayers *et al.*, 2022; Wackett, 2004). Databases like NCBI contain DNA and amino acid sequences from a multitude of origins, including metagenomic projects, accessible for scientists to screen and work with (Ferrer *et al.*, 2005). Furthermore, when looking at the family of organisms that were proven to harbor enzymes that are capable of degrading plastics, it might be possible to find other organisms within this group that share homologue enzymes. It is possible that these organisms reside in challenging environments and have evolved in a manner that makes the enzymes they produce even more powerful (Bollinger *et al.*, 2020b). However, this way only already known pathways of degradation can be found. Novel pathways are necessary especially for plastics like polyethylene. For those polymers, only the degradation through oxidizing of the polymer chain is known (Sanluis-Verdes *et al.*, 2022). Secondly, to bypass the problem of difficulties growing most microorganism in laboratory environments, metagenomics can be applied (Lodhi *et al.*, 2023; Stewart, 2012). For this the DNA of all organisms inhabiting a certain area like for example deep-sea sediment is harvested and screened. The obtained DNA can then be integrated into plasmids and the respective protein can be produced by a host organism like *E. coli* and screened for different activities. These functional screenings can then be done in high throughput on for example agar plates containing the respective substrate of interest (Molitor *et al.*, 2020). With a functional metagenome and high throughput screening assays like agar plate-based assays (Molitor *et al.*, 2020), novel degradation pathways might be found (Kaul & Asano, 2012; Lorenz & Eck, 2005).

### 1.3.1. The (*Halo*-)*Pseudomonas pertucinogena* lineage

Recently the *Pseudomonas pertucinogena* clade has been described as a promising lineage with biotechnological potential (Bollinger *et al.*, 2020b). Peix *et al.* (2018) were the first to classify the *P. pertucinogena* clade comprising of nine marine and seven land born species. Bollinger *et al.* (2020b) realized that members of this group have been mentioned in different studies regarding the identification of novel biocatalysts relevant for biotechnological applications. Most of the species were first described in the past thirteen years (Bollinger *et al.*, 2020b). Since it seemed like a clade with a lot of potential yet not a lot of research, they analyzed the potential on basis of bioinformatic data.

They found that members of this group have a versatile metabolism and are producing a variety of proteins being able to degrade hydrocarbons (Bollinger *et al.*, 2020c) mostly from oil spills making them potentially important for restoring the health of aquatic systems after ship accidents. In addition, most of the *P. pertucinogena* species seem to be cold and salt tolerant, showing an adaption to marine habitats. This is especially true for the species *P. pelagia*, which was found in the Arctic Ocean associated with the green algae *Pyramimonas gelidicola* showing that this genus has the potential of surviving in very low temperatures (Hwang *et al.*, 2009).

*Pseudomonads* are generally known for being able to metabolize a wide range of carbon sources. Comparatively, the *P. pertucinogena* group seems to be more limited regarding its carbon degradation potential (Sanchez *et al.*, 2014).

Rudra and Gupta (2021) reevaluated the evolutionary relationships of species from the family *Pseudomonadaceae* and saw in the genus *Pseudomonas* one clade branching out. Due to these 19 species mainly being halotolerant, they proposed a novel genus *Halopseudomonas gen. nov.* They clustered species from the *Pseudomonas* clade based on the flagella FlgN protein commonly shared by all members of the *Pertucinogena* clade as well as 23 other conserved signature indels and found those 19 species in the *Halopseudomonas pertucinogena* clade (Rudra & Gupta, 2021). Compared to the clustering shown by Bollinger *et al.* (2020b) the new genus *H. pertucinogena* consists of 11 more species namely *H. gallaeciensis*, *H. jilinensis*, *H. yangmingensis*, *H. laoshanensis*, *H. nanhaiensis*, *H. neustonica*, *H. phragmitis*, *H. profundis*, *H. salina*, *H. saliphila*, and *H. abyssi*. *Pseudomonas populi* did cluster with *H. pertucinogena* in the publication by Bollinger *et al.* (2020c) but not in the one by Rudra and Gupta (2021).

Based on the new clustering by Rudra and Gupta (2021), I will refer to the *P. pertucinogena* lineage in this thesis as *H. pertucinogena* or simply *Halopseudomonas*.

### 1.4. Aim

The extensive use of plastic materials like recalcitrant polyesters has led to a dramatic littering problem in our environment. This motivates the search for novel biocatalysts hoping that appropriate enzymes can be used to degrade and even recycle plastic waste. The use of polymer-active enzymes represents a promising solution for breaking down polymers into their individual components to be able to produce 'virgin' plastic again. In this work, several questions in the context of the plastic problem will be addressed to expand the knowledge on occurrence, diversity, and biochemical mechanistic.

To do this, a new collection of enzymes and enzyme variants acting on polyesters and polyester containing co-polymers should be established to aid plastic waste handling. The focus of this work is specifically on:

1. Does the metagenome from plastic accumulation zones in the North Atlantic Ocean contain sequences of known polyester degrading enzymes?
2. How does the natural diversity of polyester hydrolytic enzymes from closely related organisms shape their biochemical characteristics?
3. Can general rules be derived from sequence and biochemical information and is it possible to transfer this knowledge to increase the performance of respective enzymes?

For the first question, I intended to analyze samples taken during a research cruise in the North Atlantic Ocean. I analyzed the bacterial community using metagenome sequencing combined with Hidden-Markov-Model based homology search, enrichment cultivation on different polyesters and functional screening for active isolates.

For the second question, I investigate the *Halopseudomonas spp.* lineage. Closely related organisms have differentiated in different environments, while retaining beneficial homologue enzymes. I explore if some of these homologue enzymes have improved plastic degrading capabilities, and how their biochemical characteristics differ. I analyze them phenotypically for the presence of polyester hydrolases. I clone, express, and characterize the resulting enzymes regarding different relevant factors important for applications of their polyester hydrolase abilities. By having a set of highly similar enzymes, I provide better insight into structure-function relationships by comparative analysis of biochemical characteristics.

Finally, I perform rational mutagenesis of the best performing polyester hydrolases at amino acid positions that were found to be important in existing literature. I elucidate the impact of these positions on the enzyme's polyester degrading behavior, temperature tolerance, and pH sensitivity.

## 2. Material and Methods

### 2.1. Working with bioinformatics

#### 2.1.1. Online Databases and tools

In this work the database of the National Center for Biotechnology Information (NCBI (Sayers *et al.*, 2022)) of the National Library for Medicine, used for sequence comparison, was searched using the tool BLAST (Camacho *et al.*, 2023), to identify organisms as well as find protein sequences.

The online tool ProtParam (Gasteiger *et al.*, 2003) was used for calculating different parameters of protein sequences. Both Databases were used with standard parameters.

For the percentage identity matrix, the online tool Clustal Omega Multiple Sequence Alignment (Madeira *et al.*, 2022) using the default parameter was used.

#### 2.1.2. Alignment Tools

Alignments were done with the alignment tools MEGA11 (Tamura *et al.*, 2021) for the neighbor joining tree, as well as BioEdit version 7.2.5 (Hall, 2011) using the default parameters and the ClustalW algorithm.

#### 2.1.3. UCSF ChimeraX

Bioinformatical comparisons of protein structures were computed using UCSF ChimeraX (Pettersen *et al.*, 2021). The implemented tool matchmaking, alignment and the AlphaFold implementation were used with standard parameters.

#### 2.1.4. Python

Python (Van Rossum G, 2009) is a programming language with add-ons to do mathematical calculations. For the analysis of photometric activity data, a program code was written to identify the linear range (i.e., the initial enzyme activity) to calculate a more reliable and transparent slope.

First an amount of points  $N$  is defined. With this defined  $N$  the program looks through all points in time, makes the linear regression and checks if the  $R_2$  is larger than 0.95. If that is the case the program saves the value and looks for the next point. If it finds a larger linear regression with an  $R_2$  over 0.95 it saves this value.

After this, the calculated slopes were used to subtract the blank from the values and do further calculations depending on the type of assay. The Script can be found on GitHub under [https://github.com/RebeckaMo/Enzyme\\_photometric\\_activity](https://github.com/RebeckaMo/Enzyme_photometric_activity).

#### **2.1.5. CloneManager9**

Clone Manager9 was used for the analysis of DNA sequences, primer design, as well as plasmid map construction and calculations for the restriction ligation cloning.

### **2.2. Working with DNA**

#### **2.2.1. Preparation of primer**

Primers were ordered from Eurofins Genomics with the purification method HPSF at a synthesis scale 0.01  $\mu\text{mol}$ . The primers were delivered in lyophilized form and adjusted with ddH<sub>2</sub>O to a concentration of 100 pmol/l. For use in PCRs the primers were 10 x diluted with ddH<sub>2</sub>O to a concentration of 10 pmol/l. A list of the used primer can be found in the Appendix Table 9.

#### **2.2.2. Polymerase chain reaction (PCR)**

Polymerase chain reaction is a method for amplifying DNA. For this purpose, the chemical listed in Table 2 are mixed accordingly.

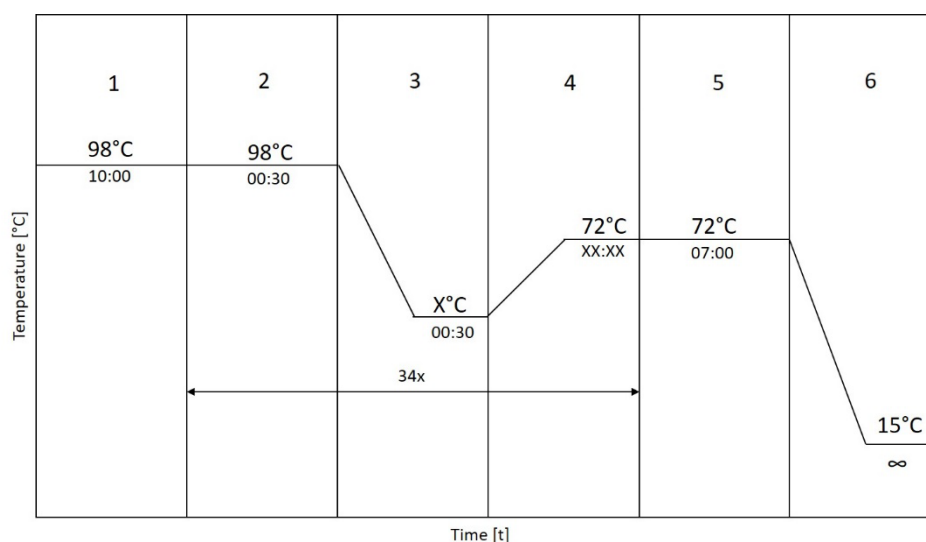
**Table 2: PCR ingredients and volumes.** The volume of the template DNA is dependent on the ng/ $\mu\text{l}$  concentration and needs to be adjusted accordingly.

50-100	ng	Template DNA
10	$\mu\text{l}$	5x Phusion HF-buffer (Thermo Fisher Scientific, USA)
2.5	$\mu\text{l}$	Reverse Primer (10 pM)
2.5	$\mu\text{l}$	Forward Primer (10 pM)
1.5	$\mu\text{l}$	DMSO (Thermo Fisher Scientific, USA)
1	$\mu\text{l}$	dNTP Mix (10 mM ea.) (Thermo Fisher Scientific, USA)
0.5	$\mu\text{l}$	Phusion High-Fidelity DNA Polymerase (Thermo Fisher Scientific, USA)
Add 50	$\mu\text{l}$	ddH <sub>2</sub> O

At last, the Phusion polymerase should be added since it will start its activity as soon as it is not kept cool anymore.

When everything is mixed, the reaction tubes are put into the Biometra TAdvance (Analytik Jena, Germany) PCR Cycler with the temperature and time protocol listed in Figure 7.





**Figure 7: PCR cycle temperature and time.** The annealing temperature in step 3 is dependent on the primer sequences and must be calculated using an online tool or an appropriate formula. The amplification speed of the polymerase and the length of the desired DNA fragment determine the elongation time in step 4.

The success of the PCR is subsequently evaluated by visualizing the DNA on an agarose gel as mentioned in 2.2.4 and identified according to the size of the amplified DNA fragment.

### 2.2.2.1. Quick-Change PCR

Modified according to Edelheit *et al.* (2009).

A quick and easy solution for changing single amino acids in proteins is a mutagenesis by Quick-Change PCR using an already existing plasmid encoding the gene of interest as a template.

For this, primer pairs were constructed that contain the triplet of interest. To stabilize this short non-complementary sequence, the triplet is flanked by at least 15 bp that are complementary to the template sequence for at least 30 nucleotides. With these primers, the PCR mix was set up according to Table 3.

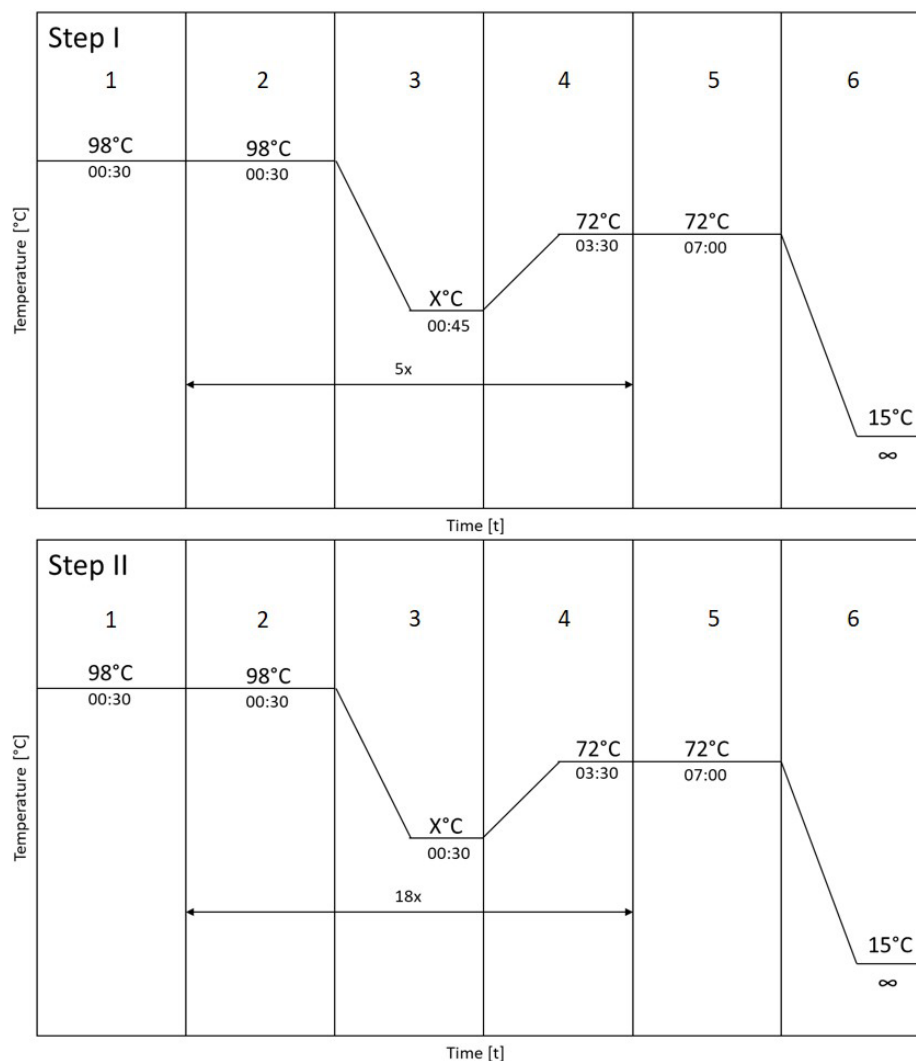
**Table 3: Quick-Change PCR mixture ingredients for 25 µl reaction mixture in total per primer.** Reaction mixtures for the forward and the reverse primer, respectively, were set up separately to avoid the formation of dimers during the first cycles. The volume of the template DNA is dependent on the ng/µl concentration and needs to be adjusted accordingly.

5	µl	5x Phusion HF-buffer (Thermo Fisher Scientific, USA)
0.5	µl	10 mM dNTP-Mix (Thermo Fisher Scientific, USA)
50-100	ng	Template DNA
0.5	µl	Forward or Reverse Primer (10 pM)
0.75	µl	DMSO (Thermo Fisher Scientific, USA)

0.25  $\mu$ l Phusion High-Fidelity DNA-Polymerase (Thermo Fisher Scientific, USA)

Add 25  $\mu$ l ddH<sub>2</sub>O

Both Primers were used individually for amplifying the single stranded whole plasmid DNA in step I. In step II, both reactions were combined (Figure 8).



**Figure 8: Quick-Change PCR cycle temperature and time graph** for step I with separated primers and step II with mixed primers. Instead of the X the appropriate calculated annealing temperature was used.

After the plasmids have been amplified, the template plasmid was digested by addition of 1  $\mu$ l of *DpnI* (Thermo Fisher Scientific, USA) to the mixture and incubation for 16 h at 37°C with subsequent heat inactivation at 80°C for 20 min. Unwanted components were removed by using the NucleoSpin Gel and PCR Clean-up Kit (Macherey-Nagel, Germany). After this, 2.5  $\mu$ l of the DNA solution were used to transform competent cells (see 2.3.1).

### **2.2.3. Cloning**

#### **2.2.3.1. Restriction and ligation cloning**

For introduction of gene fragments into a plasmid, several different techniques were used. One of these techniques is hydrolysis and ligation. For this purpose, the gene of interest is amplified using the PCR method mentioned in 2.2.2 with a primer pair containing a short sequence in the beginning for the restriction enzyme to reside on. Additionally, a sequence with the recognition motif of the used restriction endonuclease, followed by a complementary sequence to the gene of interest was added. In addition, a His-Tag is C-terminally fused to the construct using the primer if the plasmid based His-Tag is not in frame with the used restriction endonucleases. The His-tag was used to facilitate purification and tracking of the protein of interest.

The gene of interest is checked for size using agarose gel electrophoresis as mentioned in 2.2.4 and purified using the NucleoSpin Gel and PCR Clean-up Kit (Macherey-Nagel, Germany). 1 µg of the purified gene of interest as well as 100 ng of vector isolated according to 2.2.5 were then hydrolyzed with the appropriate restriction enzymes (Thermo Fisher Scientific, USA) according to the manufacturer manual. The DNA insert fragments with the now formed sticky ends were digested using 1 µl of FastAP (Thermo Fisher Scientific, USA) and purified again using the NucleoSpin Gel and PCR Clean-up Kit (Macherey-Nagel, Germany). Then, the insert and vector in a ratio of one part vector and two parts inserts were ligated using a T4-DNA-Ligase (Thermo Fisher Scientific, USA) according to the manufacturer's manual. The reaction was inactivated at the respective temperature according to the manufacturer's protocol. 2.5 µl of the so formed plasmid were used to transform chemical competent cells as stated in 2.3.1.

#### **2.2.3.2. One-step sequence- and ligation-independent cloning (SLIC)**

Modified according to Jeong *et al.* (2012).

The one-step sequence- and ligation-independent cloning (SLIC) is a fast and easy method to insert a gene of interest into a vector when there is no appropriate restriction site accessible, based on sequence homology.

For this, the primer must be designed to have at least 15 bp homology to the ends of the vector at the desired integration site of the gene of interest. Another 15 bp homology of the primer needs to be with the gene of interest outer sites. The gene of interest was

amplified using the PCR method stated in 2.2.2. The vector was linearized using the appropriate restriction endonuclease and both, vector, and amplified gene of interest, were purified using the NucleoSpin Gel and PCR Clean-up Kit (Macherey-Nagel, Germany). The linearized vector and gene of interest were mixed in a molar ratio of 1:2. The rest of the digestion mixture consists of 1x BSA (New England Biolabs GmbH, Germany) solution, 1x NEB Buffer 2 (New England Biolabs GmbH, Germany), 0.2 µl of T4 DNA polymerase (3 U/µl, New England Biolabs GmbH, Germany). The mixture was added up with ddH<sub>2</sub>O to 10 µl. The mixture was incubated at room temperature for 2.5 min and stopped by incubating the mixture on ice for 10 min. Chemically competent cells were transformed with the plasmid according to 2.3.1.

#### **2.2.4. Agarose gel electrophoresis**

With the agarose gel electrophoresis, DNA can be visualized as well as separated by size. For this 1 % Agarose (Nippon genetics Europe, Germany) was mixed with 0.5xTBE-buffer (22.25 mM Tris, 22.25 mM boric acid, 0.625 mM EDTA) and boiled until no agarose beads were visible anymore. After cool-down of the agarose solution to approximately 60°C, 4 µl per 100 ml of the DNA dye Midori Green Advance (Biozym Scientific, Germany) was added to the solution. The mixture was poured into an appropriate mold. After polymerization, the gel is placed in a gel chamber filled with TBE-buffer. A voltage of 120 V for 20 min separated the DNA. The dyed DNA was visualized using blue light of a wavelength of 490 nm.

#### **2.2.5. Isolation of circular plasmid DNA from bacterial cells**

Bacterial cells transformed (2.3.1) with plasmid DNA were used to inoculate 10 ml LB medium (Carl Roth GmbH, Germany) supplemented with the appropriate amount of antibiotic according to the antibiotic resistance coded for on the plasmid. The cells were incubated for 24 h at 37°C and under agitation of 130 RPM. The cells were harvested, and the DNA isolated using the innuPREP Plasmid DNA Mini Kit 2.0 (Analytik Jena, Germany) according to manufacturer manual. The amount of isolated DNA was measured using a NanoDrop 2000c (Thermo Fisher Scientific, USA) using the Nucleic Acid method according to the manufacturers basic specifications using UV/VIS absorption at 260 nm. DNA solutions were stored at -20°C.

### **2.2.6. Isolation of metagenomic DNA from sediment**

To isolate the total DNA from the frozen marine sediment samples (2.3.2), the DNeasy PowerSoil Kit (Qiagen, Germany) was used. The environmental DNA was isolated according to the manufacturers' protocol and stored at -20°C until further use.

### **2.2.7. Analysis of metagenomic DNA**

The sequencing and analysis of the metagenomic DNA was done by Novogene (Beijing, China). For a thorough analysis an Amplicon Metagenomic Sequencing and a Shotgun Metagenomics library was prepared. In the Amplicon Metagenomic Sequencing, the 16S-ribosomal DNA sequenced, and the most probable species were detected giving an overview over the bacterial community in the sample. In the Shotgun Metagenomic library every available DNA fragment was sequenced. The bioinformatic analysis was also conducted by Novogene.

## **2.3. Working with bacterial cells**

### **2.3.1. Preparation and transformation of chemical competent cells**

Modified according to Hanahan (1983).

An overnight culture of *E. coli* cells was added to 500 ml LB-medium (Carl Roth GmbH, Germany) to an initial OD<sub>580nm</sub> of 0.05. The cells were incubated at 37°C until they reached a cell density equivalent to an OD<sub>580nm</sub> of 0.4-0.5. The cells were chilled for 10 min on ice and harvested for 10 min with 2,790 g at 4°C. The pelleted cells were resuspended in 35 ml sterile FB-buffer (100 mM KCl, 67.5 mM CaCl<sub>2</sub>, 10 % (w/v) glycerin, 10 mM potassium acetate, pH 6.4) and again incubated on ice for 20 min. The cells were washed with another centrifugation step at 2,790 g and 4°C for 10 min and resuspended in 8.6 ml FB buffer. The resulting cell suspension was portioned into 100 µl aliquots and immediately frozen at -80°C until further use.

For transformation, one aliquot was thawed on ice for 20 min. The plasmid of interest was added to the cells which were again incubated on ice for 20 min. The cells were heat-shocked at 42°C for 90 sec and immediately placed on ice again. 700 µl of LB-medium (Carl Roth GmbH, Germany) was added and the cells were left to regenerate for an appropriate time between 30 min and 3 h at 37°C, according to the antibiotic resistance used. In the meantime, LB-agar plates were poured using LB-medium with the addition of 1.5 % (w/v)

agar-agar and the appropriate antibiotic. After regeneration, the cells were plated on selective antibiotic plates and incubated for 24 h at 37°C.

### 2.3.2. Sampling of bacterial cells from Deep-Sea sediment

During the cruise SO279 of the German research vessel Sonne from 04.12.2020-05.01.2021 to the area of the North Atlantic Ocean garbage accumulation zone samples of deep sea sediment were taken (Beck *et al.*, 2021). Sediment samples were taken, with a Box-Core device, on each station, from different depths (Table 4). Around 2 x 50 ml of sediment were sampled from each Box-Core using a clean metal spoon into 50 ml falcon tubes. One 50 ml falcon tube was kept at 4°C with the addition of 10 ml of filtered seawater after sampling to keep the bacteria alive for enrichment. The other 50 ml falcon tube was frozen at -20°C for later extraction of metagenomic DNA.

**Table 4:** Sampling points from the cruise SO279.

<b>Station</b>	<b>Boxcore samples SO279</b>	<b>Timestamp</b>	<b>Latitude</b>	<b>Longitude</b>	<b>Depth (m)</b>
<b>1</b>	SO279_8-1BC	09.12.2020 09:14	47° 15,035' N	010° 06,216' W	4428
<b>3</b>	SO279_25-1BC	14.12.2020 08:39	31° 16,048' N	024° 48,707' W	5496
<b>4</b>	SO279_39-1BC	16.12.2020 12:20	30° 53,545' N	029° 18,836' W	4333
<b>5</b>	SO279_60-1BC	19.12.2020 09:06	31° 21,398' N	034° 02,274' W	4397
<b>6</b>	SO279_72-1BC	20.12.2020 13:24	33° 17,647' N	034° 29,505' W	3592
<b>7</b>	SO279_85-1BC	21.12.2020 23:47	33° 08,612' N	033° 46,715' W	3674
<b>9</b>	SO279_104-1BC	27.12.2020 15:54	35° 00,002' N	020° 59,980' W	5191

### 2.3.3. Enrichment cultures

For better handling the sediment of stations 2-9 (Table 4) were pooled before enrichment. Station 1 was kept individually since it was not taken in the North Atlantic garbage accumulation zone. The bacteria in the sediment were enriched for growth on Impranil DLN-SD using 10 ml of the minimal medium Bushnell-Haas Broth (Thermo Scientific, USA) depleted of hydrocarbons and temperatures of 10°C and 20°C with the addition of 10 mM NH<sub>4</sub><sup>+</sup> (Joint *et al.*, 2010) at an agitation of 50 RPM for aeration. After one month of incubation time, the cultures were used to inoculate a subsequent new enrichment round in fresh media for another month.

After every enrichment round, the cultures were harvested by centrifugation at 5,000 RPM for 10 min and the pellet resuspended in 100 µl of the respective media and plated on agar plates containing Impranil DLN-SD and the respective culture media. The plates were then incubated at room temperature in the dark for one week.

### 2.3.4. Production of proteins

The production of proteins was conducted using the T7 expression system of the chemically competent *E. coli* strain derived from BL21(DE3) called LOBSTR (LOW Background STRain) with the genotype: F ompT hsdSB(rB mB ) gal dcm (klts857 indl sam7 nin5 lacUV5-T7gene1) and additional point mutations of the genes ArnA and SlyD (Andersen *et al.*, 2013).

For the start of an expression culture, chemically competent LOBSTR cells were transformed as described in 2.3.1 with the plasmid of choice appropriate for T7-expression. The cells were incubated in 10 ml of LB-medium (Thermo Fischer Scientific, USA) with the appropriate antibiotic as well as 0.5 % of glucose to inhibit expression in the pre-culture as much as possible to avoid stress for the cells. After 24 h of incubation at 37°C, 500 ml of auto-induction medium (AI-medium) according to Studier (2005) were inoculated with an OD<sub>580nm</sub> of 0.05 of cells. AI-medium utilizes the preference of *E. coli* cells for glucose over lactose. After the glucose is depleted, after approximately four hours, lactose is metabolized, and the induction starts. The cells were placed at an appropriate temperature varying according to the protein expressed (Table 5) and incubated under agitation of 160 RPM for 24 h. The cells were harvested by centrifugation at 4°C and 6,000 RPM for 30 min and stored at -20°C until further use.

The *E. coli* expression cells C43 (DE3) (Miroux & Walker, 1996) are commonly used for expression of difficult or toxic proteins. C43 (DE3) cultures were handled the same as mentioned in 2.3.1, but inoculated into LB-medium (Thermo Fisher Scientific, USA) with target gene expression induced by applying 0.2 mM IPTG to the cultures when a cell density equivalent to an OD<sub>580nm</sub> of 0.4 was reached. The incubation was performed as mentioned above. The expression conditions of the proteins expressed for this work are summarized in Table 5.

**Table 5: List of expression conditions to obtain the characterized enzymes.** AI stands for autoinduction medium, LB-AI stands for LB-medium with added lactose, glucose, and glycerol according to the AI-medium protocol. All media were prepared with 100 µg/ml ampicillin.

Enzyme name	Origin organism	Host organism	Expression medium	Expression temperature	Shaking frequency	IPTG concentration
ISPETase	<i>I. sakaiensis</i>	LOBSTR	AI	30°C	160 RPM	-
Haes_PE-H	<i>H. aestusnigri</i>	LOBSTR	AI	30°C	160 RPM	-
Haes_PE-H_Y250S	<i>H. aestusnigri</i>	LOBSTR	AI	30°C	160 RPM	-
Hoce_PE-H	<i>H. oceani</i>	LOBSTR	LB AI	15°C	160 RPM	-
Hsab_PE-H	<i>H. sabulinigri</i>	C43	LB	20°C	160 RPM	0.2 mM

<i>Enzyme name</i>	<i>Origin organism</i>	<i>Host organism</i>	<i>Expression medium</i>	<i>Expression temperature</i>	<i>Shaking frequency</i>	<i>IPTG concentration</i>
<i>Hbau_PE-H</i>	<i>H. bauzanensis</i>	LOBSTR	AI -lactose	15°C	160 RPM	-
<i>Hpac_PE-H</i>	<i>H. pachastrella</i>	LOBSTR	LB AI	30 °C	160 RPM	-
<i>Hpel_PE-H</i>	<i>H. pelagia</i>	LOBSTR	AI -lactose	30 °C	160 RPM	-
<i>Hlit_PE-H</i>	<i>H. litoralis</i>	LOBSTR	LB AI	15°C	160 RPM	-
<i>Hxin_PE-H</i>	<i>H. xinjiangensis</i>	LOBSTR	AI -lactose	15°C	160 RPM	-
<i>Hfor_PE-H</i>	<i>H. formosensis</i>	LOBSTR	AI	30°C	160 RPM	-

## 2.4. Working with proteins

### 2.4.1. Purification of proteins using an IMAC

Proteins with a C- or N-terminally fused His-Tag can be purified from a culture or a cell lysate by affinity binding of the His-tag to nickel at Ni-NTA beads (Crowe *et al.*, 1994).

The purification follows up on the in 2.3.4 described expression of proteins. The fresh or frozen cell pellet were resuspended in lysis buffer (20 mM Na<sub>2</sub>HPO<sub>4</sub>, 500 mM NaCl, 10 mM Imidazole, pH 7.4) and lysed using the Bandelin (Berlin, Germany) Sonoplus HD 2070 generator with the Sonoplus KE 76 tip with 40 % power for three times five minutes. After lysis, the cell debris was separated from the soluble parts by centrifugation at 4°C and 17,400 RPM for 20 min. The column was filled with 2.5 ml Ni-NTA agarose (Qiagen, Germany) and washed with 3 CV ddH<sub>2</sub>O. After this, the column was equilibrated with 3 CV lysis buffer and the soluble fraction of the cell lysate was put onto the column. This step of binding to the column was prolonged by leaving the cell lysate on the column and stirring for 5 min. After this, the column was washed with 15 CV of wash buffer (20 mM Na<sub>2</sub>HPO<sub>4</sub>, 500 mM NaCl, 30 mM Imidazole, pH 7.4). The elution step was conducted like the incubation of the soluble fraction on the column using 8 ml of the elution buffer (20 mM Na<sub>2</sub>HPO<sub>4</sub>, 500 mM NaCl, 500 mM Imidazole, pH 7.4). After 5 min, the elution fraction was collected and concentrated using a Vivaspin20 centrifugal filter (VWR, USA) with a cutoff of 10,000 MWCO to a volume of 2.5 ml. This concentrated elution fraction was again purified by a size exclusion chromatography (PD10 desalting column, GE Healthcare Bio-Sciences AB, Sweden) according to the manufacturer's protocol with the storage buffer (100 mM KPO buffer, 100 mM NaCl, pH 7.2). The eluted protein in storage buffer was aliquoted into 1 ml fractions and stored at -20°C. 10 µl of each step of the purification process was saved and checked on an SDS-PAGE according to the method described in 2.4.2. The protein concentration was measured using the NanoDrop2000c (Thermo Fisher



Scientific, USA) with the A280 method stating the size and extinction coefficient of the measured enzyme according to the ProtParam tool (Gasteiger *et al.*, 2003).

#### 2.4.2. SDS-PAGE

Modified according to Laemmli (1970).

SDS-PAGE samples were prepared mixing one part of 2xSDS-PAGE sample buffer (0.2 M Tris-HCL, 0.4 M DTT, 277mM 8 % (w/v) SDS, 6 mM bromophenol blue, 4.3 M glycerol) with one part of the sample. The buffer-sample mixture was cooked at 99°C for 10 min to ensure full denaturation of the proteins.

Proteins were separated using the Invitrogen NuPAGE 4 to 12 % Bis-Tris 1.0 mm Mini Protein Gel (Thermo Fisher Scientific, USA) system with the NuPAGE MES SDS Running buffer (Novex, USA) according to the manufacturer's protocol.

The separation was conducted at 150 V for 15 min followed by another step at 200 V for 45 min. As a size standard, the PageRuler Prestained Protein Ladder (Thermo Fischer Scientific, USA) was used.

The gels were stained with the Bio-Safe Coomassie Stain (BioRad, USA) according to the manufacturer protocol. The gels were documented using the Intas advanced fluorescence imager (Intas science Imaging Instruments GmbH, Germany) using the settings for SDS documentation.

#### 2.4.3. Esterase activity assay

Modified according to Winkler and Stuckmann (1979).

Esterase activity can be measured through the hydrolysis of 4-nitrophenyl esters. The hydrolysis leads to the release of the yellow 4-nitrophenolate that can be photometrically measured at a wavelength of 410 nm. The relative and volumetric esterase activity can then be calculated using the Beer-Lambert formula. The volumetric activity was calculated using the formula:

$$\frac{\Delta OD_{410} [\text{min}^{-1}] * \text{vol. in MTP} [\text{ml}] * \text{dillution factor}}{d [\text{cm}] * \epsilon [\text{mM}^{-1} * \text{cm}^{-1}] * \text{sample volume} [\text{ml}]} * \text{enzyme concentration} \left[ \frac{\text{mg}}{\text{ml}} \right] = \frac{U}{\text{mg}}$$

(Nolasco-Soria *et al.*, 2018) with an extinction coefficient  $\epsilon = 10 \text{ mM}^{-1}\text{cm}^{-1}$

A 20-x substrate stock solution was made by solving 20 mM 4-nitrophenyl ester (4-nitrophenyl-butyrate (pNPB), 4-nitrophenyl-hexanoate (pNPH)) in acetonitrile. From this stock solution a 1/20 solution with 100 mM Potassium-phosphate buffer with 100 mM

NaCl (pH 7.2) or 20 mM Tris-buffer with 100 mM NaCl (pH 8). For substrates with a fatty acid chain length longer than C6, 1 mg/ml gum Arabic was added as an emulator. 10 µl of the enzyme solution (2.4.1) was mixed with 190 µl of the substrate solution in a 96-well plate (BRANDPlates®, BRAND GmbH+CO KG, Germany). Increase of absorbance at 410 nm was monitored over 10 min with a measurement every 30 sec using an Infinite M1000 Pro photometer (Tecan Austria GmbH, Austria) starting immediately after the application of the substrate solution.

#### **2.4.4. Measurement of thermic stability**

The thermal stability of an enzyme was assessed with a nano differential scanning fluorimetry (nanoDSF) using the Prometheus device by NanoTemper (NanoTemper Technologies GmbH, Munich, Germany). The nanoDSF capillaries were filled with a solution of 1 mg/ml enzyme in 100 mM potassium-phosphate buffer with 100 mM NaCl (pH 7.2). The denaturation was scanned in a range between 20 and 99 °C at a heating rate of 1°C per minute.

#### **2.4.5. Detection of polyester degradation**

##### **2.4.5.1. Ultra-performance liquid chromatography (UPLC)**

Modified according to Bollinger *et al.* (2020c).

The products of enzymatic degradation of PET and PU-foam were identified using an UPLC. The reaction was conducted using 190 µl 100 mM potassium phosphate buffer pH 7.2 with 100 mM NaCl and 10 µl enzyme in storage solution with an end concentration of enzyme of 1500 nM. Due to the long incubation time, more enzyme is used. The substrates were then applied as solid pieces of around 5 mg of PET-foil amorphous (Goodfellow Cambridge, United Kingdom) or polyester-polyurethane foam (Covestro, Germany). The polyester PET was also tested as a powder, derived from amorphous PET-foil and ground using a CryoMill MM400 (Retsch GmbH, Germany) with a frequency of 20 Hz for 2 min after pre-cooling the 35 ml stainless steel jars with one 20 mm diameter stainless steel grinding ball in liquid nitrogen for 5 min. The solutions were incubated in centrifugal filters (10,000 MWCO, VWR Avantor®, USA) for 24–168 h at 30°C. Afterwards, the reaction was stopped by ultrafiltration in a centrifuge at 15,000 RPM for 30 sec to remove enzyme and residual solid substrate. The reaction products were filled in HPLC Screw Neck Vials (Waters GmbH, USA) and frozen at -20°C until further use.

For the measurement of PET oligomers, monomers and building blocks standards were created ranging from 0.0078 mM up to 1 mM of the degradation products BHET, MHET, and TPA.

For PET hydrolysis an Acquity UPLC BEH C18 column (1.7  $\mu\text{m}$  particle size) (Waters GmbH, USA) in an Acquity UPLC (Waters GmbH, USA) was used. The method described by (Bollinger *et al.*, 2020c) was used. The temperature of the column was kept at 35°C. As standards, TA (Thermo Fisher Scientific chemicals, USA) and BHET (Sigma Aldrich, USA) were used. Since MHET is difficult to synthesize, MHET standard kindly provided by Jo-Anne Verschoor at the Institute of Microbial Science in the laboratory of Han de Winde at the University of Leiden, Netherlands was used.

For PU-foam hydrolysis, a Supelco (Merck KGaA, USA) TitanC18 column with a particle size of 1.9  $\mu\text{m}$  was used. The mobile phase consisted of A ddH<sub>2</sub>O with 0.1 % formic acid and B MeOH with 0.1 % formic acid. The effluent was monitored at  $\lambda = 206 \text{ nm}$  with a flow rate of 0.21 ml/min. The program started at a concentration of 99 % A and 1 % B for 4 min. Then the concentrations were changed to 5 % A and 95 % B until they were changed back after 6 min to 99 % A and 1 % B. The amount was kept for 3 more minutes until the program finishes after 9 min. The temperature of the column was kept at 30°C. Adipic acid was used as a standard with concentrations ranging from 0.1 mM up to 100 mM.

#### **2.4.5.2. Polyester-polyurethane optical density assay**

Modified according to Islam *et al.* (2019).

Impranil DLN-SD is a polyester-polyurethane coating material with aliphatic polyester segments. It is distributed as Impranil DLN-SD (Covestro, Germany) a formulation of nanoparticles in water with a white and opaque appearance. Due to its opacity and liquid texture, Impranil DLN-SD suspension can be easily used in clearing assays to monitor polyester-polyurethane degradation.

For this, 2 % of Impranil DLN-SD dispersion was mixed with 100 mM potassium-phosphate buffer with 100 mM NaCl (pH 7.2). 100  $\mu\text{l}$  of this suspension was mixed with 100  $\mu\text{l}$  of enzyme solution prepared as in 2.4.1 mentioned with a concentration of 50 nM. The final concentration of the Impranil DLN-SD in a 96-well plate (BRANDPlates®, BRAND GmbH+CO KG, Germany) was then 1 % in 200  $\mu\text{l}$ , which yields an OD<sub>580nm</sub> of approximately 0.8.

The clearing of Impranil DLN-SD was monitored in an Infinite M1000 Pro photometer (Tecan Austria GmbH, Austria) at a wavelength of 580 nm for 10 min with interval times of 20 sec at temperatures between 30 and 50°C.

#### **2.4.5.3. pH activity optimum determination using polyester-polyurethane**

Modified according to Islam *et al.* (2019).

This assay was conducted as the assay mentioned in chapter 2.4.5.2 but with a set of Britton-Robinson buffers (40 mM boric acid, 40 mM phosphoric acid, 40 mM acetic acid) with a pH adjusted between 3 and 12 instead of the potassium-phosphate buffer. The buffer with the pH of interest was then mixed with 1 % Impranil DLN-SD and 190 µl of this substrate solution was mixed with 10 µl of enzyme solution in a 96-well plate (BRANDPlates®, BRAND GmbH+CO KG, Germany). The Impranil DLN-SD degradation was monitored in an Infinite M1000 Pro photometer (Tecan Austria GmbH, Austria) at a wavelength of 580 nm for 30 min with interval times of 1 min at 30°C.

#### **2.4.5.4. Fluorescein pH sensitive assay**

Fluorescein is a fluorescent pH sensitive dye that can be used to effectively measure the acidification of media. At a pH higher than 7 fluorescein shows a strong fluorescence at a wavelength of 510 nm. This sensitivity can be used to monitor plastic degradation by detecting the released acid groups.

2 mM of potassium phosphate buffer (pH 8) was mixed with 50 µM fluorescein. In a 96-well plate (BRANDPlates®, BRAND GmbH+CO KG, Germany), 10 µl of the enzyme solution was mixed with 190 µl of the fluorescein solution. The substrates were added in solid form as cut PU-foam squares of around 50 mg. The fluorescence after excitation at 498 nm was then monitored at 510 nm for a period of 4 h of incubation at 30°C in an Infinite M1000 Pro photometer (Tecan Austria GmbH, Austria) with measurements every 5 min. To minimize evaporation effects the 96-well plate was covered with a transparent lid and glued shut using evaporation safe tape.

#### **2.4.5.5. Impranil DLN-SD assay plates**

LB-agar was heated to a temperature of 60°C. 440 µl of Impranil DLN-SD was added to 50 ml of LB-agar and mixed. This mixture was poured into petri dishes and cooled down before use (Molitor *et al.*, 2020).

### 3. Results and Discussion

Besides all our efforts to recycle and reuse plastic materials, we still have not found a good solution for the end-of-life treatment of plastic waste. Most plastic tends to disintegrate physically (e.g. because of UV radiation and mechanical stress) over its lifespan and ends up as microplastic in our waters.

Enzymes might contribute to a good solution to containing this flood of plastic in the future. With plastic-active enzymes, it would be possible to degrade plastic into its building blocks under ambient conditions, as opposed to other recycling processes like pyrolysis. This way plastic concentrations could be reduced in, for example wastewater, before it gets disposed of into the ocean.

With plastic already having been present in the environment for decades, nature might have had time to adapt to this new carbon source. Yoshida *et al.* (2016) have found a bacterium in a PET recycling facility possessing two enzymes specialized in PET degradation. This finding indicates that there might be more, already adapted organisms out there.

However, finding new enzymes can be challenging. Sequence databases, e.g. provided by the National Center for Biotechnology Information (NCBI), contain millions of DNA and protein sequences, as well as environmental metagenomes from sites polluted by plastics. This is therefore a potential gold mine for not yet characterized biocatalysts. Using homology searches, enzymes with patterns homologous to sequences present in already known enzymes, such as the *ISPETase* can be found and identified as explained in 1.3.

However, this way of searching can only deliver enzyme candidates with motif patterns associated with polyester degradation that are already known (Mican *et al.*, 2024). To find truly novel enzymes with possibly new ways of degrading plastic, a functional screening is the best way (1.3). Taking samples from a heavily polluted site, such as the ocean floor right under plastic accumulation zones seems like a reasonable approach. Organisms in these areas might have already found a way to utilize the constant stream of carbon in an otherwise nutritionally scarce environment. With enough evolutionary pressure, new variants develop comparably quickly because of the short generation times of many microbes. In experimental settings using enrichment cultures, this sometimes only takes a few months (Cui *et al.*, 2008).

Another approach would be to combine two strategies. Taking samples and searching in these samples for already known homologue enzyme variants. If these enzyme variants can

be found it is a good hint that the sampled areas are a breeding ground for potentially novel degradation pathways. Due to horizontal gene transfer and evolutionary pressure, gene variants are shared in the microbial communities and can adapt to other niches and potentially similar carbon sources (Sobecky & Hazen, 2009).

In the following chapters, the approach of searching for new enzymes from the oceans, and searching for new enzymes in databases using homologies, are examined, and described.

### **3.1. Activity-based uncovering of novel polyesterases from marine samples**

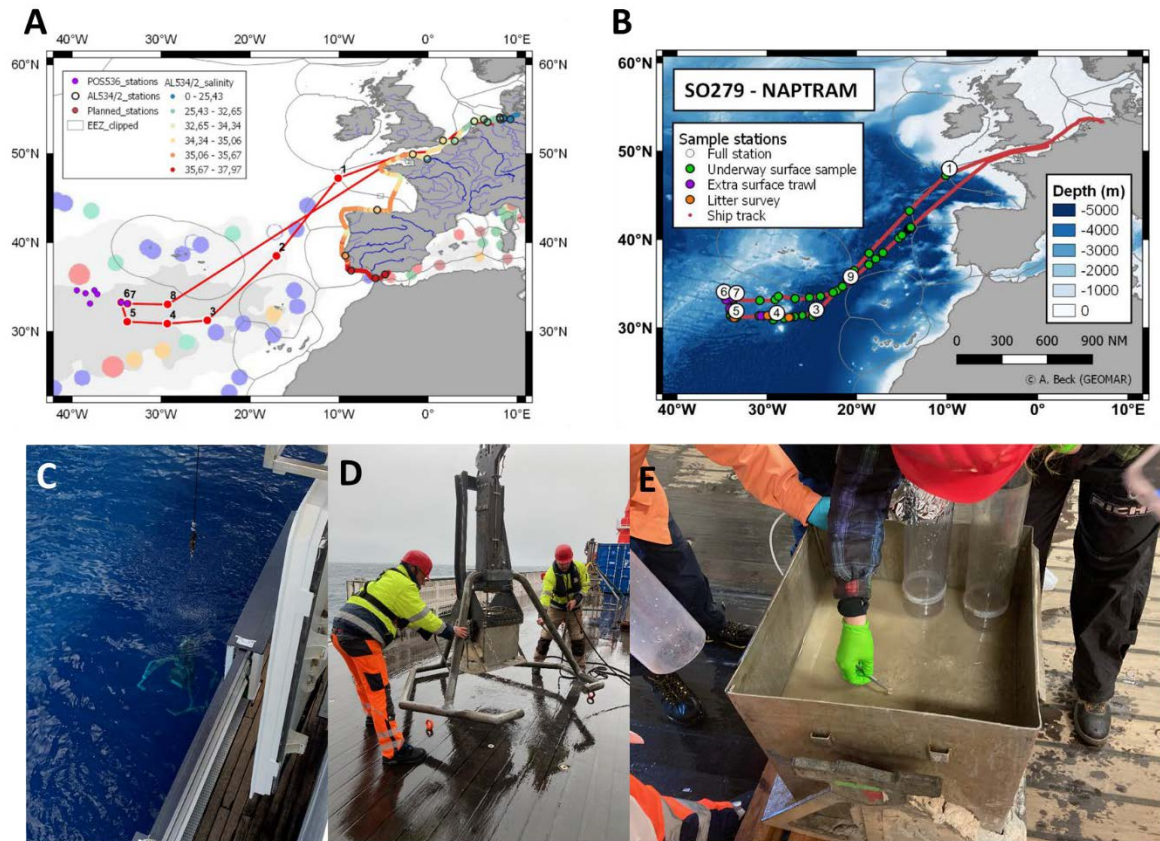
Sequence based screening has proven to be of high value for the identification of functional enzymes but is limited to the available set of sequence data (Mican *et al.*, 2024). Therefore, the exploitation of pristine habitats by metagenomics is needed to broaden the available sequence space. This needs to be supported by functional screening studies, to assign proper functions to the newly identified proteins.

Currently, publications on marine microbial communities describe microbial diversity in the water column above the sediment level, mainly at the ocean surface. Sediment is rarely sampled and analyzed. In addition, most publications discuss the Pacific Ocean; the Atlantic Ocean is not yet in the focus of interest. Therefore, more data on the bacterial composition of the sediment in the North Atlantic Ocean, especially regarding plastic degradation, is valuable for the global scientific community (Amaral-Zettler *et al.*, 2020; da Silva *et al.*, 2013). What is known is that plastic waste of all kinds accumulates in the ocean gyres (van Sebille *et al.*, 2015). Some plastic sinks due to biotic and abiotic factors (Amaral-Zettler *et al.*, 2021; Kaiser *et al.*, 2017). In these deep-sea environments nutrients are scarce. In their search for new carbon sources, organisms living in deep-sea sediment might find ways of transforming this new, not yet digestible, carbon source into food. These organisms can be harvested and investigated from deep-sea sediment samples and further analyzed in the laboratory.

#### **3.1.1. Analysis of environmental DNA from deep-sea sediment**

During the SO279 research cruise in 2020, titled NAPTRAM (Beck *et al.*, 2021), one of the main aims was to investigate the distribution of plastic in the water column of the north Atlantic Ocean. During this cruise, I gathered sediment samples from the deep-sea of the North Atlantic gyre (Figure 3).

Sediment was sampled at different locations and depths in the North Atlantic gyre, as well as in the Bay of Biscay (Figure 9). After sampling, the samples were immediately cooled at 4°C or frozen at -20°C to prevent degradation of the DNA or the death of the bacteria.



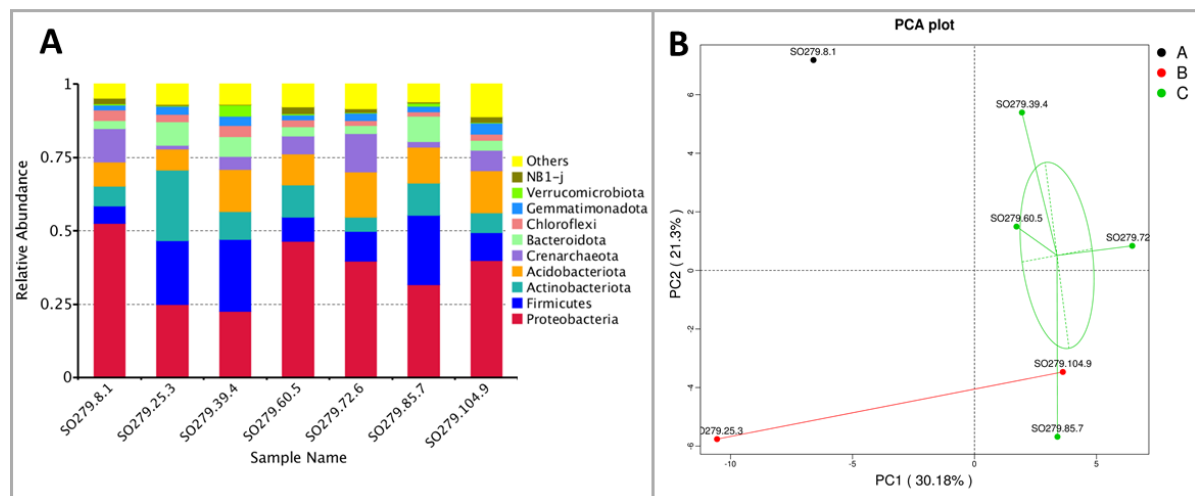
**Figure 9:** (A) Map of the planned sampling stations of the research cruise SO279 with the inner plastic accumulation zone shown in grey (Beck *et al.*, 2021). The inner plastic accumulation zones are defined according to Cozar *et al.* (2014). The red line indicates the proposed route of the expedition. The colorful dots indicate sampling stations of previous expeditions (B) Map of the actual sampling stations of the research cruise SO279 (Beck *et al.*, 2021). The red line indicates the cruise route. Sampling stations, two and eight, were left out due to bad weather conditions. Samples were taken from locations indicated by the white circles using a box core device. (C) Box Corer while resurfacing after sampling. (D) Box Corer on deck after sampling before opening. (E) Sampling of the Box Core on deck. Pictures taken in 2020 by Rebecka Molitor (C) and Mikael Kaandorp (D-E).

Woodall *et al.* (2014) sampled deep-sea sediment from the North Atlantic close to the continental shelf and analyzed them for microplastic particles. In 50 ml of sediment, the authors found around 10 pieces of polyester fibers, showing that polyester is present in the deep-sea sediment. In a recent pre-print publication, Materic *et al.* (2023) investigated the nanoplastic composition in the North Atlantic gyre in more detail. They searched for nanoplastic particles throughout the water column up to 30 m above the ocean floor but not in the sediment. Right above the ocean floor, the authors found mainly PET particles in concentrations of  $6.1 \pm 2.1$  ng/ml seawater. In addition, they discovered that the

nanoplastic concentrations were not evenly distributed, but that they were higher close to the continental shelf, as well as inside of the North Atlantic gyre. This led to the hypothesis that nanoplastic and microplastic particles accumulate on the ocean floor of the North Atlantic gyre. This indicates that PET particles are most probably present in the above-mentioned sediment samples of cruise SO279.

Back in the laboratory, the environmental DNA was extracted using the DNeasy PowerSoil Kit (Qiagen, Germany) according to the manufacturer's specifications. DNA amounts of around 1 µg per 250 mg of sediment were extracted. This low amount of DNA was likely due to the low density of actively growing microorganisms in the deep-sea sediment (Sogin *et al.*, 2006). While this low amount of DNA is sufficient for sequencing, it was not enough material for the construction of a metagenomic library.

As a start, I wanted to get insight into the bacterial composition as well as class relationships of the deep-sea sediment samples. To do this, the extracted DNA was analyzed via 16S sequencing (Figure 10).



**Figure 10: Relative abundance of bacterial phyla at the different stations in the marine sediment and the principal component analysis (PCA) of their class relationship.** (A) 16S ribosomal RNA analyzed and bioinformatically pictured by Novogene (Beijing, China). The sample name consists of the cruise name SO279, separated by dots, the box-core number according to the D-Ship data repository, and the sample station as the last number (Figure 9B). (B) The PCA analysis was done by Novogene with the shotgun sequencing taxonomy results. For visualization, the samples were sorted into groups A, B, and C and clustered according to the sample location proximity and sampling depth before PCA with PC1 and PC2 being the principal component 1 and 2. Group A is the out-group containing only sampling station 1, sampled on top of the continental ridge. Group B consists of the sample stations 3 and 9 which are outside the gyre. Group C includes all the sampling stations inside the gyre.

Comparing the composition of the samples to global beta-diversity (Zinger *et al.*, 2011) shows that the amount of proteobacteria at stations 1, 5, 6, and 9 is very similar to the



diversity in deep-sea benthic environments. The beta diversity of proteobacteria at stations 3, 4, and 7 seems to be more comparable to the beta diversity of coastal benthic communities, however. This is odd considering that the sampling depth of all samples was below 3,000 m but might be due to the limited knowledge of bacterial compositions in the deep sea. The firmicutes composition at stations 3, 4, and 7, also seems to be more like the beta diversity of coastal benthic environments rather than deep-sea benthic environments. In addition, the general amount of actinobacteria is similar to the global beta diversity of overall benthic environments, with no clear favorable environment recognizable. All in all, the microbial composition of the sediment samples seems to be comparable to global benthic communities, with no clear difference between coastal and deep-sea benthic environments.

To investigate if there might be a phyla composition in the sediment samples that has characteristics of bacterial compositions often found around certain plastics, I compared it to an experiment where the authors grew such communities in the deep-sea. A team of scientists planted different plastics and reference materials in the deep-sea of the North Atlantic close to the United States for a period of 719 days. Their goal was to evaluate the growing behavior of microbial communities on different plastic substrates (Agostini *et al.*, 2021). The microbial community that was found forming on polyester resembles the composition of the community in the sediment samples at stations 1, 5, 6, and 9. Mainly for the phyla of proteobacteria, actinobacteria, and bacteroidota the composition is similar. Only for stations 3, 4, and 7 the composition resembles the one found on gravel. This might indicate less plastic content of the sediment.

Due to the challenging nature of evaluating the plastic concentration in sediment samples, the plastic concentrations could not be determined in the laboratory. Hence, only comparisons to reported plastic concentrations found in literature can be made.

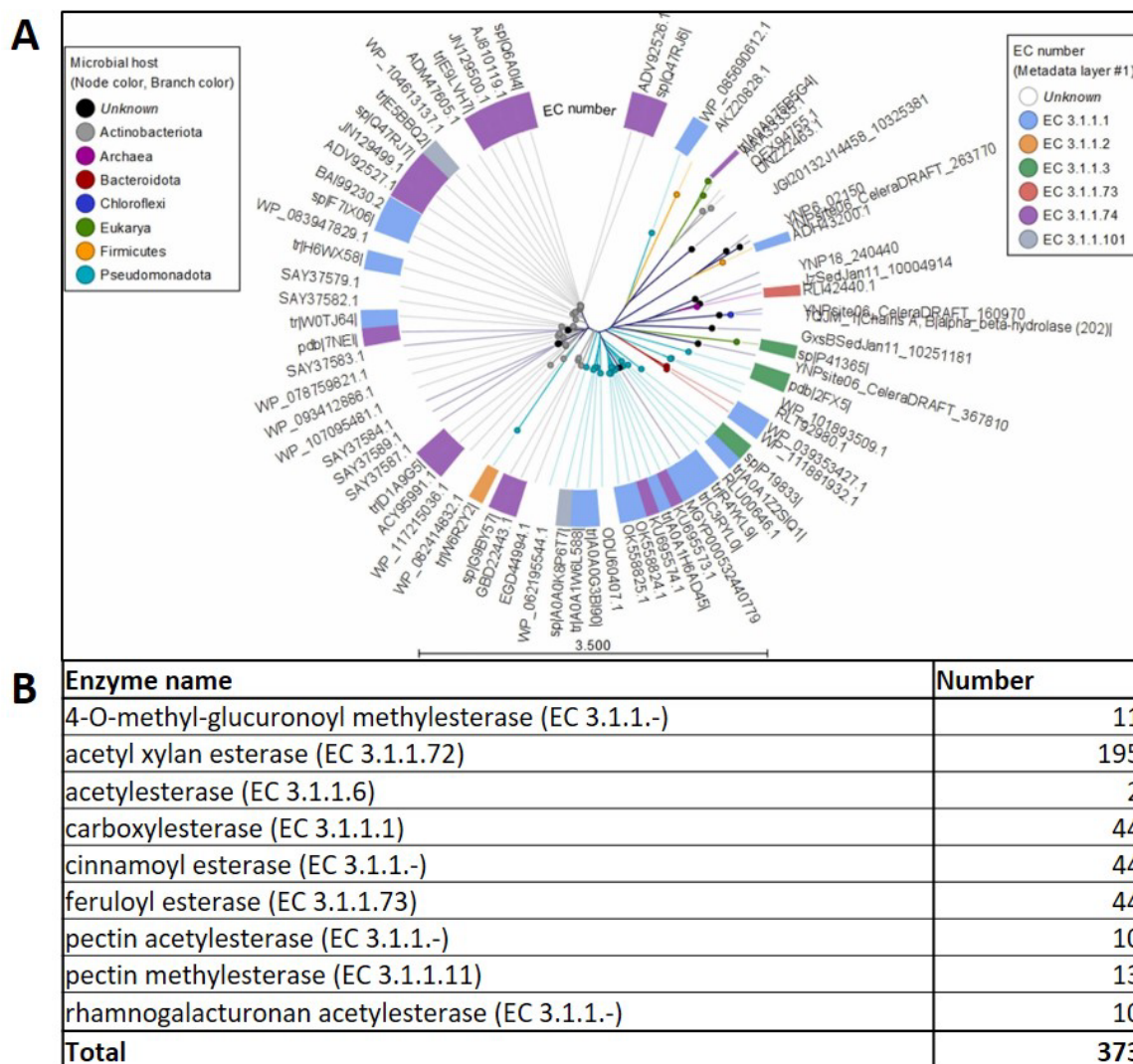
To shed more light on potential correlations of the different phyla in connection with the sampling depth and sampling site, a Principal Component Analysis (PCA) was requested with the same phyla present in Figure 10A. This analysis tries to simplify complex data by representing data consisting of many variables by a few important ones. The variables are compressed into the X and Y-axis principal components, with PC1 accounting for the most variation and PC2 for the second most variation (Figure 10B). The PCA analysis shows a clear clustering of the communities at stations 4, 5, and 6. These stations are close in

proximity to each other and located inside the North Atlantic gyre (Figure 3). However, judging by proximity, station 7 should also be very similar to stations 4, 5, and 6 but clusters further away in the PCA. Also, station 9 is according to the PCA more closely related to sampling stations 4, 5, and 6, even though it is just outside of the gyre and at a depth below 4,000 m. The considerable distance in the PCA analysis between the first sampling station and the rest of the sampling stations is to be expected, because of the physical distance between the sampling stations, but also due to the proximity of the sampling station to the English Channel, a highly frequented shipping route, as well as to Europe. As mentioned earlier, Zinger *et al.* (2011) found that bacterial communities in sediment differ depending on the proximity to coastal areas. The second visible differing point is sampling station 3. This station was the deepest at a depth of over 4,300 m and might therefore differ in phyla composition.

It is apparent that species that are often associated with plastic degradation are present in all samples. Since the most abundant plastic in the deep sea is polyester (PET) due to its high density, I look for enzymes that can degrade polyester. According to the PAZY (Buchholz *et al.*, 2022) database, most PET degrading enzymes identified so far originated in bacteria that belong to the proteobacteria, actinobacteriota, bacillota, bacteroidota, chloroflexota, or even archaea. All these families can be found in the samples. This raises the question of whether maybe relevant genes can be found in the sample set.

To evaluate this, a second analysis in the form of a shotgun sequencing was performed. This can give more insight into the presence of potential plastic degrading genes/sequences. Novogene identified 843,910 open reading frames (ORFs) with 257,632 genes containing a start and stop codon. The average length of a gene is 457.07 bp with a GC content of 53.02 %.

According to the PAZY database, most PET degrading enzymes belong to the esterases class (EC 3.1.1). Thomsen *et al.* (2023) have constructed a phylogenetic tree with all currently characterized PETases. In the tree (Figure 11A) the different genes with the EC numbers are shown in colors including their host organisms.



**Figure 11: (A) Phylogenetic tree of all currently known and characterized PETases (Thomsen *et al.* (2023) published under creative commons license CC BY) and (B) table of esterases identified in the sediment samples. (A) shows a phylogenetic tree with the outer colors defining the EC classifications and the node colors defining the host phyla (Thomsen *et al.*, 2023). (B) shows a table of all found and identified esterases in all samples and sampling stations of the research cruise SO279.**

Most characterized enzymes were assigned to the class of carboxylesterases (EC 3.1.1.1) and were found in the microbial host *Proteobacteria*. Accordingly, I searched the annotated genes in my sediment samples for enzymes that belong to this class since they could potentially be PET degraders. In the annotated genes, 373 genes belonged to the esterases (Figure 11B). According to PAZY, PET degrading enzymes mainly belong to the carboxyl esterases (EC 3.1.1.1) or the cutinases (EC 3.1.1.74). Interestingly, 44 feruloyl esterases (EC 3.1.1.73) were present in the samples. This seems particularly interesting since only recently a paper was published finding the first PETase from an archaeon, which happens to be a feruloyl esterase (Perez-Garcia *et al.*, 2023). This enzyme is also remarkable since it

is the first PETase with a unique lid structure supporting the PET degradation (Perez-Garcia *et al.*, 2023). This shows that the sampling site diversity has potential in harboring enzymes that are potentially degrading PET.

However, sequence annotations alone could not provide enough information to determine if there is a potential polyester hydrolase candidate. To look further into this and to potentially identify candidates over their homologue sequences, Pablo Perez-Garcia of the University of Hamburg used a Hidden Markov Model (HMM) to identify sequences with potential for polyester hydrolysis. He found 41 potential PET degrading enzymes mainly belonging to the esterases (EC 3.1.1.1). However, those sequences were already known, so no new genes were identified in this data set.

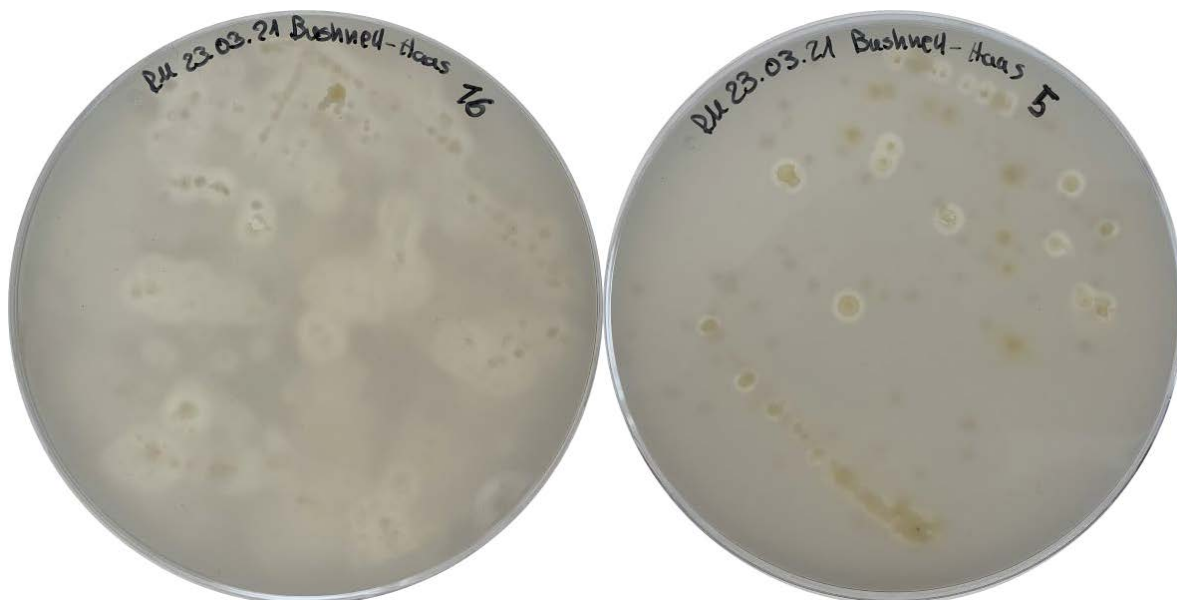
Since an HMM can only find sequences that are homologue to already known pathways, we require another method that can identify novel pathways of polyester degradation.

All in all, this analysis shows that there lies potential at the bottom of the ocean. However, future investigations are necessary to harvest the full potential of this breeding ground for novel enzymes.

### **3.1.2. Enrichment culturing on polyester substrates as sole carbon source**

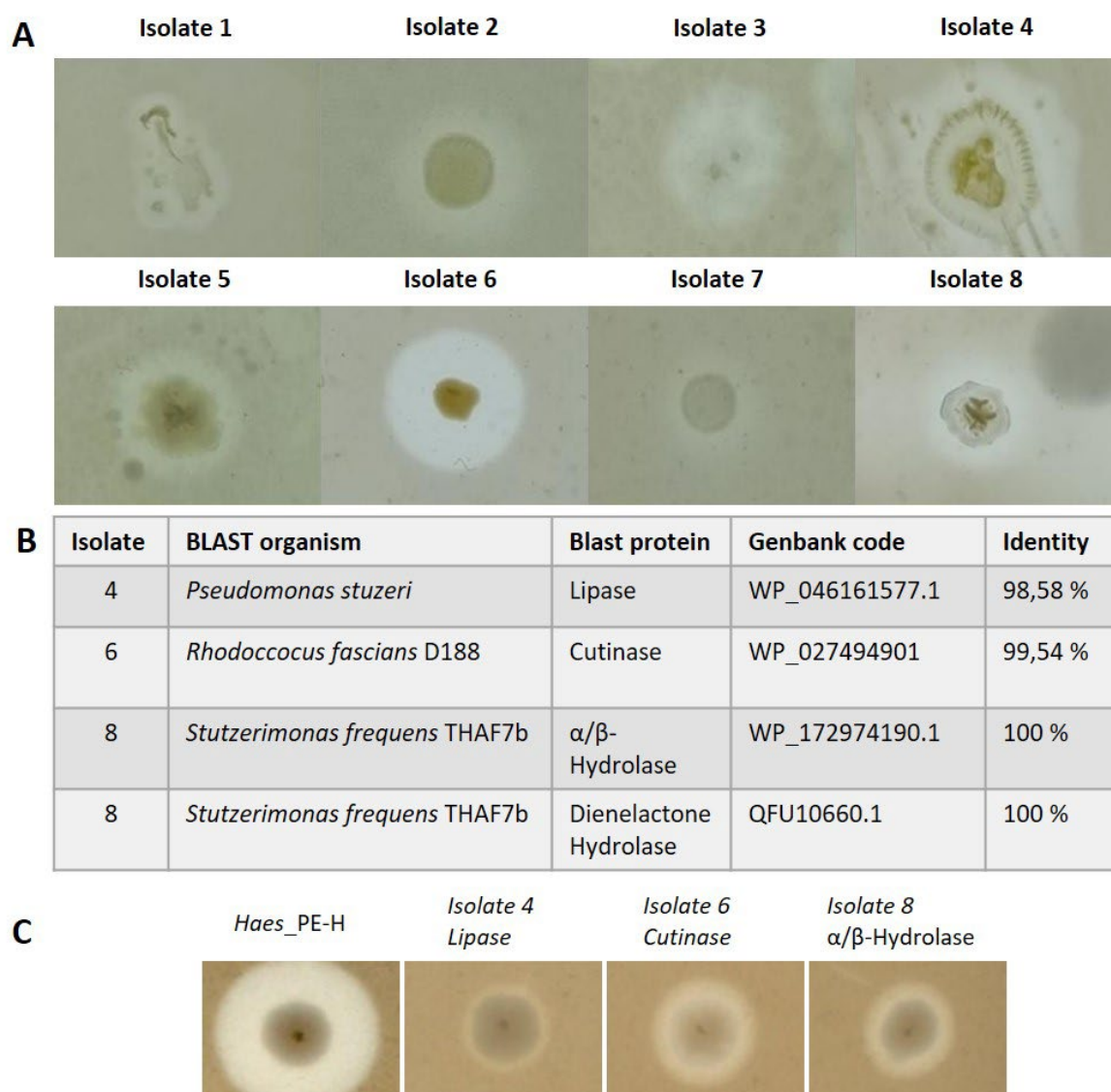
Another way of searching for polyester degradation activity, without the need for a lot of initial biomasses, would be to enrich the existing plastic degrading bacteria on polyester. This way overlooked bacteria can still be identified over their activity. Although, non-cultivable and slowly growing organism will be lost this way, enrichment cultivation is a powerful tool to increase the chances for positive hits (Madhuri *et al.*, 2019). I conducted two rounds of enrichment cultivations (chapter 2.3.3), each for one month, with Impranil DLN-SD as the only carbon source. Since the pressure of the deep sea cannot be reproduced in laboratory settings, barophilic bacteria are excluded from the start. The cultures were inoculated with the sediment and incubated at temperatures between 10 and 20°C to speed up the growing process. Given the results of the community analysis, stations 3-9 were pooled to reduce the workload. Samples from station 1 were treated individually, since it showed significant differences to the other stations. After one month of incubation, and significant visible turbidity of the growth medium, 1 ml of bacterial suspension was used to inoculate into fresh media and incubated for another month. To isolate organisms capable of polyester hydrolysis, an aliquot of each enrichment culture was plated on agar

plates containing Impranil DLN-SD as sole carbon source for halo formation analysis. The halo formation assay showed positive hits (Figure 12). This proves that there are polyester hydrolases present in deep-sea sediment.



**Figure 12: Impranil DLN-SD agar plates with halo formation of the enrichment cultures.** Enrichment was done over the course of two months at 10°C in Bushnell-Haas medium with Impranil DLN-SD as the only carbon source and agitation of 50 RPM. After two consecutive rounds of enrichment cultures, growing for one month each. 100 µl of the turbid solution was inoculated onto Bushnell-Haas agar plates containing Impranil DLN-SD and incubated at room temperature for one week.

In an associated master thesis, Tobias Horbach (2023) afterwards identified eight organisms using partial 16S-rDNA sequencing, that were able to degrade plastic on indicator plates (Figure 13A).



**Figure 13: Organism identified by Horbach (2023) Modified according to Horbach (2023).** (A) The organisms were incubated for 2 weeks at room temperature on indicator plates with Impranil DLN-SD. (B) Identified organism with putative PE-H homologue enzymes and the annotation of the closest hit according to BLAST, GenBank identifier and percentage identity of the closest hit with the respective protein sequence obtained from the sequenced genome of the isolates. (C) Homologous expression of the putative PE-H homologues in the host organism *E. coli* LOBSTR on indicator plates with Impranil DLN-SD.

The organisms were identified using NCBI as members of *Pseudomonas*, *Stutzerimonas* as well as *Rhodococcus* (Figure 13B). He then looked for the whole genome sequences of those species. Using the HMM from Pablo Perez-Garcia of the University of Hamburg with known sequences of polyester hydrolases, he was then able to identify three novel polyester hydrolases from organisms not yet known for polyester hydrolysis, such as *Rhodococcus* sp. or *Pseudomonas stutzeri*. Cloning and expression of these genes in *E. coli* confirmed polyesterase activity via indicator plates with Impranil DLN-SD (Figure 13C).

These results are interesting when comparing them to the previously mentioned identification using the HMM from the University of Hamburg on the eDNA sequencing by Novogene. These specific genes were not found in the eDNA shotgun sequencing. However, around 38 different *Rhodococcus sp.* species were found in the shotgun and 16S sequencing. This might mainly be due to the newly found enzyme from *Rhodococcus sp.* being smaller than the known PETases used in the Hamburg HMM and therefore being overlooked by the HMM.

In conclusion, this indicates that using only tools like HMM to identify new sequences might limit the amount and quality of novel found sequences. Going different paths to metagenome sequencing and subsequent HMM like enrichment cultures, can yield sufficient new sequences for enzyme discovery.

### 3.2. Sequence-based compiling of a set of homologous polyester hydrolases for a comparative characterization

Finding new sources for enzymes from activity-based screenings of strain libraries or the metagenomic approach are promising techniques. However, they are very time-consuming and therefore limited. All over the world, scientists have been sequencing metagenomic samples. Those sequences are published in repositories like the database NCBI. With interesting enzymes as a template, it is easy and quick to search for homologues. Compared to one single metagenomic library, these databases harbor millions of sequences. Sets of homologue enzymes can then be characterized in a laboratory setting to see if they show higher activities compared to the homologue. Homologue enzymes might then be promising new targets for industrial applications.

Already characterized enzymes may constitute a good starting point to search for interesting new strains. Haernvall *et al.* (2017a), Haernvall *et al.* (2017b), and Bollinger *et al.* (2020c) investigated polyester hydrolyzing enzymes from a nearly unexplored lineage of marine bacteria: the *Halopseudomonas pertucinogena* lineage formerly known as *Pseudomonas pertucinogena* (Rudra & Gupta, 2021). They showed after genomic analysis, genes that could produce interesting biomolecules for industrial applications. As such, especially the polyester hydrolases seemed promising. All available proteomes of *Halopseudomonas* spp. were then further analyzed for homologue enzymes to the polyester hydrolase from *H. aestusnigri* (Bollinger *et al.*, 2020c). All strains except for *H. xiamenensis* and *H. profundus* did possess a homologue enzyme with high sequence identities (Table 6) that were subsequently cloned and expressed in the heterologous host organism *E. coli* and then further characterized. However, due to halo formation of *H. xiamenensis* on the indicator plates it is reasonable to assume that this organism evolved a different polyester hydrolyzing enzyme variant, that was not further addressed in this work and might be interesting for subsequent identification.

The homologies and general relationship of the PE-Hs can be seen in Figure 14. Figure 14B shows that all the amino acid sequences of the homologues are identical up to 94.08 % between *Haes*\_PE-H and *Hpac*\_PE-H. This underlines the close genetic relationship of the *Halopseudomonas* family. Having such a conserved gene sequence might also indicate an evolutionary pressure on keeping this enzyme variant. In Figure 14A this relationship is shown in the Neighbor-joining tree, indicating which enzymes are more closely related.

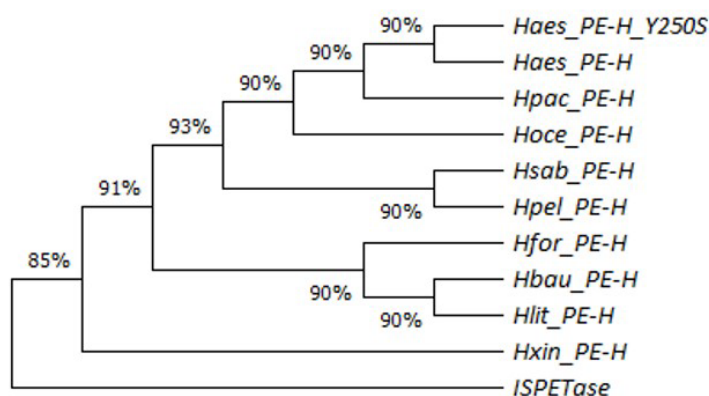


Here some enzymes show closer relationships than others based on their amino acid sequences and conserved domains according to Clustal Omega.

**Table 6:** List of all enzymes compared in this thesis with PDB numbers, NCBI accession numbers and first publication.

Enzyme name	Organism of origin	PDB/AlphaFold Number	NCBI Blast	First proven activity
ISPETase	<i>Ideonella sakaiensis</i>	6ANE	<a href="#">WP_054022242.1</a>	(Yoshida et al., 2016)
Haes_PE-H	<i>Halopseudomonas aestusnigri</i>	6SBN	<a href="#">WP_088276085.1</a>	(Bollinger et al., 2020c)
Haes_PE-H_Y250S	<i>Halopseudomonas aestusnigri</i>	6SCD		(Bollinger et al., 2020c)
Hoce_PE-H	<i>Halopseudomonas oceani</i>	A0A2P4EZRO	<a href="#">WP_170062967.1</a>	this work
Hsab_PE-H	<i>Halopseudomonas sabulinigri</i>	A0A1H1UUH5	<a href="#">WP_231701947.1</a>	this work
Hbau_PE-H	<i>Halopseudomonas bauzanensis</i>	8AIT	<a href="#">WP_036989706.1</a>	(Avilan et al., 2023)
Hpac_PE-H	<i>Halopseudomonas pachastrella</i>	A0A1S8DKK6	<a href="#">WP_083724990.1</a>	this work
Hpel_PE-H	<i>Halopseudomonas pelagia</i>	A0A2A4AWW4	<a href="#">ANP21910.1</a>	(Haernvall et al., 2017a)
Hlit_PE-H	<i>Halopseudomonas litoralis</i>	A0A1H1RJ19	<a href="#">WP_090272969.1</a>	this work
Hxin_PE-H	<i>Halopseudomonas xinjiangensis</i>	A0A1H1PFY8	<a href="#">WP_172829808.1</a>	this work
Hfor_PE-H	<i>Halopseudomonas formosensis</i>	A0A1I6BKY1	<a href="#">WP_090538641.1</a>	(de Witt et al., 2023)

**A**



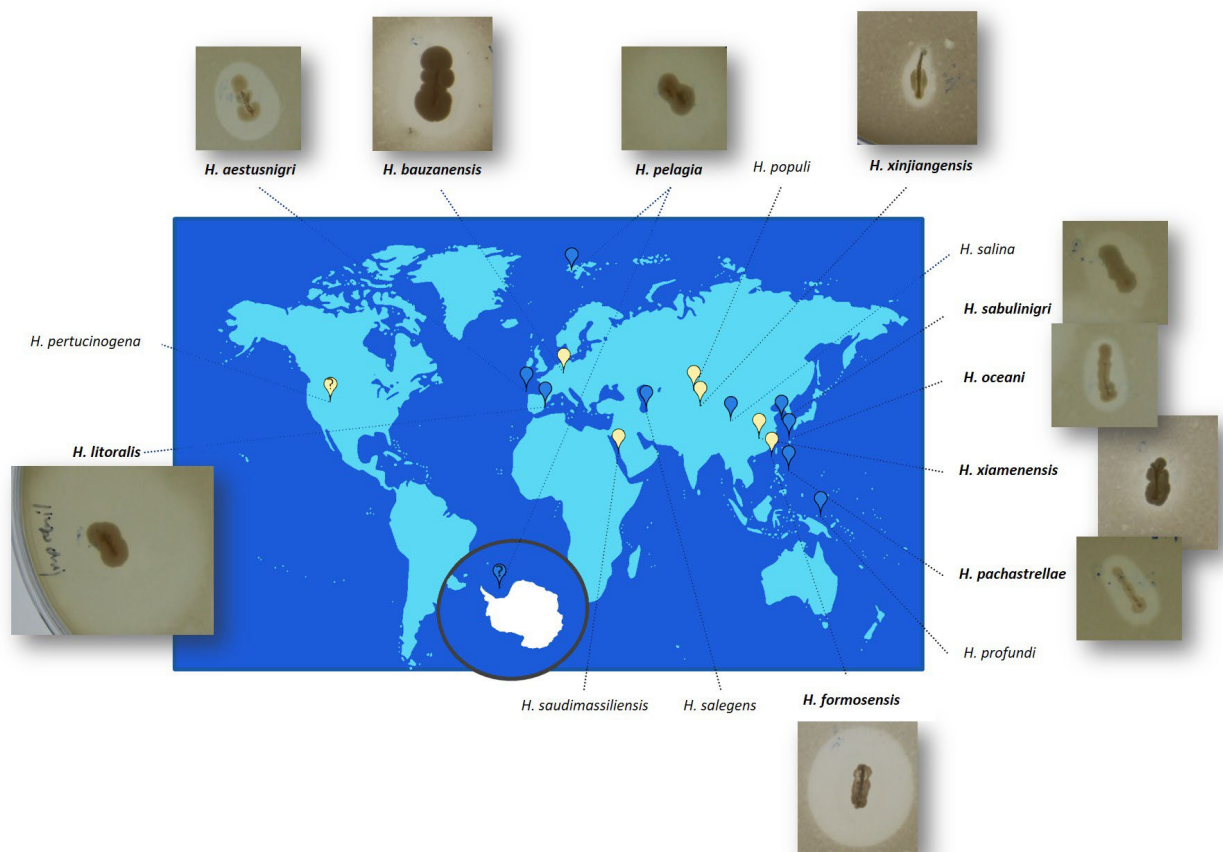
**B**

ISPETase	100.00	47.55	46.34	44.56	47.39	45.10	47.90	47.55	47.55	49.12	49.12
Hxin_PE-H	47.55	100.00	68.65	70.87	71.19	73.75	73.14	72.76	72.70	73.18	72.52
Hpel_PE-H	46.34	68.65	100.00	74.92	68.28	72.28	70.63	70.96	70.07	75.17	74.17
Hsab_PE-H	44.56	70.87	74.92	100.00	75.91	76.41	76.38	76.08	74.75	74.09	72.43
Hoce_PE-H	47.39	71.19	68.28	75.91	100.00	87.13	91.75	91.75	78.62	75.50	73.84
Hpac_PE-H	45.10	73.75	72.28	76.41	87.13	100.00	93.75	94.08	79.14	78.33	76.33
Haes_PE-H_Y250S	47.90	73.14	70.63	76.38	91.75	93.75	100.00	99.67	78.29	77.33	76.00
Haes_PE-H	47.55	72.76	70.96	76.08	91.75	94.08	99.67	100.00	78.48	77.67	76.33
Hfor_PE-H	47.55	72.70	70.07	74.75	78.62	79.14	78.29	78.48	100.00	83.11	82.45
Hbau_PE-H	49.12	73.18	75.17	74.09	75.50	78.33	77.33	77.67	83.11	100.00	88.41
Hlit_PE-H	49.12	72.52	74.17	72.43	73.84	76.33	76.00	76.33	82.45	88.41	100.00

**Figure 14:** (A) Neighbor-joining tree with distances indicated as percentage and (B) percent identity matrix for the *Halopseudomonas* PE-H homologues. ISPETase is used as an outgroup. The names of the enzymes are comprised of the

abbreviated organism name as the first four letters together with the abbreviation of polyester hydrolase (PE-H) (Table 6). Mutations are marked as an addition at the end.

We analyzed the activity of all eight *Halopseudomonas* strains that were retrievable from DSMZ (German Collection of Microorganisms and Cell Cultures GmbH, Leibniz Institute, Germany) on Impranil DLN-SD agar plates in relation to the activity of *H. aestusnigri* that was described in Bollinger *et al.* (2020c). Additionally, a *H. formosensis* isolate from a compost in Würselen/Germany (de Witt *et al.*, 2023) was included into the study. Most of them showed polyester hydrolase activity indicated by halo formation upon the degradation of the polyester (Figure 15). It is noticeable that all strains seem to be producing a polyester hydrolase, and we found varying degrees of polyesterase activity: especially the strain *H. litoralis* showed an enormous halo formation (Figure 15). The screening method and part of the results were published in Molitor *et al.* (2020).



**Figure 15: Distributional map of the *Halopseudomonas* clade.** Modified according to Bollinger *et al.* (2020b). The organism highlighted in bold were ordered from the DSMZ and tested for polyester hydrolysis activity. The strains were inoculated on LB-agar-plates containing Impranil DLN-SD and incubated at 25°C for 24 h.

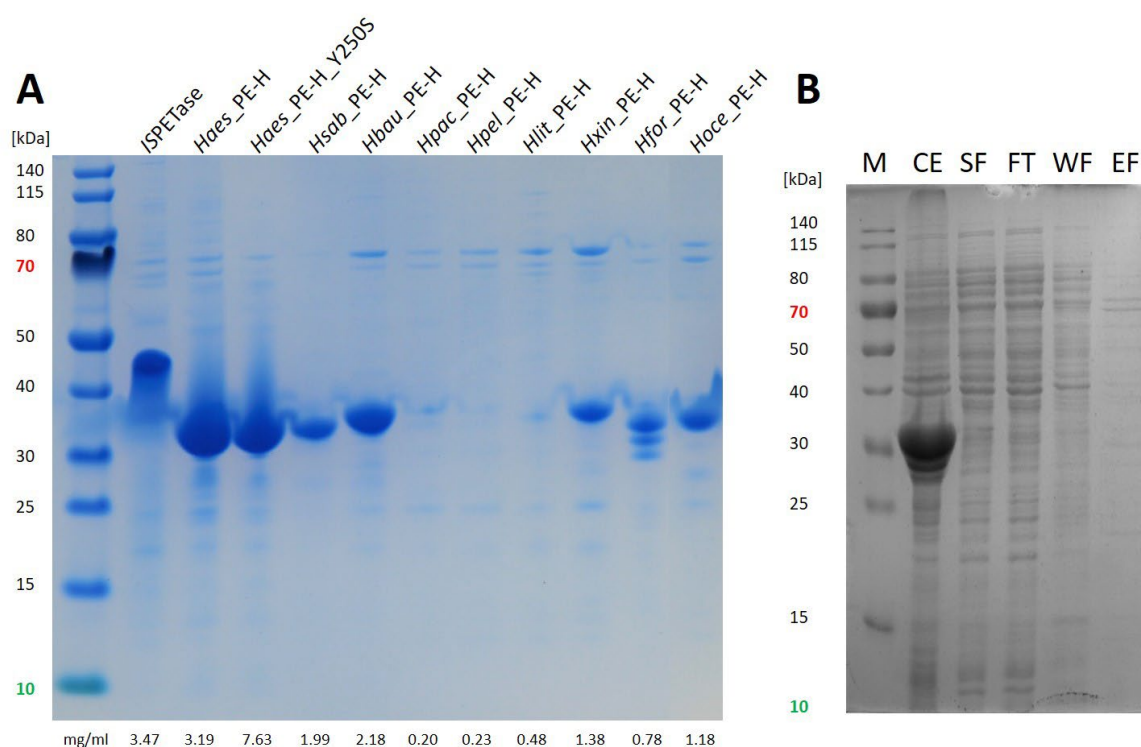
Based on these results, a set of homologues polyesterases should be established for comparative evaluation experiments. Therefore, *Haes*\_PE-H homologues from the *H. pertucinogena* clade that were available at the DSMZ (German Collection of Microorganisms and Cell Cultures GmbH, Leibniz Institute, Germany) were cloned and transferred into the host organism *E. coli* for heterologous expression and purification. The enzymes were then characterized, and the activities compared to each other, as well as to literature.

In this study, the enzymes were first characterized according to their efficiency including how easily they are expressible and if purification is possible, as well as if the enzymes need any cofactors or are inhibited. In the second part, the stability was evaluated by checking temperature and pH related stability. Lastly, the specific and unspecific activities towards polyester was assessed. Efficiency on how good an enzyme is expressible as well as purified is a principal factor for the usage of this enzyme.

### **3.2.1. Expression and purification of *Halopseudomonas* PE-Hs**

The identified homologues of *Haes*\_PE-H (Figure 15) were expressed and purified. Even though the enzymes are highly similar with amino acid identities up to 94.08 % (Figure 14), the expression behavior varied massively between the enzymes, which required the development of different production protocols for individual enzymes. The enzymes *Hsab*\_PE-H, *Hbau*\_PE-H, *Hxin*\_PE-H, *Hfor*\_PE-H and *Hoce*\_PE-H were expressed in soluble form and therefore obtained in high yields (Figure 16A).

Some enzymes however, like *H. pelagia* PE-H (*Hpel*\_PE-H, syn. PpelaLip (Haernvall *et al.*, 2017a)), *H. litoralis* PE-H (*Hlit*\_PE-H), and *H. pachastrellae* (*Hpac*\_PE-H) were expressible but mainly formed insoluble inclusion bodies (Figure 16B).



**Figure 16: (A) Coomassie Blue stained SDS-gel of all expressed enzymes with measured concentrations after purification from the soluble fraction of the *E. coli* cell lysate.** 2.5  $\mu$ l of each enzyme was applied. **(B) SDS-gel of the purification of *Hpel*\_PE-H.** The SDS-PAGE of *Hlit*\_PE-H showed a similar pattern and is therefore not shown. Lanes contain the marker (M), cell extract (CE), the soluble fraction (SF), flow through (FT), wash fraction (WF), and the elution fraction (EF). 2.5  $\mu$ l of each fraction was applied.

Those enzymes were not correctly expressed and folded and were therefore only purified in low quantities. Attempts were made in an associated bachelor thesis, by Lisa Hoppe (2020) to refold *Hlit*\_PE-H and *Hpel*\_PE-H according to a protocol published by Haernvall *et al.* (2017a) for *Hpel*\_PE-H. This did not result in more soluble protein (Figure 16B). However, a low amount of *Hlit*\_PE-H, as well as *Hpel*\_PE-H was measurable and visible in the SDS-gel after purification from the soluble fraction of *E. coli* expression strains. Despite the low yields, activity confirmation for *Hlit*\_PE-H and *Hpac*\_PE-H using *p*NPH was successful, hence active proteins could be obtained for both enzymes. *Hpel*\_PE-H was not produced in quantities usable in the assays and was therefore not further characterized.

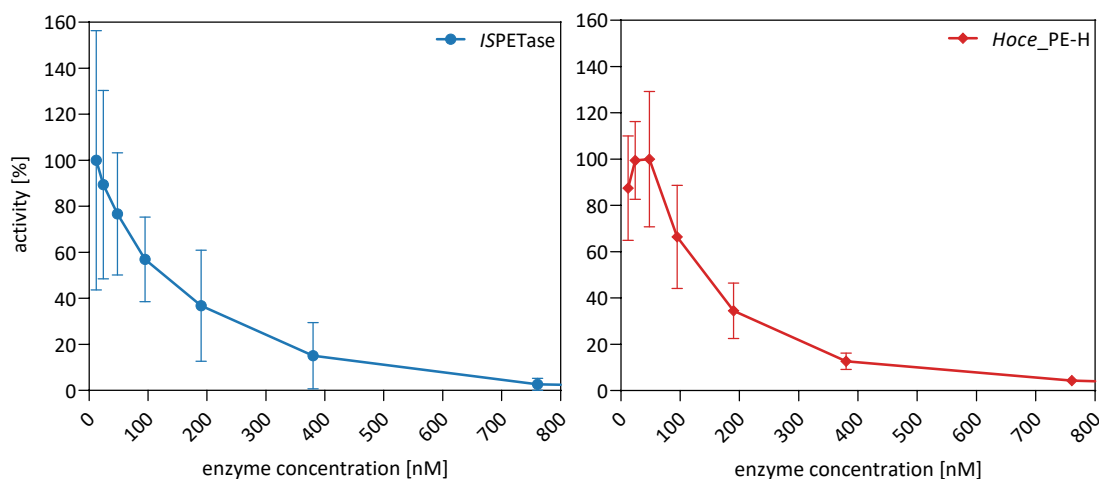
After an optimization step, most of the enzymes were expressed and purified with concentrations exceeding 0.1 mg/ml with most enzymes reaching concentrations of more than 1 mg/ml. Besides this high concentration of purified enzyme there were also barely any impurities with most enzymes as seen on the SDS-gel (Figure 16A).

Some impurities visible in Figure 16A around the size of 70 kDa were always present, however did not interfere with measurements due to the low concentrations.

To exclude the overestimation of enzyme concentrations due to a suboptimal ratio of target enzyme and contaminating proteins in these cases, I based the comparative characterization on relative activities related to the optimal conditions, rather than relying on the specific activities with *p*NPH as the substrate.

### 3.2.2. Concentration dependent inhibition of polyester hydrolases

When testing the activity of the enzymes after purification on easy substrates like *p*NPH, it was noticeable that higher concentration of enzyme did not yield higher activities. All experiments showed the same relationship for the investigated enzymes, with activity inhibition at high enzyme concentrations. In Figure 17 the approximate amount of enzyme for maximum enzyme activity is shown as an example for *ISPETase* and *Hoce*\_PE-H. With dilution of the enzyme solution, the activity rises until a concentration of approximately 100-50 nM is reached where most enzymes have the highest activity. At higher concentration, the activity decreased again.



**Figure 17: Relationship of enzyme concentration and enzyme activity.** Activity of two example enzymes of the characterized enzyme set on the substrate *p*NPH at 30°C for 10 min with varying enzyme concentration. Enzyme activity is relative to the highest activity of every enzyme. The graph of the residual enzymes of the set can be found in the appendix.

Avilan *et al.* (2023) noted in their publication, that interfacial biocatalysts active on polyesters show an interesting relationship between enzyme amount and activity. They saw that the activity of *ISPETase* was not following the classic Michaelis-Menten kinetic, a

hyperbolic relationship, but rather increases with less used enzyme until the point of highest activity was reached, then decreased again. In this paper, the authors also discussed the *Hbau*\_PE-H (PbauzCut, Avilan *et al.* (2023)) which is showing this behavior. This behavior has already been seen by other interfacial active enzymes (Baath *et al.*, 2021; Mukai *et al.*, 1993; Scandola *et al.*, 1998; Wei *et al.*, 2014).

Interfacial active enzymes with substrates containing less surface compared to soluble substrates, face the issue that the limited space on the surface is at some point saturated with enzymes. After this point, excessive enzymes might interfere with the sitting position of the enzymes on the substrate, changing the orientation of the sitting enzymes. Without the right orientation, these enzymes lose their ability to hydrolyze the substrate. Having less enzyme in the mix helps the enzymes to not interfere with each other's position, rendering the hydrolysis more efficient (Avilan *et al.*, 2023; Scandola *et al.*, 1998). However, this cannot completely explain this behavior, since *p*NPH is a water-soluble substrate. Therefore, no such behavior should be seen here. However, Avilan *et al.* (2023) also stated that different factors come into play for different enzymes, and that every enzyme reacts differently under different conditions. They state that dynamic properties of the enzymes, like regions around the active center, thermostability, and the solution conditions like pH and other additives, might also influence the concentration-dependent inhibition.

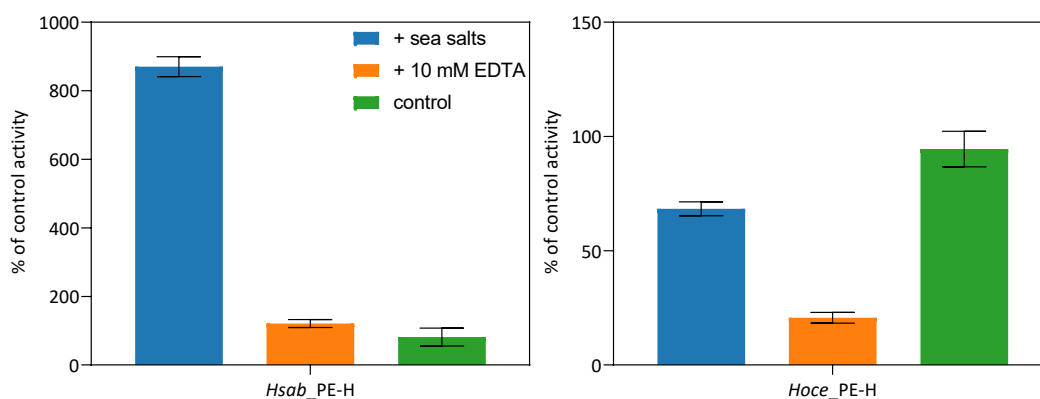
According to the results obtained here, the subsequent experiments were conducted applying enzyme concentrations of 50 nM with an exception for the measurement done in the UPLC, where concentrations of 1500 nM were applied due to long incubation times and the addition of DMSO which can stop the inhibition according to Avilan *et al.* (2023).

### 3.2.3. Ion dependency of PE-H activity

Enzyme activity is dependent on a multitude of factors. Among others, some enzymes are dependent on additives or cofactors for their activities. These additives can have stabilizing as well as destabilizing effects and therefore need to be monitored for efficient enzymatic activity (Bisswanger, 2014).

After defining the correct enzyme concentration for the assays, the enzymes were tested for dependency on ionic cofactors such as components present in seawater like calcium, sodium, or potassium. Since some enzymes like *Hoce*\_PE-H, *Hpel*\_PE-H, *Haes*\_PE-H, and *Hsab*\_PE-H were found in association with the ocean, those seawater components seem to

be the most likely cofactors. For this, the enzyme activity was tested with the substrate *p*NPB in the presence of the complex forming EDTA or sea salt in concentrations found in the oceans (artificial sea water medium (Smith & Ferrer-Gonzalez, 2018)). With 10 mM EDTA most enzymes from the set showed unchanged activity compared to the control group (data not shown). Only *Hsab*\_PE-H as well as *Hoce*\_PE-H are inactive or show significantly reduced activity (Figure 18).



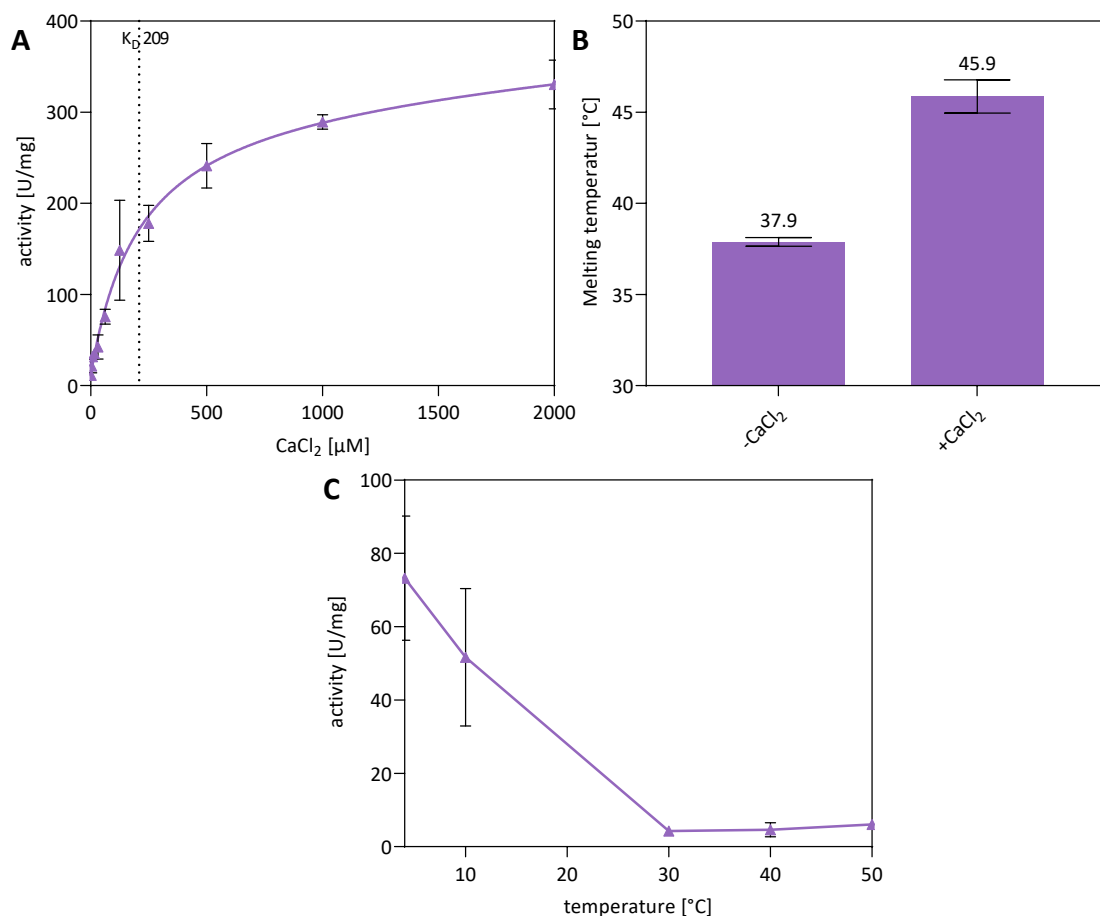
**Figure 18: pNPB assay of the enzymes *Hsab*\_PE-H and *Hoce*\_PE-H in the presence of 10 mM EDTA or puffer with average conditions of sea salt.** The enzyme activities were measured in 100 mM potassium phosphate buffer at 30°C for 10 min. Activities are calculated relative to the activity of the control without the addition of EDTA or sea salts. The activity of *Hsab*\_PE-H in the control was not measurable and therefore inactive.

In contrast to *Hsab*\_PE-H, *Hoce*\_PE-H does have activity in potassium phosphate buffer without EDTA. This might indicate an effect of certain salts on the activity of *Hoce*\_PE-H, but that very low concentrations are sufficient. *H. oceani* was found in deep-sea samples with normal oceanic salt concentrations (Wang & Sun, 2016). However, also other *Halopseudomonads* were found in the ocean like *H. pelagia* that do not show this behavior. With salts always available in the bacteria's natural environment, they might be utilized for stabilizing the enzymes' three-dimensional structure. However, since the activity of *Hoce*\_PE-H was not influenced by the addition of oceanic salts compared to 100 mM phosphate buffer conditions, no further checks for the exact cofactor were made.

The polyester hydrolase *Hsab*\_PE-H is from the organism *H. sabulinigri*, isolated from beach sand on the island of Jeju in South Korea (Kim *et al.*, 2009). Since *Hsab*\_PE-H was not active with 100 mM phosphate buffer concentrations, but only with the addition of marine salts, more testing was conducted. In an associated bachelor thesis, Laura Valvason (2020) tested a variety of different salts present in marine environments and found that the addition of



$\text{Ca}^{2+}$  leads to increased activity. Further testing of *Hsab*\_PE-H showed that its half-maximal activity was reached with the addition of around 209  $\mu\text{M}$   $\text{CaCl}_2$  (Figure 19A).



**Figure 19: Calcium dependency of *Hsab*\_PE-H (A)** *p*NPH assay in Tris-buffer with increasing  $\text{CaCl}_2$  concentrations. Without  $\text{CaCl}_2$  there is barely any activity with the substrate *p*NPH. With the addition of  $\text{CaCl}_2$  to the solution, the activity exponentially grows with  $\text{CaCl}_2$  concentration until a plateau at around 1 mM of  $\text{CaCl}_2$  concentration was reached. The  $K_D$  was calculated the same as the  $K_M$  in a Michaels-Menten Kinetic would be calculated. It describes the amount of calcium where  $V_{\max}/2$  is reached. The diagram **(B)** shows the changes in melting temperature measured by nanoDSF (NanoTemper, Germany) that are noticeable with or without addition of  $\text{CaCl}_2$ . The melting temperature of *Hsab*\_PE-H in phosphate-buffer changes significantly between the addition of  $\text{CaCl}_2$  (+ $\text{CaCl}_2$ ) or without  $\text{CaCl}_2$  (- $\text{CaCl}_2$ ) at various temperatures with the lowest being  $4^{\circ}\text{C}$ . **(C)** *Hsab*\_PE-H activity on the substrate *p*NPH without  $\text{CaCl}_2$  addition. The enzyme activity was measured in 100 mM potassium phosphate buffer with 100 mM NaCl for 3-10 min at different temperatures.

Considering the calcium phosphate precipitation of  $\text{CaCl}_2$  in phosphate buffer, using a phosphate-buffer with *Hsab*\_PE-H might not be as efficient as using a Tris-buffer. However, since the aim was to look at distinctive characteristics of the enzymes at different temperatures, using a phosphate-buffer is more advantageous, since it is temperature independent. Indeed, Tris-buffer appeared less advantageous for the thermostability



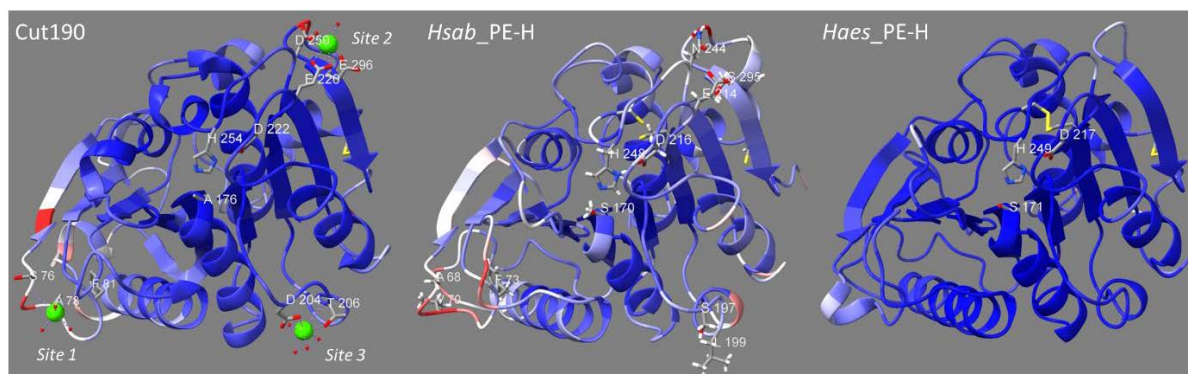
measurements of *Hsab*\_PE-H (data not shown). This might be due to pH changes in Tris-buffer with a raising temperature. In terms of initial activity of the *Hsab*\_PE-H, the amount of  $\text{Ca}^{2+}$  needed for activity is low enough for the  $\text{Ca}^{2+}$  to stay soluble in the phosphate buffer. This was confirmed by detecting no changes in activity in phosphate buffer and tris-buffer, each 209  $\mu\text{M}$  of  $\text{CaCl}_2$ , for *Hsab*\_PE-H.

This calcium dependency has been described in other polyester degrading cutinase-like enzymes. Liu *et al.* (2022) characterized an enzyme from the deep-sea *Nocardiopsaceae* family, showing calcium activation. With calcium the enzyme performed twice as well. However, it did have activity without calcium, as opposed to *Hsab*\_PE-H which shows almost no activity without calcium. In literature a few cutinase like enzymes with polyester hydrolase activity are known to have increased hydrolyzation ability with the addition of  $\text{Ca}^{2+}$ . Most of them are not completely dependent on ambient temperatures compared to the addition of  $\text{Ca}^{2+}$ . One of those enzymes is PHL7. Richter *et al.* (2023) saw an improvement in thermostability of the polyester hydrolase PHL7 by up to 7°C after the addition of  $\text{Ca}^{2+}$  or  $\text{Mg}^{2+}$ . The PET-degrading cutinase like enzyme Cut190 has an up to 16°C higher thermostability with up to 300 mM  $\text{Ca}^{2+}$  (Miyakawa *et al.*, 2015). An increase in thermostability in the same magnitude than PHL7 was visible in *Hsab*\_PE-H (Figure 19B). With the addition of  $\text{Ca}^{2+}$  the thermostability increased by 8°C.

Structurally, enzyme catalysis is dependent on the interplay of two factors. Structural rigidity as it allows for keeping a certain three dimensional form, as well as flexibility for allowing to adapt to substrates and to perform its catalytic function (Georlette *et al.*, 2004). Finding a balance between those two opposing factors is important in finding the most efficient enzyme. Psychrophilic enzymes show a stronger structural flexibility compared to mesophilic as well as thermophilic enzymes. This flexibility helps keep the structural integrity yet flexibility in environments that provide lower thermal energy. Less flexibility on the other hand helps thermophilic enzymes at higher temperatures to not fall apart in environments with higher thermal energies (Georlette *et al.*, 2004). Checking the temperature activity of *Hsab*\_PE-H without the addition of  $\text{Ca}^{2+}$ , it was noticeable that *Hsab*\_PE-H was inactive at higher temperatures above 30°C, however showed activity at lower temperatures between 4-10°C (Figure 19C). This indicates that  $\text{Ca}^{2+}$  dependency is most likely due to stabilization effects of the  $\text{Ca}^{2+}$  ions on the three-dimensional structure that can also partially be obtained at lower temperatures.

To enable insight into the structure, the crystal structure of the enzyme *Hsab*\_PE-H was solved by the Center for Structural Studies (CSS) of the Heinrich Heine University Düsseldorf with a resolution of 1.2-2.0 Å but without Ca<sup>2+</sup> and hence in the form that showed activity below 10°C.

When comparing the b-factor, a factor for measuring thermic stability and therefore flexibility of a protein structure, for *Hsab*\_PE-H and the homologous and Ca<sup>2+</sup> dependent Cut190 (Numoto *et al.*, 2018), it is noticeable, that especially at the calcium binding sites, it is equal with *Hsab*\_PE-H showing generally a bit more flexibility in *Hsab*\_PE-H (Figure 20).

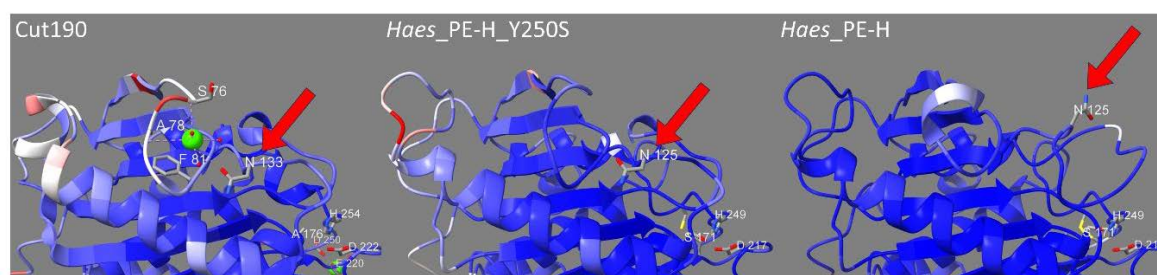


**Figure 20: Comparison of the crystal structure of Cut190 with *Hsab*\_PE-H and *Haes*\_PE-H.** The structure visualization of the enzymes are colored by b-factor with the default settings of ChimeraX. Dark blue are parts that are very stable. More flexible parts are colored from white to red. The active center is oriented in the middle of the structure and the side chains are shown as sticks colored by atom. Disulfide bridge forming cysteine side chains are shown as sticks and colored in yellow and ionic calcium is colored in green in the structure of Cut190. The homologue regions for the three calcium binding sites in *Hsab*\_PE-H to Cut190 are shown in sticks. The PDB numbers of the structures are *Haes*\_PE-H (6SBN) and Cut190 (5ZNO). The structure of *Hsab*\_PE-H has not yet been published so far.

Comparing this to a highly homologue enzyme to *Hsab*\_PE-H, *Haes*\_PE-H (Bollinger *et al.*, 2020c), this flexibility is very pronounced. While structurally the *Hsab*\_PE-H and *Haes*\_PE-H are more equal (RMSD = 0.454 Å), areas with higher flexibility, as indicated by the b-factor, are more similar between *Hsab*\_PE-H and Cut190 (Figure 20). *Haes*\_PE-H seems to be very rigid according to the b-factor, which is underlined by the lack of activity of *Haes*\_PE-H at low temperatures (3.2.5)(Figure 20).

Numoto *et al.* (2018) proposed three interaction sites of Ca<sup>2+</sup> in their structural analysis. In interaction site 1, Ca<sup>2+</sup> is coordinated by the main chain carbonyls of three amino acids forming with three water molecules an octahedral geometry in a loop structure (Miyakawa *et al.*, 2015; Numoto *et al.*, 2018). In the loop structure the Ca<sup>2+</sup> interacts with the nearby N133, pulling it closer and subsequently connecting it with G80 opening the structure in a so-called open form. In this open form, the active site cleft is opened for bulkier substrates

to enter after which the  $\text{Ca}^{2+}$  detaches again bringing the enzyme into an engaged form in which the hydrolysis can happen. After this,  $\text{Ca}^{2+}$  needs to bind again to reform the open state and release the reaction product (Numoto *et al.*, 2018). Site 2 and 3 are coordinating two more  $\text{Ca}^{2+}$  molecules similar to site 1, aiding in the enzymatic activity by stabilizing the structure further (Numoto *et al.*, 2018). Comparing the crystal structures of *Hsab*\_PE-H and Cut190 (PDB: 5ZNO)(Figure 20) both show similarities at the  $\text{Ca}^{2+}$  binding and interaction motifs found. Comparing this to the *Hsab*\_PE-H structure, interaction site 3 as explained by Numoto *et al.* (2018) seems to differ from the structure of *Hsab*\_PE-H at this position with both homologue amino acid positions being different residues than in Cut190 (Figure 20). This might indicate this position not being able to bind  $\text{Ca}^{2+}$  in *Hsab*\_PE-H. Interestingly, comparing the structures of *Haes*\_PE-H and the improved *Haes*\_PE-H\_Y250S with the  $\text{Ca}^{2+}$  bound and unbound states of Cut190 and *Hsab*\_PE-H, differences between the  $\text{Ca}^{2+}$  interacting N133 of Cut190 and the respective position in the PE-H are visible (Figure 21).



**Figure 21: Comparison of the environment of Cut190 position N133 in  $\text{Ca}^{2+}$  bound state with the homologue regions of *Haes*\_PE-H\_Y250S and *Haes*\_PE-H based on the crystal structures.** The structure models of the enzymes are colored by b-factor with the default settings of ChimeraX. Dark blue are parts that are very stable. More flexible parts are colored from white to red. The active center is orientated to the right of the structure and the side chains are shown as sticks colored by atom. Disulfide bridge forming cysteine side chains are shown as sticks and colored in yellow and ionic calcium is colored in green in the structure of Cut190. The amino acid residue N133 of Cut190 and N125 of *Haes*\_PE-H is orientated to the top of the structure. The PDB numbers of the structure are *Haes*\_PE-H\_Y250S (6SCD), *Haes*\_PE-H (6SBN), Cut190 (5ZNO).

In *Haes*\_PE-H wild type enzyme, the position of the homologue asparagine residue is comparable to the position in the  $\text{Ca}^{2+}$  unbound state of Cut190 and *Hsab*\_PE-H. The more PET active variant *Haes*\_PE-H\_Y250S has the asparagine like the  $\text{Ca}^{2+}$  bound Cut190 (Figure 21). This might indicate that the N133 of Cut190 might be an important amino acid for PET activity since the *Haes*\_PE-H\_Y250S variant is significantly more active on PET substrates than the *Haes*\_PE-H wild type.

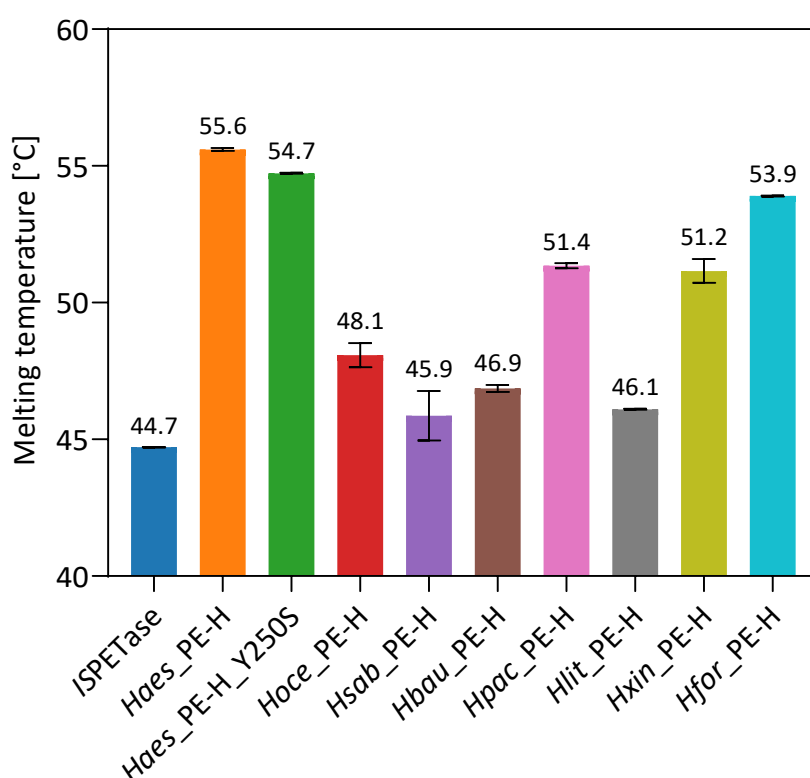
Overall, the activity at low temperatures as well as the structural analysis of the high b-factor with the homologies to Cut190 the  $\text{Ca}^{2+}$  dependency might be due to a high flexibility of the structure of *Hsab*\_PE-H. It might also be assumed that the stabilization mechanism, due to the homologue  $\text{Ca}^{2+}$  interaction sites as well as general structural homology, might be like that of Cut190.

#### **3.2.4. Thermal stability**

Temperature is a key factor for enzyme activity. However, not just for the enzyme but also for future applications. Since especially micro- and nanoplastics are not efficiently filtered in wastewater treatment plants, enzymes that are able to degrade plastics at temperatures around 10°C could be used for more efficient wastewater treatment. Additionally, industrial applications may need enzymes that are able to degrade plastic at more ambient temperatures due to high costs of energy. So far only heat tolerant enzymes have been screened for, due to a better accessibility of the polyester by enzymes at the polyester's glass transition temperatures. Therefore, the structural melting points defined as the temperature at which half of the enzymes are unfolded were determined.

The structural melting curves of the enzymes were recorded using the NanoDSF technique. The structural melting curves are calculated by looking at the aromatic amino acids tryptophan and tyrosine. These amino acids can be excited at a wavelength of  $\lambda = 280 \text{ nm}$  and the resulting fluorescence is measured at 350 and 330 nm. This ratio differs between if the amino acid being hidden inside the tertiary structure or having contact with the polar solvent.

Shown in Figure 22 are the measured melting temperatures of the enzyme set.



**Figure 22: Melting temperatures of the investigated homologous PE-H from *Halopseudomonas* spp.** The melting point was determined as the maximum of the first derivatives of the melting curves measured by nanoDSF with a temperature range of 20-99°C. The enzymes had concentrations between 0.1 - 1 mg/ml and were measured in 100 mM Potassium phosphate buffer, pH 7.2. The mean melting temperature of three measurements is written on top of the bar. The *Hsab*\_PE-H was measured in its active state with added 500  $\mu$ m  $\text{CaCl}_2$ .

Wild typical *ISPETase*, used as the benchmark enzyme, showed a melting temperature of 44.7°C, which is in agreement with the published data for this enzyme (Brott *et al.*, 2022). The set of *Halopseudomonas* PE-Hs were determined as overall slightly more and hence moderately thermostable with a range from 45.9°C for *Hsab*\_PE-H and up to 55.6°C for the *H. aestusnigri* PE-H (*Haes*\_PE-H) described by Bollinger *et al.* (2020c). The melting temperature for the rest of the enzymes lies somewhere in between these two values. The enzymes do not reach the glass transition temperature of PET at 65°C, however.

The difference in melting temperatures of up to 10°C between the enzymes from the different *Halopseudomonas* species is surprising, considering the high sequence identities (Figure 14). However, all of them were less thermostable than the thermophilic cutinases like LCC or engineered *ISPETase* variants like DuraPETase and ThermoPETase that can maintain structure and activity near the glass transition temperature of PET (Brott *et al.*, 2022). Regarding biocatalytic PET degradation, this would be an asset, as mentioned

before. Enzymatic degradation of PET at low temperatures seems to be considerably slower, due to the enzymes not being able to easily attach to polymer chains within constrained areas of the polyester. However, the application of enzymes at lower temperatures has received increased focus as of lately. Mesophilic enzymes are more useful in processes where high temperatures are not possible, as for example in wastewater treatment plants. The degradation of polyesters with lower glass transition temperatures may benefit from such enzymes. Mesophilic enzymes might therefore be a solution for more ambient temperature processes if they happen to be just as active as their temperature stable variants.

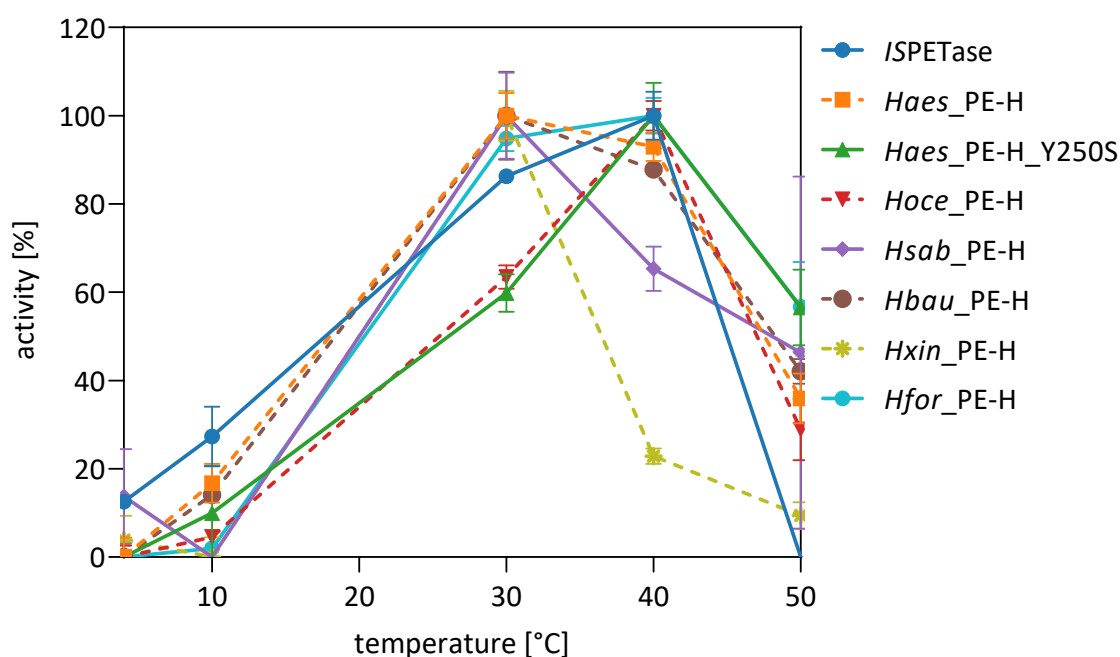
The observed melting temperatures are in good agreement with the flexibility of the enzymes with available crystal structures (indicated by the inherent b-factors), with rigid enzymes having higher melting points, and flexible enzymes having lower melting points.

### **3.2.5. Temperature dependent activity**

The optimal functional temperature of enzymes is a mixture of three variables according to the equilibrium model. On one hand, the activity rises with temperature due to an effect on the catalytical reaction. On the other hand, the enzyme is in an equilibrium with an inactive form, and will eventually get fully denatured with temperature and becomes irreversible inactivated (Daniel *et al.*, 2008). Finally, these processes are also dependent on the time the enzyme must withstand the assay.

Depending on the individual enzyme, the ideal temperature for maximum activity changes. As seen in the previous chapter, the melting temperature and therefore stability is dependent on the enzyme structure. This is also true for the activity of the enzymes at different temperatures, limiting the possible application conditions. A wide range of temperatures was assessed here, ranging from 4°C to 50°C. Temperatures between 4°C and 10°C are usually found in wastewater treatment facilities, and are therefore important to consider for usage of enzymes in such environments. Temperatures up to 50°C and higher are usually present in industrial facilities and in composting facilities.

Visible in Figure 23 are the temperature activity profiles of the tested enzymes. Most enzymes show the highest activity at around 40°C. This seems reasonable since most enzymes have a melting point just above 40°C. At this temperature, the structure of the enzymes is the most flexible.



**Figure 23: Temperature-dependent activity of the investigated homologous PE-H from *Halopseudomonas* spp.** Comparison of the enzymes, showing a bell-shaped activity curve with pNPH for 10 min at a temperature range between 4°C and 50°C and 50 nM enzyme. The activity is shown as relative activity in relation to the maximum activity of each enzyme. The enzyme preparations *Hlit*\_PE-H and *Hpac*\_PE-H did not show sufficient activity for reliable results in this setup.

Accordingly, most enzymes showed only 60 % or 10 % residual activity at 50°C. The highest residual activity at 50°C was shown by the enzyme *Haes*\_PE-H\_Y250S (Bollinger *et al.*, 2020c) as well as the enzyme *Hfor*\_PE-H. Both are also the enzymes that show the highest temperature stability as seen in Figure 22, and most rigidity in the crystal structure for *Haes*\_PE-H (Figure 20). *Hfor*\_PE-H in comparison to *Haes*\_PE-H has a higher temperature spectrum with the overall highest activities between 30 and 50°C.

The *Hfor*\_PE-H is an enzyme derived from *H. formosensis*, an organism found in compost (de Witt *et al.*, 2023). Since temperatures during compostation can rise up to 60°, and the organism was found to be active at 60°C (de Witt *et al.*, 2023), it is reasonable to assume that this enzyme can withstand temperatures of up to 60°C.

The most cold tolerant enzyme seems to be *Hsab*\_PE-H. This is supported by the results presented in 3.2.3 indicating for *Hsab*\_PE-H a flexibility that high that stabilization by  $\text{Ca}^{2+}$  ion is apparently necessary to maintain activity at temperatures higher than room temperatures (Figure 20). However, *ISPETase*, despite being more flexible in the crystal structures and having a low thermal melting point, seems to be temperature tolerant up

until 40°C. *ISPETase* does show different structural characteristics to the rest of the enzyme set, since it's a part of the type IIb PETases, in contrast to the other enzymes of the set being type IIa PETases. Some structural features might make the flexible *ISPETase* more temperature stable compared to *Hsab*\_PE-H.

Surprisingly, *Hoce*\_PE-H did not seem to be very cold active, despite being found at cold temperatures. At a temperature below 30°C, the activity is very low.

Not only for the enzyme itself but also for the applications in the context of artificial polyester degradation, temperature is an important factor. Plastics structures are very dependent on temperatures for production as well as their rigidity and use. Temperature and mechanical forces determine the degree of crystallinity in PET. Lower degrees of crystallization and higher degrees of amorphous PET are faster and easier for most enzymes to depolymerize. Especially at higher temperatures, the amorphous PET gets more mobile and easier to access for enzymes (Thomsen *et al.*, 2022). This means that PET depolymerization generally happens faster at higher temperatures, especially around the glass transition temperature of PET between 65°C-81°C, depending on the degree of crystallization (Tarazona *et al.*, 2022). Few enzymes are active at these high temperatures and are therefore engineered to be more temperature stable for industrial PET-waste degradation (Brott *et al.*, 2022; Tournier *et al.*, 2020).

Besides solid PET plastic, there are also other polyesters of interest, e.g. PET microfibers from clothing, alternative packing polyesters like PBAT or PBS, and coating materials for textiles or e.g. fishing nets, like Impranil DLN-SD. Compared to the melting temperature of PET of 260°C, Impranil DLN-SD has a melting temperature of only 175°C-200°C according to the manufacturer, which indicates that the glass transition temperature might be lower as well. These polyesters are ideal for mesophilic polyester hydrolases to degrade. This might be advantageous for some processes. The industrial degradation of plastic is energy intensive due to the optimal temperature for enzymatic degradation being equal to the glass transition temperature of the polyesters. Another useful application could be the use as an additional filtering system in wastewater treatment plants. Since temperatures in those facilities are usually equal to the ambient temperature, mesophilic enzymes could effectively filter out micro- and nano plastic particles.

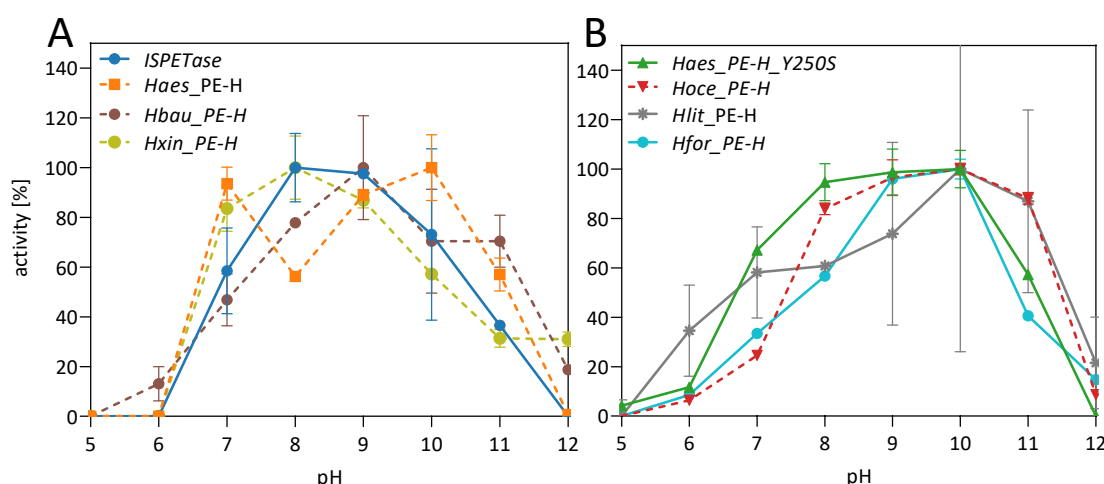


### 3.2.6. pH dependent activity

The pH is a crucial factor in enzyme activity and stability. Enzymes have an optimal pH in which their activity ( $V_{\max}$ ) and surface charge is optimal for the substrate binding and for reactions in the active center, making it most efficient (Tijskens *et al.*, 2001). This spectrum depends on the enzyme.

The enzyme activity in a pH-spectrum follows a bell-shaped curve. Important for this behavior is the protonation of the functional groups of the amino acids responsible for the activity and the native three-dimensional structure of the enzyme. The differences in protonation at certain pH values can break the enzymes' structure, making it irreversibly inactive (Bisswanger, 2014).

For the enzyme set, most of the enzymes have their pH-optimum  $V_{\max}$  in the alkaline range between pH 8 up to pH 10 (Figure 24). This was to be expected since most literature-known serine hydrolases and polyester hydrolases show a  $V_{\max}$  in this pH-range (Chen *et al.*, 2020).



**Figure 24: pH optimum for the enzyme set.** 50 nM of the respective enzyme was measured in Britton-Robinson buffer with the corresponding pH and 0.5 % (v/v) Impranil DLN-SD for 10 min at 30°C. Activity was determined as the decrease of turbidity measured via absorption at 600 nm. The values are normalized according to the pH with the highest activity. *Hsab*\_PE-H did not show sufficient activity on Impranil DLN-SD in Britton-Robinson buffer due to interactions of the buffer with  $\text{CaCl}_2$  and the anionic Impranil DLN-SD. *Hpac*\_PE-H did not show sufficient activity on Impranil DLN-SD due to low enzyme concentrations. *Haes*\_PE-H activity at pH 8 was not determinable with an enzyme concentration of 50 nM. This concentration was applied here for all enzymes for comparability reasons because of concentration dependent enzyme inactivation (3.2.2). (A) shows the enzymes with the activity max around pH 8 and (B) shows the enzymes with their activity max at pH 10.

The nature of cutinases as serine hydrolases is that the active serine needs to be deprotonated by the active histidine to function. This is probably only possible in a more

alkaline environment, since the active serine is also mostly close to the proteins surface to access the polymer chains, and therefore exposed to the medium (Baker *et al.*, 2012). In addition, the more acidic the enzyme environment of the serine hydrolases is, the more hydrophobic the surface of the enzymes gets (Baker *et al.*, 2012). This makes it easier for the hydrophobic polyester substrate to attach to the active site (Tournier *et al.*, 2023). However, also the hydrophobic surfaces of the enzymes will attach.

Some enzymes in the set show a preference towards less basic conditions like the *Hxin*\_PE-H, and others more towards alkaline conditions like the *Hoce*\_PE-H. Both enzymes originate from a more alkaline environment in the ocean. The pH value of the oceans is usually around 8.1 (Jiang *et al.*, 2019), with lower pH values in the deep sea (Park, 1966). Together with the alkaline pH necessary for serine hydrolases and cutinases to function, as well as the pH distribution in the oceans, the observed pH activities are to be expected. Overall, most enzymes show polyesterase activity in an alkaline pH and have a pH range between pH 7 and 11.

pH dependent activity is especially interesting when looking at the general nature of polyester degradation in water-based solutions. Due to the release of monoacids like MHET and diacids like TA during the degradation of PET, the solution turns acidic, rendering most polyester hydrolases useless if not controlled (Tournier *et al.*, 2023). Using an acid tolerant polyester hydrolase would cease the need for titration of the solution, which, especially in large scale would be beneficial. This makes these enzymes especially interesting for industrial applications or for their use in wastewater treatment plants, where a low pH could result in unwanted reactions.

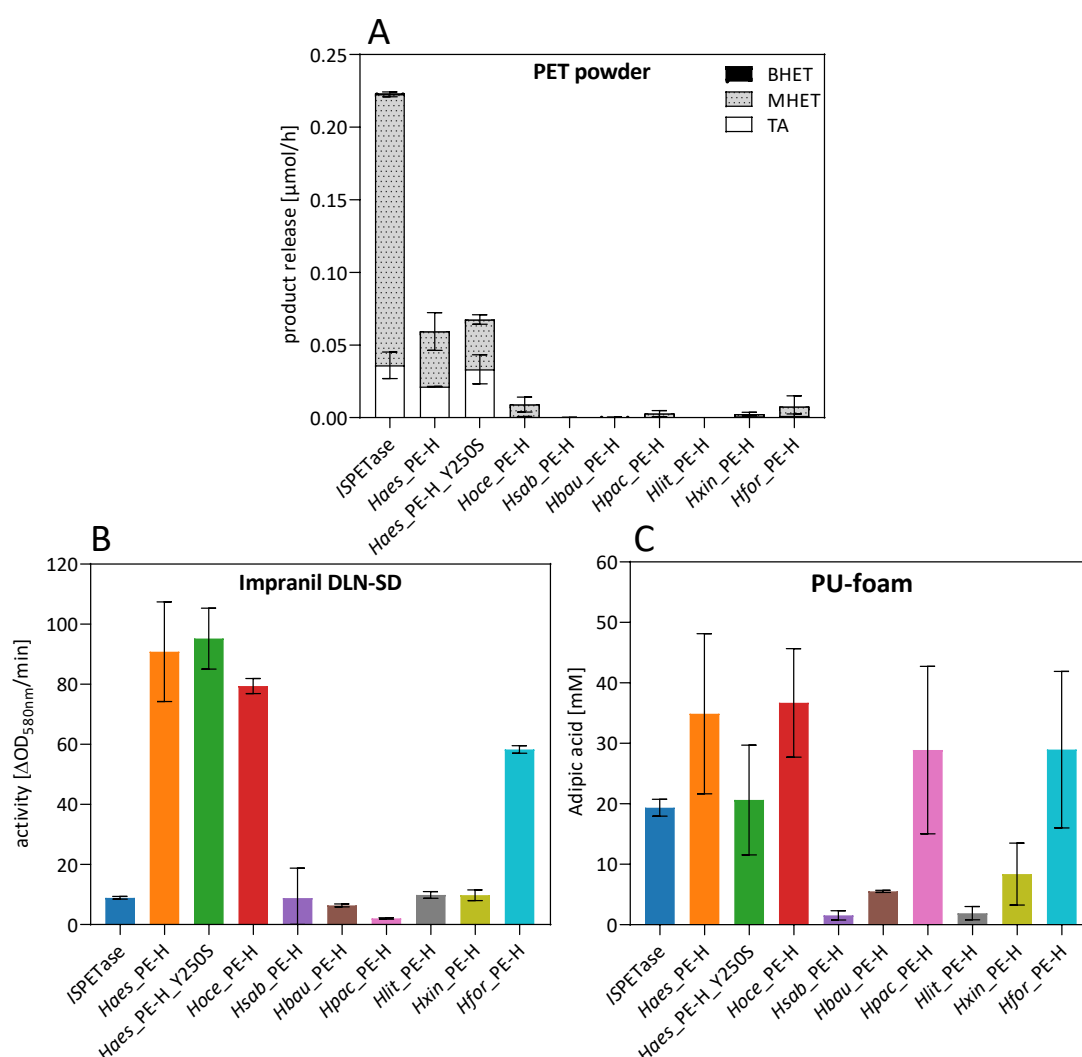
### **3.2.7. Analysis of polyester degradation**

Since PET is one of the plastics produced in the highest volumes (Figure 1) there is a need for sustainable waste treatment of this material. In recent years a multitude of PET degrading enzymes have been described, with the earliest one being described in 2016 (Yoshida *et al.*, 2016). Even though PET is the polymer with the highest production volume, other polyesters are also of interest, especially polyester blends like polyester-polyurethane foam or dispersions (Impranil DLN-SD). In this chapter, the degradation activity of the enzyme set for different polyester substrates with different compositions is analyzed. First, aromatic PET in the form of powder and film is analyzed, followed by the

aliphatic polyester-polyurethane blend Impranil DLN-SD. Lastly, the degradation of a polyester-polyurethane foam blend was analyzed.

PET is a challenging yet homogenous aromatic polyester. Due to its rigid structure, long chain length and hard to access surface, most esterase type polyester hydrolases have difficulties degrading it. In addition, most PET for the consumer market has different crystallinities depending on the usage. This ranges from crystalline rigid structures to more amorphous, less organized, structures that are more accessible. PET gets even more accessible for most enzymes when the organized chains are broken open, especially in ground PET (Thomsen *et al.*, 2023). This powdered PET is the most accessible form of PET and therefore a great substrate for testing PET degradation of enzymes.

In Figure 25A the activity of the enzyme set on powdered PET and PET-foil was tested. The powder was derived from amorphous PET foil and was ground using a CryoMill MM400 (Retsch GmbH, Germany) with a frequency of 20 Hz for 2 min after pre-cooling the 35 ml stainless steel jars with one 20 mm diameter stainless steel grinding ball in liquid nitrogen for 5 min. The activity was measured by looking at the degradation products like the monomers BHET and MHET, as well as the building block terephthalic acid (TA) in an UPLC. Samples were taken every 24 h over the course of 5 days.



**Figure 25: Polyester degradation activities of the enzyme set.** (A) Enzymatic activity of 1500 nM enzyme solution on cryo-mill-powdered PET over 96 h of incubation at 30°C. Samples were taken every 24 h and measured after filtration (MWCO 10,000) in an UPLC. The activity was measured as release of BHET, MHET or TA per hour in  $\mu\text{mol}$  [ $\mu\text{mol/h}$ ]. BHET was only detectable for ISPETase and is visible on top of the column. (B) Impranil DLN-SD clearance assay measuring the activity of 50 nM enzyme solution with 1 % Impranil DLN-SD as substrate for 10 min at 30°C and measured in a photometer at 580 nm. Activities are shown as the difference of the optical density of the solution at 580 nm per minute [ $\Delta\text{OD}_{580\text{nm}}/\text{min}$ ]. (C) Enzymatic activity on PU-foam over 96 h of incubation at 30°C with 1500 nM enzyme. Samples were taken after 96 h and measured after filtration (MWCO 10,000) in an UPLC-PDA.

Most noticeable is that ISPETase is the most active enzyme followed by Haes\_PE-H as well as Haes\_PE-H\_Y250S. This is not completely surprising regarding the described preference of ISPETase for aromatic polyester substrates over aliphatic substrates (Austin *et al.*, 2018). However, the product inhibition of MHET on ISPETase is very apparent. While BHET is efficiently converted to MHET, there is barely any released TA. This shows that a MHETase

is necessary for the full degradation of PET to overcome the stagnation between the steps of MHET release and the release of TA.

After these highly active reference enzymes, the most active variants from the enzyme set are again *Hoce*\_PE-H as well as *Hfor*\_PE-H. All activities were low compared to the *ISPETase* degradation ability. *Hoce*\_PE-H and *Hfor*\_PE-H, which generally showed the highest activities on the other substrates, only have low activity on PET. It is, however, visible that most of the released substrate was MHET, which might indicate an inhibition of further degradation due to the presence of MHET. They were not able to release any TA but fully degraded BHET to MHET. The same test was conducted with amorphous PET film; however, no activity was seen besides the activity of the reference strains (Appendix Figure 39).

To see the spectrum of polyester hydrolase activity, additionally polyester blends should be checked. Impranil DLN-SD is a polyester-polyurethane that is an easy-to-handle aliphatic polyester-polyurethane blend formulized into a dispersion of nanoparticles. Due to its liquid state, it is easy to use in high throughput activity assays. Figure 25B shows the activity of the enzyme set on Impranil DLN-SD.

From the reference enzyme *ISPETase* it is most noticeable that *ISPETase* seems to have only limited activity. Austin *et al.* (2018) postulated for *ISPETase* a preference for aromatic polyester substrates, and almost no activity for aliphatic substrates, as they detected only minor activities for aliphatic substrates, which would explain the low activity on Impranil DLN-SD. However, *ISPETase* did not reduce the optical density of the Impranil DLN-SD suspension as expected during the previously described pH-dependent activity assessment, but rather led to increased optical density and precipitate, specifically at acidic pH. This might be due to transesterification reactions or maybe crosslinking reactions happening at these low pH values. *Haes*\_PE-H and *Haes*\_PE-H\_Y250S showed almost the same activity and are in the whole set the most active. For the new enzymes, the best activity was shown by *Hoce*\_PE-H as well as by *Hfor*\_PE-H. The rest showed roughly the same amount of activity as the *ISPETase*.

In cooperation with the IBG-1 of the Forschungszentrum Jülich aiming to characterize the performance of a novel *H. formosensis* isolate, we have looked into the Impranil DLN-SD degradation by *Haes*\_PE-H and *Hfor*\_PE-H (de Witt *et al.*, 2023) on molecular level. After 10 min of incubation, we analyzed the reaction products using GC-ToF-MS (*Gas chromatography time-of-flight* mass spectrometry). We found that in the reactions with

both enzymes (neopentyl glycol), adipate, and 1,6-hexandiol were accumulated which matches the proposed composition of Impranil DLN-SD. Notably, monoesters of adipic acid were not detected. Since the enzymes from this set are highly homologous, these might also be the reaction products for the rest of the enzyme set. Interestingly, the same degradation products were detected in the culture supernatant of *H. formosensis* cultures growing on Impranil DLN-SD.

The best performing enzymes of the set, namely *Hoce*\_PE-H and *Hfor*\_PE-H seem to be doing very well with Impranil DLN-SD nanoparticles as their substrate and look promising for testing on substrates that are still aliphatic polyester but more difficult in structure.

To do this, a polyester-polyurethane foam was tested. This type of foam is used as a filling for mattresses or pillows as well as couches and other furniture. Due to this wide use, it is an interesting candidate for testing its biodegradability.

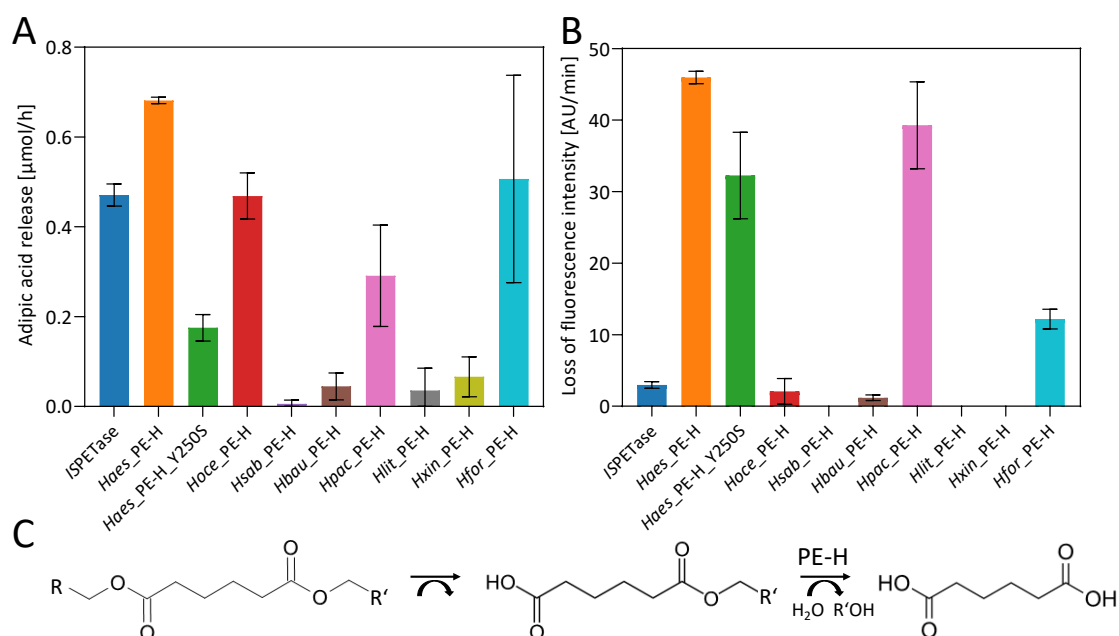
Figure 25C shows the release of adipic acid of the enzyme set from ca. 5 mg of PU-foam after 96 h of incubation. It is noticeable that after 96 h of incubation, all enzymes from the set show product release. The enzymes *Hsab*\_PE-H, *Hbau*\_PE-H, *Hlit*\_PE-H, and *Hxin*\_PE-H show the lowest activities. The enzymes *Hoce*\_PE-H and *Hfor*\_PE-H show in comparison to the reference enzymes an equal activity. Surprisingly, *Hpac*\_PE-H, rather inactive on other tested substrates, seemed to prefer PU-foam as its substrate.

These assays prove the polyester hydrolase abilities of the enzyme set, but also show that compared to easier polyesters; PET is a more challenging substrate. The enzymes also seem to have preferred substrates, with *ISPETase* for example seemingly preferring aromatic substrates and not having noticeable activity on the aliphatic substrate Impranil DLN-SD and reduced activity on PU-foam.

Esterase activity is commonly measured using pH shift assays determining the protonated species of a chosen pH indicator via its specific absorbance properties (Bollinger *et al.*, 2020a; Janes *et al.*, 1998; Pena-Garcia *et al.*, 2016). However, measuring the esterase activity in a photometer is difficult when the solid substrate i.e. PU-foam is laying on the bottom of the reaction well and blocking the path of light. To resolve this, a pH assay was adapted using fluorescein as the indicator. Free acid groups after hydrolysis lead to an acidification of the medium, and subsequently change the pH dependent fluorescence of the fluorescein, which can be determined by excitation and emission measurement from

above. This allowed us to analyze the rate of released adipic acid in comparison to the rate of general release of acidic components.

This comparison shows which enzyme might have a stronger product inhibition by having more released overall acids compared to released adipic acid (Figure 26).



**Figure 26: Comparison of adipic acid release [μmol/h] A and general acid release (Loss of fluorescence [AU/min]) B from the degradation of PU-foam. (A)** The adipic acid release [μmol/h] was measured with an UPLC-CAD for 96 h at 30°C with 1500 nM enzyme. **(B)** The overall acid release is shown as loss of fluorescence [AU/min] of the pH sensitive dye fluorescein. It was measured over 4 h at 30°C with 50 nM enzyme. The no enzyme control was subtracted from the values. **(C)** shows the general degradation pathway of a polyester-polyurethane dimer to a monomer to adipic acid.

Figure 26A-B shows the different behavior between adipic acid release and general acid release. The enzymes show very different patterns. While *ISPETase* releases more adipic acid, the general acid release is rather slow. In contrast, the *Haes\_PE-H\_Y250S*, which is designed to be closer to the *ISPETase* than wild type *Haes\_PE-H* (Bollinger *et al.*, 2020c), has less adipic acid release yet a fast general acid release. This can be interpreted as product inhibition. While the *ISPETase* seems to degrade more substrate to adipic acid, the *Haes\_PE-H\_Y250S* seems to accumulate the monoesters of PU-foam, which cannot be quantified with the UPLC-CAD due to a lack of standard materials. However, the hydrolyzed ester bonds of the PU-foam are changing the pH of the solution and can therefore be detected by loss of fluorescence of fluorescein.

Product inhibition has long been described as an important factor in regulating metabolic pathways. For industrial processes however, having product inhibition is a challenge since

this can lower the process efficiency. Barth *et al.* (2015) has described product inhibition on the polyester hydrolase TfCut2 by the degradation product MHET of the PET degradation process. In the degradation process of PET, it is degraded into the monomers BHET and MHET. Both products have roughly the same binding constant to TfCut2, with MHET being poorly hydrolysable and even inhibiting the enzyme (Wei *et al.*, 2016). For *ISPETase* this phenomenon has also been described (Erickson *et al.*, 2022). The organism of origin, *Ideonella sakaiensis* developed a MHETase that degrades the inhibiting MHET, resulting in full degradation of PET. This inhibition might also happen in the degradation of other polyesters like PU-foam with the monomer being mono ethyl adipate.

The enzymes *Haes*\_PE-H and *Haes*\_PE-H\_Y250S as well as *Hpac*\_PE-H seem to be inhibited by the monomers. Especially *Hoce*\_PE-H and *Hfor*\_PE-H seem to efficiently degrade the PU-foam to adipic acid without the monomers inhibiting the process.

To efficiently degrade the PU-foam in the future, it is necessary to either adapt the enzymes to not be inhibited by the product anymore, or to add a second enzyme to the reaction that specializes in degrading the intermediate product. For the adaptation of the enzymes, further information on how the inhibition on a structural level takes place is necessary. This might be achievable by doing random mutagenesis in the best performing enzymes and screen for variants that fully degrade the substrate and subsequent analysis of the changed structural features. For the addition of another enzyme to the reaction, such an enzyme needs to be found first. After this it is possible to either add it to the reaction or to fuse it to the respective enzyme to have a more efficient reaction in the solution. Both ways could lead to a full degradation of the PU-foam, making it more interesting for sustainable industrial applications.



### 3.3. Rational mutagenesis of PE-Hs to improve polyester conversion

After identifying certain characteristics of the enzymes, and especially after comparing them, some limitations are noticeable. These limitations, such as product inhibition, low activity, or poor thermic stability can be addressed by changing certain features of the enzyme. To overcome these limitations, the best performing enzymes in certain areas are compared to enzymes that work better in other areas, for example PET degradation. Certain features are then changed in the target enzyme and mutated accordingly (Mican *et al.*, 2024). These mutation strategies can include adding a second active site to an enzyme to elevate product inhibition or to overcome limitations by doing saturation mutagenesis at promising amino acid positions. The saturation mutagenesis can have the additional benefit, that the underlying mechanism of the limitation can be analyzed and projected on similar enzymes to overcome similar limitations.

#### 3.3.1. Addition of a second active site

As described earlier, low conversion of MHET to TA, or even inhibition of PETase by the intermediate product, hampers efficient enzymatic PET degradation. Combining PETase and MHETase activities may offer a solution. In this light, a combination of both enzymes independently or within an engineered bacterial strains from plastic component upcycling proofed to increase efficiency (Knott *et al.*, 2020; Li *et al.*, 2023; Werner *et al.*, 2021). Another approach may be engineering so-called Plurizymes. In this case, different activities on one enzyme are combined by de-novo engineering of secondary active sites. This approach yielded successful transaminase-esterases for biocatalytic casacades and esterases with extended substrate spectra (Alonso *et al.*, 2019; Roda *et al.*, 2022; Santiago *et al.*, 2018).

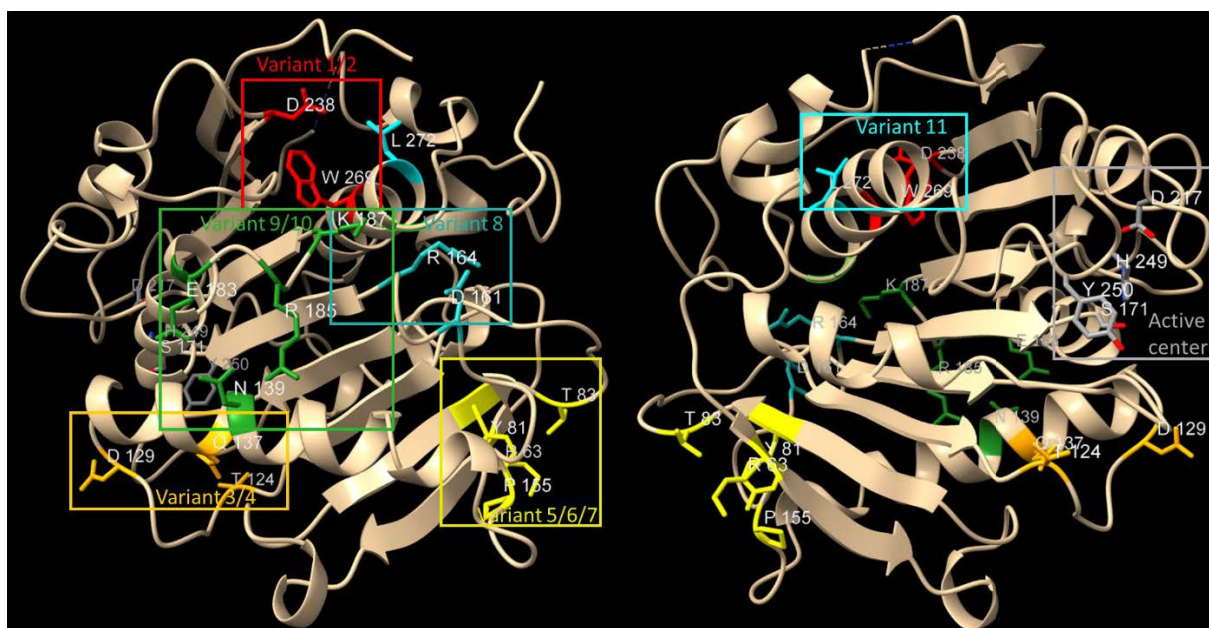
As a starting point, I used the enzyme *Haes*\_PE-H from the organism *H. aestusnigri* and its variant Y250S, both first described by Bollinger *et al.* (2020c). Since this enzyme has already been described as highly active and easy to express, other types of mutations that enhance its activity might be useful.

The additional active sites were predicted in cooperation with Manuel Ferrer, Víctor Guallar and Gerard Santiago from the Barcelona Supercomputing Center using PELE (protein energy landscape exploration) with dimer (2HE-(MHET)<sub>2</sub>) or tetramer (2HE-(MHET)<sub>4</sub>) binding and MD (molecular docking) simulation (Alonso *et al.*, 2019)(Table 7). This

additional active site was meant to enable complete PET degradation to ethylene glycol and terephthalic acid, solving the bottleneck of MHET accumulation by PE-H. The respective additional active sites are shown in Figure 27 in the crystal structure of *Haes*\_PE-H.

**Table 7: *Haes*\_PE-H variants predicted by the Barcelona Supercomputing Center to have a second active site specific for MHET degradation.**

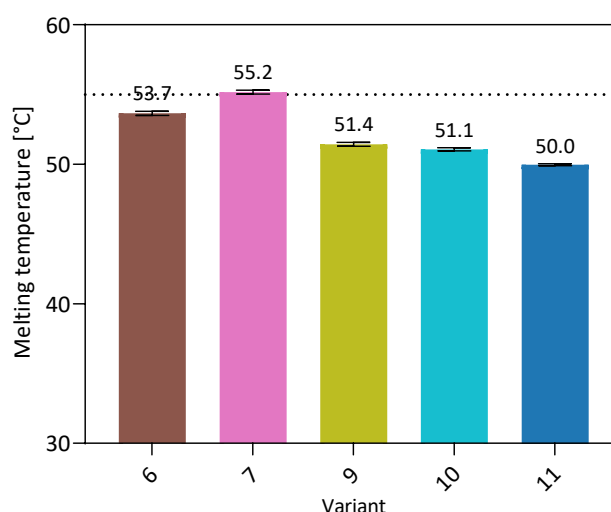
Variant	Plasmid name	Predicted function
1	<i>Haes</i> _PE-H_D238S/W269D	
2	<i>Haes</i> _PE-H_D238S/W269D/Y250S	additionally cloned into the Y250S variant
3	<i>Haes</i> _PE-H_T124L/D129H/Q137E	
4	<i>Haes</i> _PE-H_T124L/D129H/Q137E/Y250S	additionally cloned into the Y250S variant
5	<i>Haes</i> _PE-H_P155S/Y81H/R63D	active site modeled to be exclusive for MHET
6	<i>Haes</i> _PE-H_P155S/Y81H/T83E/R63A	active site modeled to be exclusive for MHET
7	<i>Haes</i> _PE-H_P155S/Y81H/T83D/R63A	active site modeled to be exclusive for MHET
8	<i>Haes</i> _PE-H_D161S/R164H/K187E	active site modeled to be for MHET and BHET
9	<i>Haes</i> _PE-H_E183S/N139H/R185D	active site modeled to be exclusive for MHET
10	<i>Haes</i> _PE-H_E183S/N139H/R185D/K187Q	active site modeled to be exclusive for MHET
11	<i>Haes</i> _PE-H_D238S/L272D	active site modelled to be capable of hydrolyzing oligomers and MHET



**Figure 27: Crystal structure of *Haes*\_PE-H (6SBN) with the Plurizyme positions marked by colored squares.** The amino acid positions of interest are shown as sticks in the corresponding color with the amino acid positions labeled. In the left picture, the structure is turned 180° to the right and the active center is on the left on the backside of the enzyme. In the right picture, the active center is seen on the right of the structure in the front.

Most of the additional active sites have been engineered to be on the backside of the enzyme, opposite the active center. Only the variants 3 and 4 are close to the active center. After successful introduction of the mutations by Quick-Change PCR, expression and purification trials were conducted. After checking via SDS-PAGE only the variants 6, 7, 9, 10, and 11 showed an expression band. Variants 1-5 and 8 could not be expressed in quantities and qualities suitable for further testing. The enzyme with the strongest expression was variant 9. An Impranil DLN-SD liquid assay showed that from the expressed variants, only variant 9 showed a reasonable activity. Further testing of activity with BHET as a substrate and MHET and TA as reaction products showed in the UPLC that only variants 7, 8, 9, and 10 were able to convert BHET to MHET. However, the desired full conversion of MHET to TA did not work (data not shown).

This indicates that the second active site was not active. Since the amount of released MHET was significantly lower than the wild-type enzyme, the original active site seemed to have been impacted by global structural changes. This was also supported by the changes in melting temperature measured using NanoDSF. The initial fluorescence ratio for all variants was increased from an AU for the wild type of about 0.7, to values between 0.8 and 0.85. This led to the assumption that the enzymes might already be partially denatured, leading to the conclusion that the addition of the second site severely influences the global stability of the protein. Considering the melting points determined, for variants 6 and 7 the melting temperature stayed approximately the same compared to the wild type enzyme (Figure 28).



**Figure 28: Melting temperatures of the investigated Plurizymes** The melting point was determined as the maximum of the first derivatives of the melting curves measured by nanoDSF with a temperature range of 20-99°C. The enzymes had concentrations between 0.1 - 1 mg/ml and were measured in 100 mM Potassium phosphate buffer, pH 7.2. The mean melting temperature of three measurements is written on top of the bar. The dotted line represents the melting temperature of the wild-type *Haes*\_PE-H.

Variants 9-11 seem to have a lower melting temperature indicating a loss in stability for those variants. In addition, to the global stability, the mutations also affect the amount of expressed enzyme.

To further continue working on the addition of a second active site, the problem of low global stability needs to be addressed. This information might also lead to further improvement of the PELE and MD simulations. Even though the enzymes were predicted by those systems to be active and stable, laboratory testing concluded that these positions do not live up to their theoretically predicted potential.

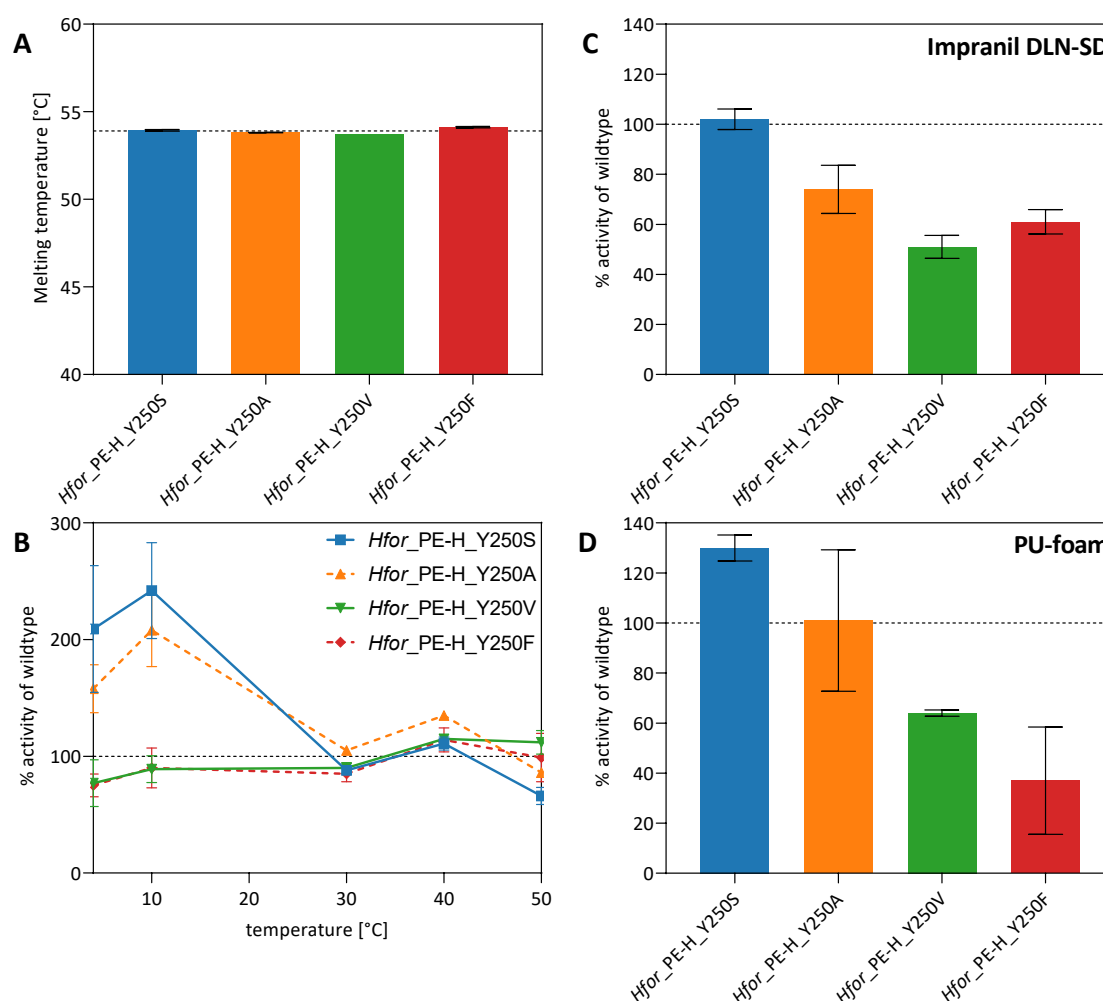
### 3.3.2. Mutagenesis between the active site histidine and disulfide bridge forming cysteine

Many groups researching PETases have already identified the amino acid position between the active site histidine and disulfide bridge forming cysteine as being important for stabilizing the active site, as well as being important for opening the active site cleft (Austin *et al.*, 2018; Avilan *et al.*, 2023; Charupanit *et al.*, 2022; Cui *et al.*, 2021; Guo *et al.*, 2022; Joho *et al.*, 2023; Joo *et al.*, 2018; Richter *et al.*, 2023; Sevilla *et al.*, 2023). Likewise, Bollinger *et al.* (2020c) found in the structure of *Haes*\_PE-H, that the amino acid position

between the active site histidine and the disulfide bridge forming cysteine as a very important position for polyester hydrolase activity.

Since this position has already proven to enhance the PET hydrolysis capabilities of *Haes*\_PE-H, *ISPETase* and many other enzymes, I aimed to assess the transferability of this approach to the most active enzymes in the set, namely *Hoce*\_PE-H and *Hfor*\_PE-H, which already show the most promising activities on aliphatic polyesters. For *Hfor*\_PE-H from the novel organism *H. formosensis* FZJ (de Witt *et al.*, 2023), selected amino acid exchanges were introduced to increase the activity even more. The selected amino acid substitutions were serine, alanine, valine, and phenylalanine. Serine was chosen since it is described by Bollinger *et al.* (2020c) and others as activity increasing. Alanine and valine were chosen as they are more hydrophobic and small residues, that might help in opening the active site cleft for the hydrophobic substrates. Phenylalanine was chosen, since it is like the wild type tyrosine however, but hydrophobic.

After mutating the tyrosine at position 250 to serine, alanine, valine, and phenylalanine in *Hfor*\_PE-H, the activity regarding different aspects was investigated (Figure 29).



**Figure 29: Relative activity of the *Hfor*\_PE-H mutants and thermal stability.** The relative activity of the mutants was calculated compared to the activity of the wild type. **(A)** Melting temperature of *Hfor*\_PE-H wild type and mutants. The melting point was determined as the maximum of the first derivatives of the melting curves measured by nanoDSF with a temperature range of 20-99°C. The enzymes had concentrations between 0.1-1 mg/ml and were measured in 100 mM potassium phosphate buffer with 100 mM NaCl, pH 7.2. The dashed line equals the melting point of the wild type enzyme **(B)** shows the relative activity of the mutant strains compared to the wild type with the substrate *p*NPH at different incubation temperatures and times between 3-10 min with enzyme concentrations of 50 nM measured in 100 mM potassium phosphate buffer, pH 7.2. The dashed line indicates the wild type activity. **(C)** shows the relative activity of the *Hfor*\_PE-H mutants compared to the wild type in percent. The activity was measured with 1 % Impranil DLN-SD (v/v) as substrate in 100 mM potassium phosphate buffer with 100 mM NaCl pH 7.2 at 30°C for 10 min and 50 nM enzyme. The dashed line indicates the wild type activity. **(D)** shows the relative activity of the *Hfor*\_PE-H mutants towards PU-foam compared to the wild type enzyme. The activity was measured as release of adipic acid over 96 h of incubation with time points every 24 h. 100 mM potassium phosphate buffer with 100 mM NaCl pH 7.2 was used at 30°C. Analysis was done with an UPLC-PDA. The dashed line indicates the wild type activity.

Even though no changes in the melting temperature could be detected (Figure 29A), the activity at different temperatures changed greatly for the mutant serine and alanine (Figure

29B). Between 4 and 10°C the mutants seem to be more active, which indicates that the mutations might influence the flexibility of the active site. As explained in chapter 3.2.3 for the enzyme *Hsab*\_PE-H, being more active at lower temperatures might indicate stabilizing effects (Georlette *et al.*, 2004), which might also be true for the *Hfor*\_PE-H variants. The mutants with the amino acid substitutions to valine and phenylalanine seem to have a more rigid active site, or at least comparable to the wild type since they have slightly more activity at higher temperatures. Overall, the mutations seem to have changed the enzymes active site stability to being either more flexible (Y250S/A) or more rigid (Y250F/V).

The activities of the mutants on different polyester substrates seem to compliment those findings. The mutant with the serine exchange shows, with the substrates Impranil DLN-SD as well as PU-foam, more activity compared to the wild type (Figure 29C-D). With PU-foam the activity increased by 30 % compared to the wild type.

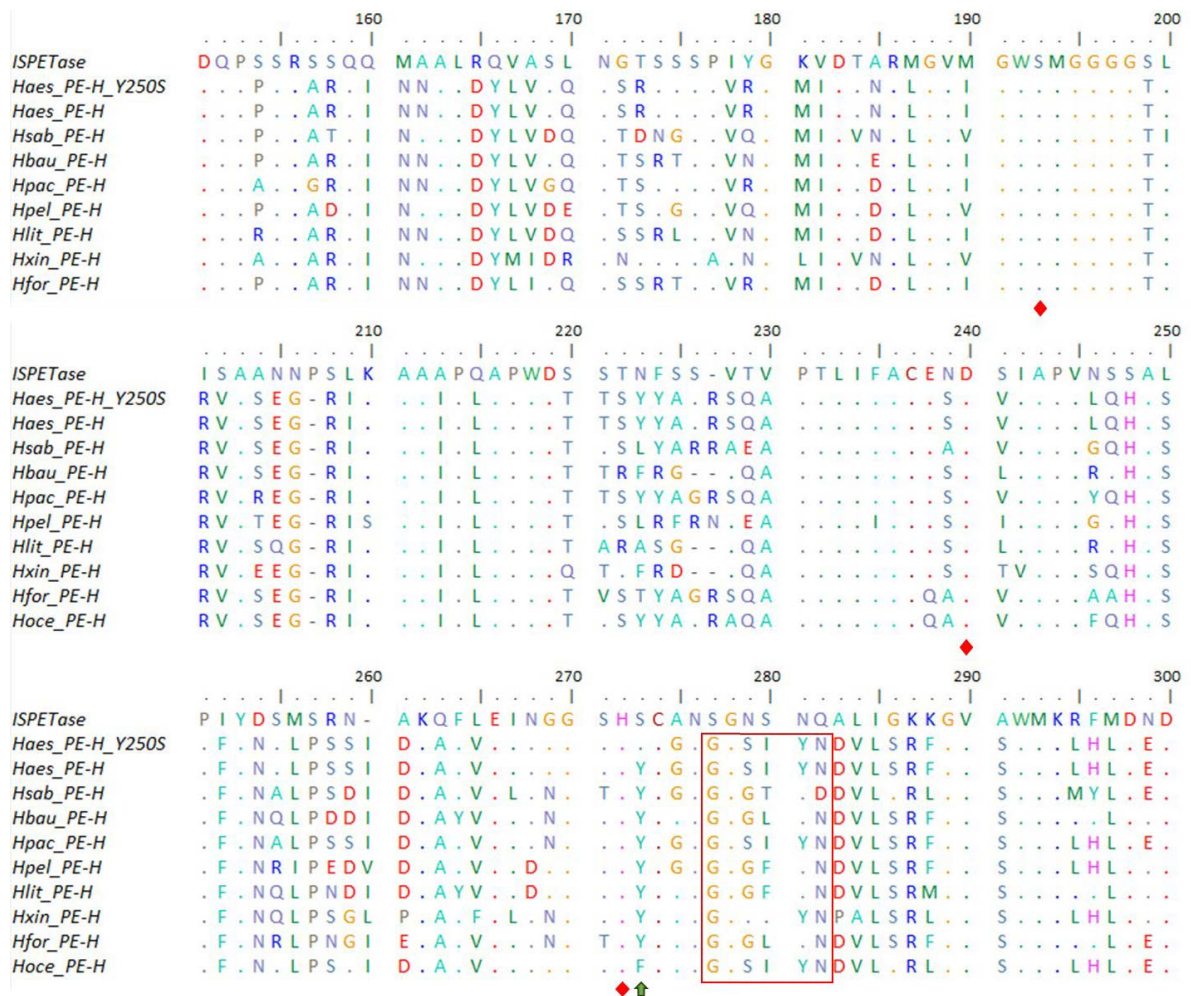
This increase in activity might be due to more flexibility of the active site, which enables the enzyme to open more for these bulky longer chain substrates (Bollinger *et al.*, 2020c; Fecker *et al.*, 2018). In comparison, the probably more rigid and larger substitutions of branched valine and aromatic phenylalanine cause a loss of activity ranging between 40 and 60 %.

These more bulky amino acids might be posing some sort of hindrance for the binding of the bulky substrates. However, phenylalanine and valine have significantly less activity compared to the wild type, even though the wild type tyrosine being very similar to phenylalanine. This indicates that there might be some other interactions of the side chains with the rest of the three-dimensional structure, or perhaps charge related interactions. A more systematic approach might bring insights into this question, as for example a saturation mutagenesis.

### 3.3.3. Saturation mutagenesis of *Hoce*\_PE-H position Y265

The enzyme *Hoce*\_PE-H from the organism *H. oceani* has shown itself as one of the most active and promising enzymes in this set. It shows high activities for some polyester substrates, even surpassing the activities of already established enzymes like the *ISPETase* as well as *Haes*\_PE-H. Especially the activity on polyester-polyurethane seems very promising since not a lot of enzymes are yet known to degrade such material. As mentioned in the previous chapter, the position right next to the active site histidine in the enzyme

ISPETase has been described as crucial for elevated polyester degradation activity (Sevilla *et al.*, 2023; Tournier *et al.*, 2020). Tournier *et al.* (2020) found this position by performing a saturation mutagenesis at the predicted MHET binding site of the LCC. They found by making use of molecular dynamics simulations, that the mutated variant has a higher affinity to MHET compared to the wild type. According to Bollinger *et al.* (2020c) this position seems to enlarge the active site cleft of the *Haes*\_PE-H. Since *Hoce*\_PE-H is a close homologue of *Haes*\_PE-H with a sequence identity of 71.19 % (Figure 14) changing this position seems promising to elevate the polyester or polyester-polyurethane degradation even further than what the *Haes*\_PE-H can do now. Notably, it was the only *Halopseudomonas* enzyme with a phenylalanine residue instead of tyrosine at the position of interest (Figure 30).



**Figure 30: Sequence alignment of all PE-H homologues with the ISPETase.** The catalytic triad is marked with red diamond. The extended loop area is marked with a red box. The position behind the catalytical active histidine is marked with a green arrow. The N-terminal signal peptide as well as the amino acids behind position 300 are not depicted. Every amino acid has a specific color for better visual understanding.

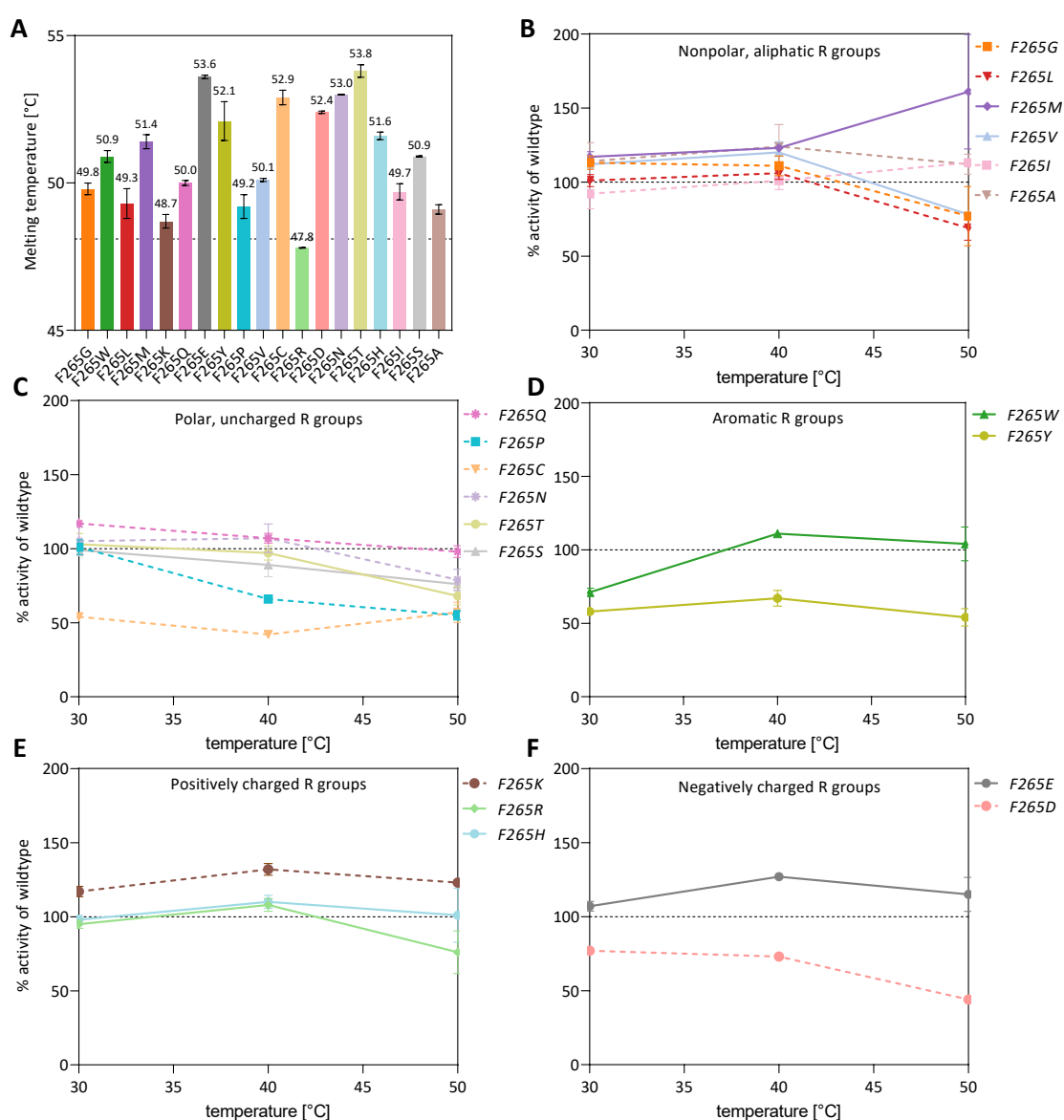


Therefore, *Hoce*\_PE-H was chosen as target for a saturation mutagenesis of the His<sub>cat</sub>+1 position (Y265 in this case) to get insight on different levels and to find out what makes this position so special.

Nadine Königshausen (2022) cloned, expressed, purified, and characterized the thermal stability and PU-foam degradation capabilities of the *Hoce*\_PE-H variants in her bachelor thesis associated to this thesis.

The first difference between the variants was the enzyme production. Compared to the wild type with an amount of 0.805 mg/ml, the variant F265V was expressed with 8.589 mg/ml, giving it 1,067 % higher yields. In fact, most of the variants had better production compared to the wild type, except for variant F265H with a somewhat lower enzyme amount. This better producibility might show the importance of this amino acid position for production in *E. coli*. This was also observed in the *Haes*\_PE-H and its variant *Haes*\_PE-H\_Y250S. While I was able to express amounts of around 8 mg/ml of the *Haes*\_PE-H, *Haes*\_PE-H\_Y250S was produced in the same conditions with amounts of around 12 mg/ml. However, in the *Hfor*\_PE-H mutants no such behavior was observed. All variants resulted in the same amount of produced enzyme. This might indicate that a better producibility of the enzyme at this position seems to be enzyme dependent.

The substitutions appear to also influence the general stability of the enzymes. The differences in melting temperature vary by 8 K with the highest temperature in the mutation F265T at 53.8°C, compared to the wild type at 48.1°C. Despite this rise in melting temperature and therefore higher stability, the enzyme does not display more activity at higher temperatures compared to the wild type (Figure 31A).

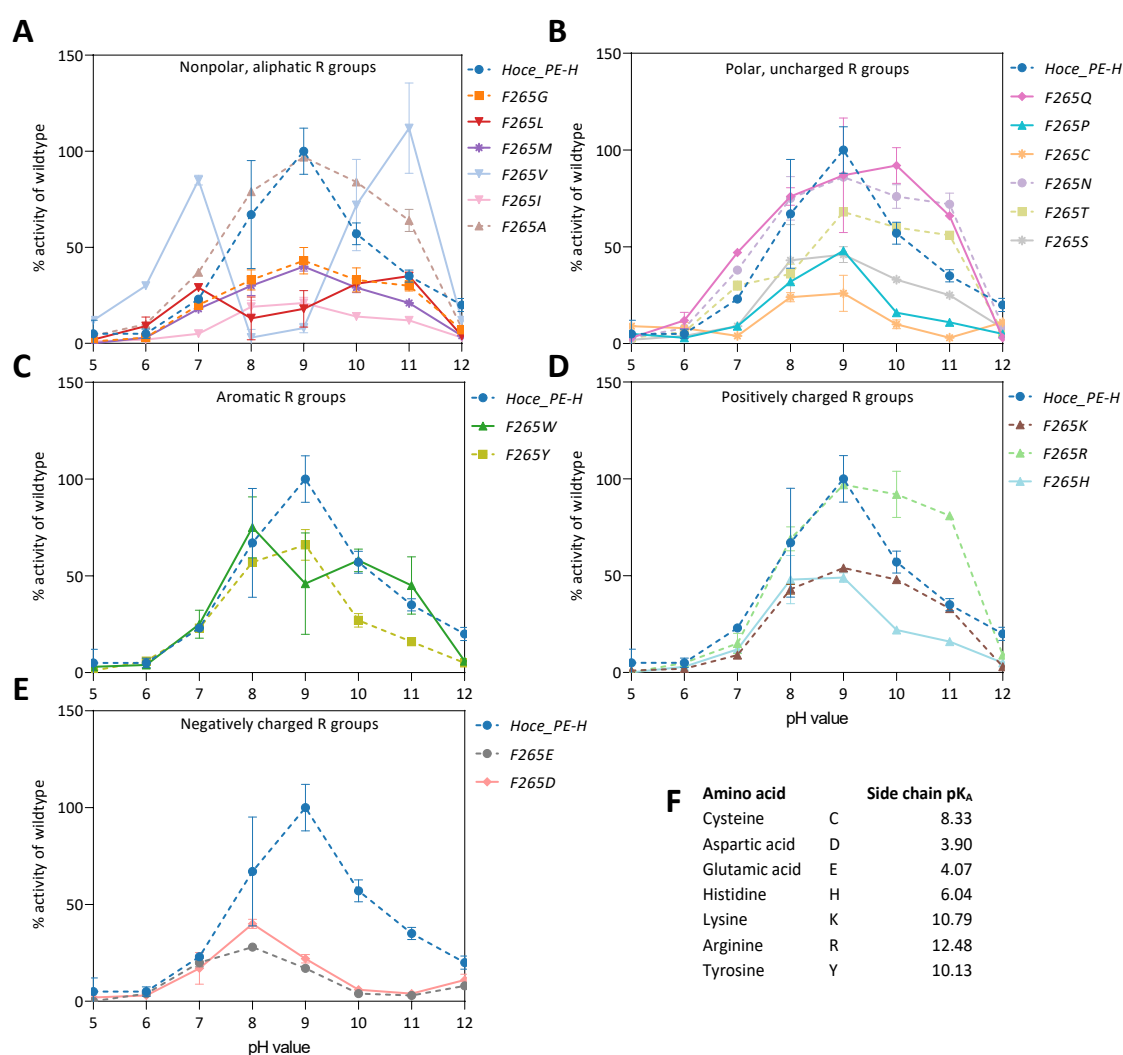


**Figure 31: Temperature stability and activity of the *Hoce*\_PE-H mutations.** (A) shows the melting temperature of the enzyme variants measured with NanoDSF with enzyme concentrations of 0.1 mg/ml. The data was obtained within associated Bachelor thesis (Königshausen, 2022) (B-F) shows the activity of the variants in 100 mM potassium phosphate buffer with 100 mM NaCl (pH 7.2) at different temperatures with the substrate *p*NPH over 10 min and 50 nM enzyme. The enzyme activity has been set relative to the enzyme activity of the wild type at the respective temperatures. The variants were separated according to the amino acid group of the interchanged amino acid. The dashed line represents 100 % of activity of the wild type enzyme.

This difference in melting temperature shows the connection between the three important parameters of psychrophilic enzymes. As discussed before, there is always a trade-off between more general stability, which makes the enzyme more resistant to higher temperatures, but which at the same time makes the active site less accessible or flexible, making these mutations less advantageous (Daniel *et al.*, 2008; Georlette *et al.*, 2004). The

most influence on flexibility seems to have the amino acid substitution F265M. Even though it has not the highest rise in temperature stability, it still seems to have the needed flexibility in or around its active site to be the most active. The variant with the highest rise in activity at higher temperatures is the F265M variant. It shows generally more activity compared to the wild type and has an exceptional rise in activity at 50°C of around 50 % more activity compared to the wild type (Figure 31B). However, there is no general correlation between higher melting temperature and higher temperature activity. The variant F265D seems to change the stability more than the active F265M variant, but does not show more activity, especially at higher temperatures.

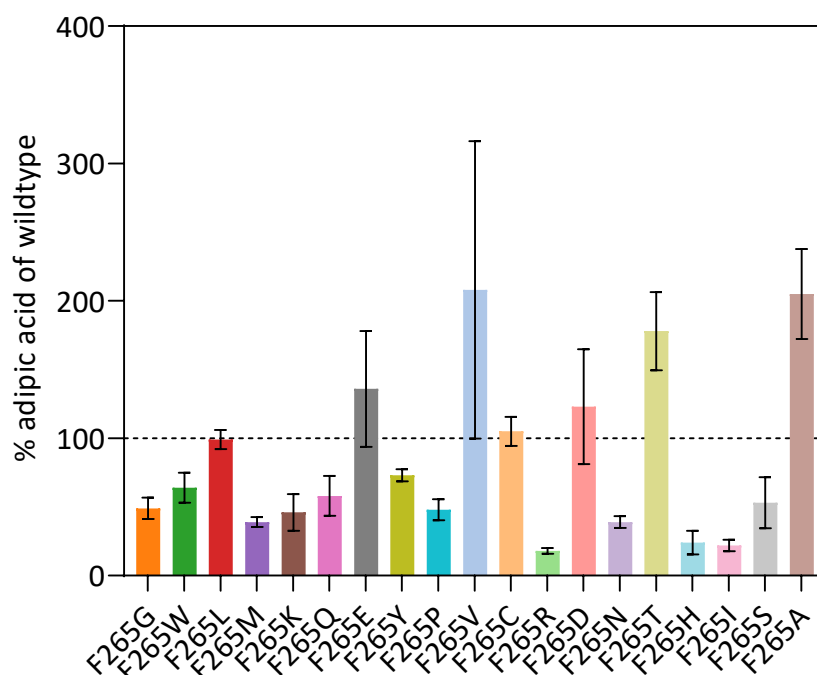
The pH activity spectrum differs remarkably between the different variants (Figure 32). Both effects (overall stability and pH dependence) cannot be explained with the classical assumption of beneficial His<sub>cat</sub>+1 mutations, i.e. the extension of the active site pocket. Hence, the mutants were bioinformatically analyzed in cooperation with Holger Gohlke at the Computational Pharmaceutical Chemistry (CPC) at the Heinrich Heine University Düsseldorf (unpublished). By looking at the amino acid changes and the corresponding behavior in addition to modeling the mutants in different environments, they were able to determine that the determinant for enhanced activity of the enzyme, is the charge of the amino acid at position 265 which changes for some residues with pH. They determined that a neutral charge of the amino acid at position 265 leads to more activity, as shown in Figure 32.



**Figure 32: pH optimum of the *Hoce*\_PE-H variants.** The data was obtained within associated Bachelor thesis (Königshausen, 2022). The activity was measured using the substrate Impranil DLN-SD. 50 nm of the respective enzyme were incubated for 10 min with 0.5 % (v/v) Impranil DLN-SD in Britton-Robinson buffer, titrated to the respective pH, at 30°C. Activity was determined as the decrease of turbidity measured via absorption at 600 nm. The activities were normalized to percentage of the highest activity of the wild type at pH 9. The amino acids are grouped according to their characteristics under normal conditions (A-E). The variant names are shortened to the amino acid substitution. (F) The amino acid side chain pK<sub>A</sub> values are depicted in the bottom right corner (Modified according to Bräse *et al.* (2008)). The F265V variant was too active for measurements at pH 8-9 and therefore show a dip.

Especially when comparing the negatively charged R groups (Figure 32E) to the positively charged R groups (Figure 32D), a shift can be observed to either more activity in physiological pH values or a shift towards basic pH values. Holger Gohlke and his group (CPC) determined the theoretical isoelectric point of every amino acid substitution and were able to see that the amino acids substitutions need to remain neutral in the respective solution.

Further looking at the activity of the variants towards polyester substrates there is an increase in activity visible towards the polyester polyurethane PU-foam regarding release of the dicarboxylic acid. Compared to the wild type, the variant F265A shows an increase in activity of around 100 % relative to the wild type (Figure 33).



**Figure 33: Released adipic acid from PU-foam of the variants relative to the released adipic acid of the wild type.** The released adipic acid was measured after 24 h of incubation at 30°C with an UPLC. 1500 nM of enzyme was used. The dashed line indicates 100 % activity of the wild type.

This change in activity might be due to generating more space at the active center (Bollinger *et al.*, 2020c). The aliphatic and small alanine residue might broaden the active site cleft compared to the bulky aromatic phenylalanine. However, also the initial change of the tyrosine residue at this position, like in *Haes*\_PE-H or *Hfor*\_PE-H, might have an impact in PU-foam degradation by forming hydrogen bonds. In the wild-type, the *Hoce*\_PE-H has a phenylalanine at this position, which might inhibit the hydrogen bond formation between the enzyme and the PU-foam, which in turn might elevate some inhibitory effects. This is also visible in chapter 3.2.7 discussing the inhibitory effect oligomeric PU has on the degradation capabilities of the enzyme set.

Another theory could be the generation of a bigger hydrophobic patch around the active site cleft (Gricajeva *et al.*, 2021). Highly hydrophobic areas ensure the attachment of the hydrophobic plastics substrate close to the active site. This can also be observed in Figure

33. The strongly hydrophobic amino acid substitutions alanine and valine show the highest activity of the set for PU-foam. However, the neutral threonine, as well as the acidic glutamic acid and aspartic acid show elevated activity towards the PU-foam. In addition, no other hydrophobic amino acid elevates the activity.

All in all, it seems that small hydrophobic amino acid substitutions close to the active center create a hydrophobic patch, as well as a broader active site cleft. This accommodates the needs of the bulky and hydrophobic PU-foam substrates the best.

### 3.4. Summarizing evaluation

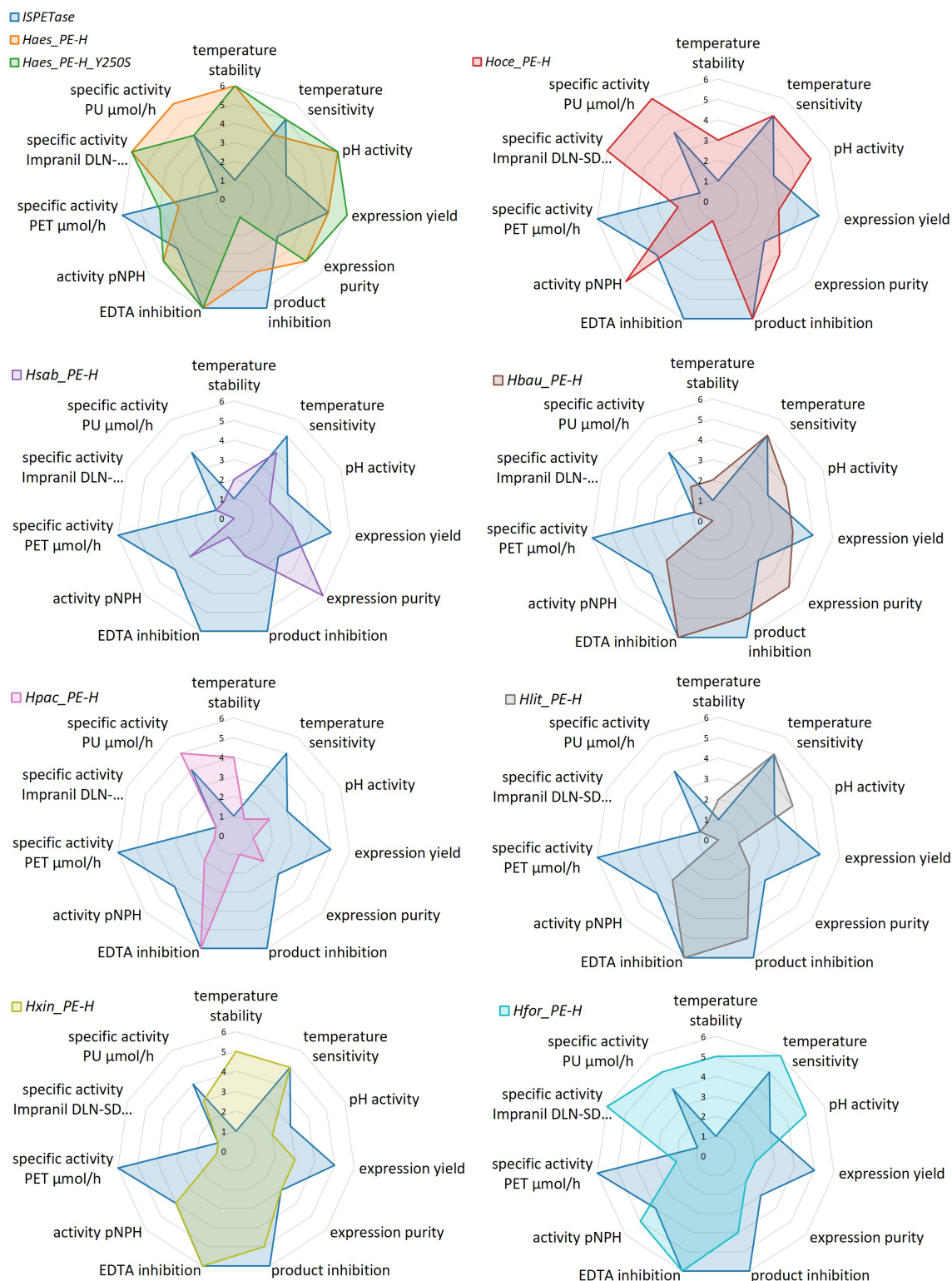
The characterization of enzymes is important to identify promising new candidates for industrial applications. In the field of plastic waste management, new enzymes are required that can degrade large quantities of plastic waste fast and in a cost-efficient manner. Enzymes that can be expressed in huge quantities with little expense are favorable. Attempts have been made to identify such enzymes using tools such as Hidden Markov Models (Danso *et al.*, 2018). However, such tools still need calibration from laboratory experiments. After characterizing, the wild-type enzymes as well as the mutated versions, the radar diagrams in Figure 34, Figure 35, and Figure 36 show an overview of the characteristics of the enzymes. Here, the characteristics are scored by a system of one to six, depending on the usefulness to the industrial application. Comparing these graphs shows which characteristics of the best performing enzymes should be addressed for enhanced activity, production, or stability.

#### 3.4.1. Insights from comparisons of wild typical *Halopseudomonas* PE-H

The enzymes in the enzyme set show a variety of differently pronounced characteristics despite their high sequence homologies (Figure 14). The enzymes are scored according to the system as explained in Table 8. Figure 34 shows the radar diagrams of the *Halopseudomonas* enzyme set.

**Table 8: Ranking of the different characteristics for the radar diagrams.** The characteristics are scored according to the max and min values of the enzyme set in the respective category.

Value	1	6
temperature stability at pH 7.2	less stable (44.7°C)	highly stable (55.6°C)
temperature sensitivity	little activity at high temperatures (<30°C)	high activity at high temperatures (>40°C)
pH activity	at low pH (optimum at 8)	at high pH (optimum at 10)
expression yield	low yield (less than 0.5 mg/ml)	high yield (more than 1 mg/ml)
expression purity	very impure	very pure
product inhibition	inhibited	not inhibited
EDTA inhibition	inhibited by EDTA	not inhibited by EDTA
activity pNPH at pH 7.2	lowest activity (0 U/mg)	highest activity (1.700 U/mg)
specific activity PET µmol/h	less than 0.01 µmol/h	more than 0.05 µmol/h
specific activity Impranil DLN ΔOD <sub>580nm</sub> /min at pH 8	less than 10 ΔOD <sub>580nm</sub> /min	more than 20 ΔOD <sub>580nm</sub> /min
specific activity PU µmol adipic acid/h at pH 7.2	less than 0.1 µmol/h	more than 0.2 µmol/h



**Figure 34: Radar diagrams of the enzyme set in relation to ISPETase.** The enzyme set was valued according to the values in Table 8. Generally, one means poor and six means great. Every enzyme is shown in comparison to the benchmark enzyme ISPETase (dark blue).

At first glance, it is noticeable that most enzymes from the set differ from the benchmark ISPETase mainly by their temperature stability and specific activity towards Impranil DLN-

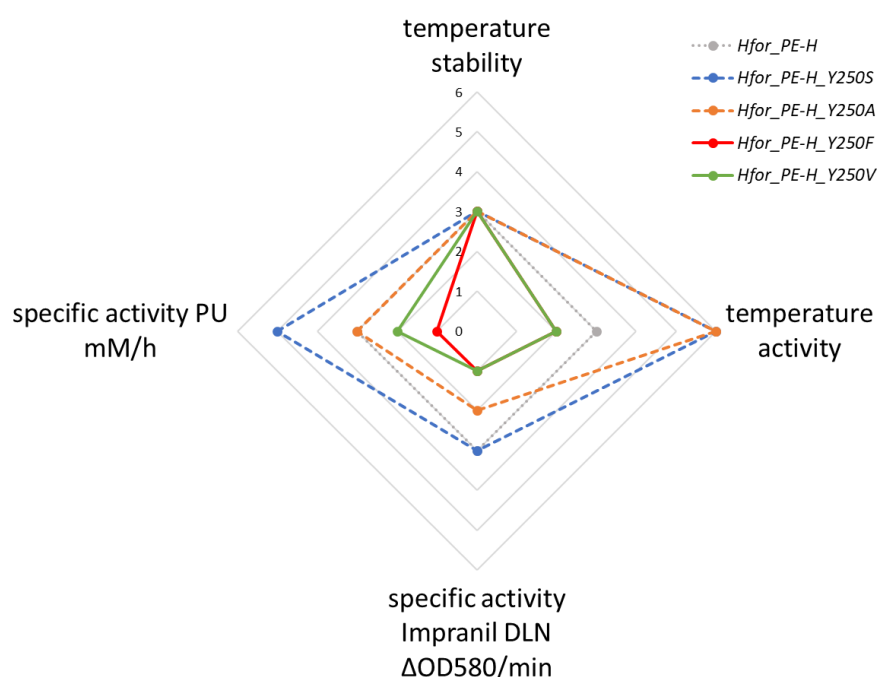


SD and PU-foam. It is noticeable, that especially *Hfor*\_PE-H and *Hoce*\_PE-H outcompete the benchmark *ISPETase* in specific activities, temperature stability and sensitivity, and pH activity. The *Haes*\_PE-H and *Haes*\_PE-H\_Y250S variants are, however, overall more active and stable compared to *Hfor*\_PE-H and *Hoce*\_PE-H.

Looking at the sequence alignment in Figure 30, there is no specific site identifiable that would explain the given results. However, the mutagenesis results were able to show some potential important sites and potential for enhanced activities.

### 3.4.2. Insights from mutagenesis experiments

Comparing the characteristics of the *Hfor*\_PE-H mutants delivers an interesting pattern. Figure 35 shows that the mutant *Hfor*\_PE-H\_Y250S has better activity at higher temperatures compared to the wild type, as well as more specific activity on PU-foam.

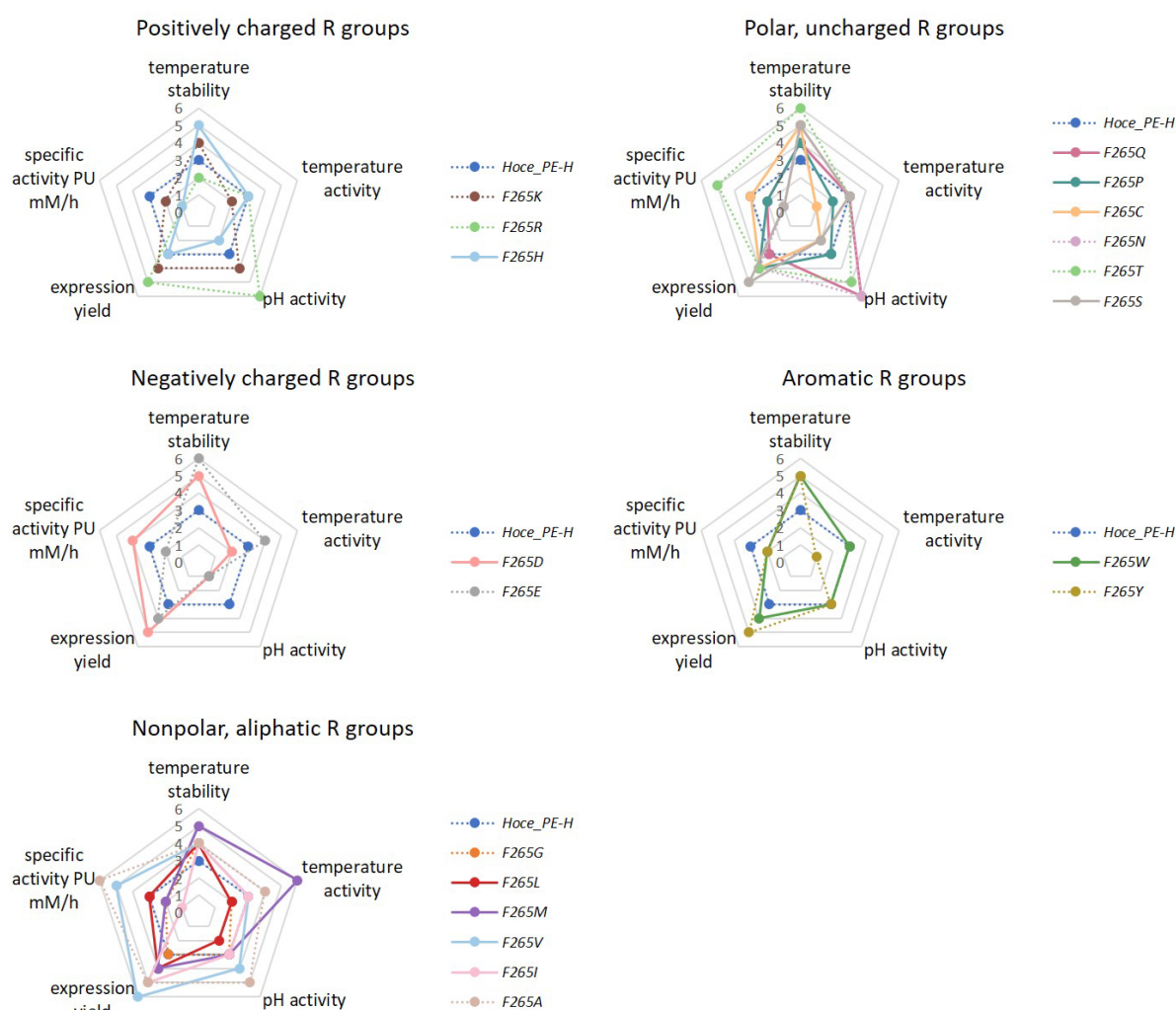


**Figure 35: Radar diagram of the *Hfor*\_PE-H mutants.** The *Hfor*\_PE-H wild type is indicated as gray dashed line. The mutants are weighted relative to the wild type activity from 1 worse to 6 better than the wild type with 3 being the same as the wild type.

Also, the variant Y250A shows enhanced activity at temperatures around 50°C, but shows no elaborate PU-foam activity, and less specific activity on Impranil DLN-SD. The variants Y250F and Y250V are overall less active than the wild type. All variants have the same temperature stability, indicating no change in the structural rigidity. Overall, the variant Y250S seems to be the best performing. This shows parallels to the findings of Bollinger *et*

*al.* (2020c) and Tournier *et al.* (2020). Here the authors also exchange the homologue amino acid at the His<sub>cat</sub>+1 position from in the case of *Haes*\_PE-H a tyrosine to a serine and in the case of LCC from a phenylalanine to an isoleucine enhancing the PET degradation or in the case of Tournier *et al.* (2020) the MHET affinity of the active site.

Comparing the *Hoce*\_PE-H variants in Figure 36, it is noticeable that temperature stability is way more influenced by the single exchange than observed with the mutants of *Hfor*\_PE-H.



**Figure 36: Radar diagrams of the *Hoce*\_PE-H mutants.** The amino acid substitutions are sorted according to their charge in a non-bound state. All enzymes are shown relative to the wild type. The mutants are weighted relative to the wild type activity from 1 worse, to 6 better than the wild type with 3 being the same as the wild type.

While the *Hfor*\_PE-H variants all have approximately the same melting temperature, the *Hoce*\_PE-Hs vary greatly with differences of up to 8°C. In addition, the activities as well as the expression yield and pH activity vary. The pH activity is especially interesting due to the connection of a higher activity for amino acid substitutions that lead to a neutral charge at

a specific pH. Looking at the PU-foam activity, the variants with changes to small hydrophobic amino acids like valine and alanine show an increase in activity up to 200 %. This might indicate better affinity and more space for the bulky and hydrophobic PU chains. Overall comparing the radar graphs of the substitutions, the F265V, F265M, and F265A variants seem to show the most improvements in overall activity and thermal stability. Those variants might be interesting candidates for future applications or further improvements for more activity, especially towards PU-foam.

## 4. Conclusion and Outlook

The goal of this work was to find, analyze, and improve polyester and polyurethane degrading enzymes. For this purpose, I formulated three research questions in the aim of this thesis:

1. Does the metagenome from plastic accumulation zones in the North Atlantic Ocean contain sequences of known polyester degrading enzymes?
2. How does the natural diversity of polyester hydrolytic enzymes from closely related organisms shape their biochemical characteristics?
3. Can general rules be derived from sequence and biochemical information and is it possible to transfer this knowledge to increase the performance of respective enzymes?

In chapter 3.1 I answered the first question by analyzing sediment samples from the North Atlantic Ocean. In these samples, I was able to find a wide variety of microorganisms and explored their polyester degrading potential using the comparative tool of HMM. Even though the HMM was not able to find novel enzymes in the sequence dataset, the approach of enriching the microbial diversity of the sediment sample on polyester resulted in the finding of polyester degrading organisms. These organisms were further evaluated by Tobias Horbach (2023) in his associated master thesis and resulted in the finding of three novel polyester hydrolases of two distinct types the PETase/bacterial cutinase similar ones (e.g. in *Pseudomonas* sp.) and an enzyme of smaller size that were not covered so far by the HMM-profile describe in Danso *et al.* (2018).

Secondly, in chapter 3.2 a collection of homologues novel polyester and polyester containing co-polymer degrading enzymes were characterized. These characterizations showed a diversity of structural motifs in otherwise highly similar enzymes with identities of more than 70 %. Despite the high sequence similarity, the enzyme *Hsab*\_PE-H showed for example a complete dependence on calcium for its activity. In addition, two enzymes *Hoce*\_PE-H and *Hfor*\_PE-H were identified as highly active and promising enzymes for further structural assessments. This knowledge opens new possibilities for directed evolution of polyester hydrolyzing enzymes. It is necessary, however, to shed light on the function of important structural parts of polyester hydrolyzing enzymes further.

In further structural assessments in chapter 3.3, an important amino acid position between the active site histidine and disulfide forming cysteine was mutated in both *Hoce*\_PE-H and

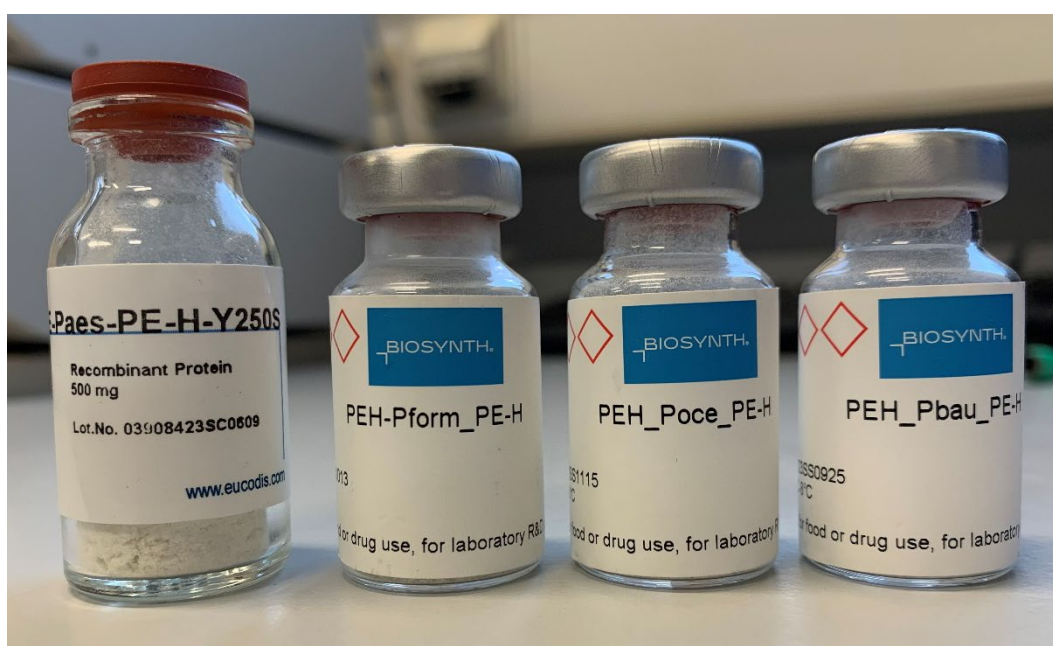
*Hfor*\_PE-H. This mutagenesis resulted in an *Hfor*\_PE-H variant that was able to degrade polyester-polyurethane foam 30 % better than the wild type enzyme by one single amino acid substitution. To elucidate the possible function of the amino acid position Nadine Königshausen (2022) performed a saturation mutagenesis on this position in an associated bachelor thesis. Trying out all possible amino acids on this position could elucidate the importance of the charge of this position for activity. Holger Gohlke and his team investigated the importance of the charge based on the laboratory results. With the information that this position can enhance activity when charged neutral, it is potentially possible to adapt similar enzymes to have higher activity in different pH values on especially polyester-polyurethane substrates and therefore aid in the further usage of polyester hydrolyzing enzymes. More experiments need to be conducted to further clarify this.

The enzyme set shows a wide spectrum of functionality towards polyester waste management. Psychrophilic enzymes, and enzymes that can be switched on with for example the addition of  $\text{CaCl}_2$ , may help in wastewater treatment in the future. Due to rising levels of waste entering the natural ecosystems every day especially in the form of microplastics, an efficient system to purify wastewater is necessary (Faber & Fritz, 2024). As de Witt *et al.* (2023) stated in their recent publication, some organisms do not possess one single polyester hydrolase, but rather have multiple hydrolases and cutinase-like enzymes that may work together in degrading polyester substrates. Preliminary experiments with cutinases from *H. formosensis* FZJ as well as from *H. litoralis* did not yet show activity towards polyester (data not shown).

In the future, coupling a polyester hydrolase with a cutinase might result in less product inhibition and potentially full degradation of the polyester substrates as seen in the degradation of *ISPETase* and *ISMHETase*. This was attempted by integrating a second active site into the PE-H from *H. aestusnigri*. This, however, did not result in a functional enzyme. It might be promising to use a linker instead to combine two enzymes and achieve better degradation of polyesters.

Besides getting an idea how different esterases might work together and which condition, the (cost-) efficient supply of ready-to-use enzyme material is an important step for application. One example would be enabling production in secretory expression systems at a larger scale. Initial trials for production with *Pichia pastoris* were conducted in cooperation with Biosynth, former Eucodis, for the most promising enzymes from the

*Halopseudomonas* PE-H set according to the discussed experiments, namely *Haes*\_PE-H\_Y250S, *Hfor*\_PE-H, *Hoce*\_PE-H, and *Hbau*\_PE-H were selected. Codon optimized genes were expressed in *P. pastoris* cultures using methanol-inducible expression at a 10 L bioreactor scale. The supernatant was concentrated, exchanged for phosphate buffer, and lyophilized, yielding >50g of material. Initial analysis of the lyophilized enzymes indicated that all four expressions yielded active enzyme (despite the glycosylation occurring in eukaryotic expression system), but, as seen for intracellular production with *E. coli*, with varying yields.



**Figure 37: By Biosynth in *Pichia pastoris* produced and lyophilized enzymes from the set.** The names were changed during this work because of the reclassification of *Halopseudomonas* species from *Paes*\_PE-H\_Y250S to *Haes*\_PE-H\_Y250S, *Pform*\_PE-H to *Hfor*\_PE-H, *Poce*\_PE-H to *Hoce*\_PE-H, and *Pbau*\_PE-H to *Hbau*\_PE-H.

This shows that the upscaling of the production of those enzymes in established industrial systems is feasible.

Interesting to see in further experiments would be the application of the best enzyme variants in environments like wastewater treatment plants to see, if the enzymes can filter out polyester fibers from the water. For this purpose, even the wild type organism could be used in wastewater treatment plants, that come from cold and salt rich habitats like *H. oceanii*.

## References

- Agostini, L., Moreira, J. C. F., Bendia, A. G., Kmit, M. C. P., Waters, L. G., Santana, M. F. M., Sumida, P. Y. G., Turra, A., & Pellizari, V. H. (2021).** Deep-sea plastisphere: Long-term colonization by plastic-associated bacterial and archaeal communities in the Southwest Atlantic Ocean. *Sci Total Environ*, 793, 148335. <https://doi.org/10.1016/j.scitotenv.2021.148335>
- Alonso, S., Santiago, G., Cea-Rama, I., Fernandez-Lopez, L., Coscolín, C., Modregger, J., Ressmann, A. K., Martínez-Martínez, M., Marrero, H., et al. (2019).** Genetically engineered proteins with two active sites for enhanced biocatalysis and synergistic chemo- and biocatalysis. *Nature Catalysis*, 3(3), 319-328. <https://doi.org/10.1038/s41929-019-0394-4>
- Amaral-Zettler, L. A., Zettler, E. R., & Mincer, T. J. (2020).** Ecology of the plastisphere. *Nat Rev Microbiol*, 18(3), 139-151. <https://doi.org/10.1038/s41579-019-0308-0>
- Amaral-Zettler, L. A., Zettler, E. R., Mincer, T. J., Klaassen, M. A., & Gallager, S. M. (2021).** Biofouling impacts on polyethylene density and sinking in coastal waters: A macro/micro tipping point? *Water Res*, 201, 117289. <https://doi.org/10.1016/j.watres.2021.117289>
- Andersen, K. R., Leksa, N. C., & Schwartz, T. U. (2013).** Optimized *E. coli* expression strain LOBSTR eliminates common contaminants from His-tag purification. *Proteins*, 81(11), 1857-1861. <https://doi.org/10.1002/prot.24364>
- Arnal, G., Anglade, J., Gavalda, S., Tournier, V., Chabot, N., Bornscheuer, U. T., Weber, G., & Marty, A. (2023).** Assessment of four engineered PET degrading enzymes considering large-scale industrial applications. *ACS Catal*, 13(20), 13156-13166. <https://doi.org/10.1021/acscatal.3c02922>
- Atiweh, G., Mikhael, A., Parrish, C. C., Banoub, J., & Le, T. T. (2021).** Environmental impact of bioplastic use: A review. *Heliyon*, 7(9), e07918. <https://doi.org/10.1016/j.heliyon.2021.e07918>
- Austin, H. P., Allen, M. D., Donohoe, B. S., Rorrer, N. A., Kearns, F. L., Silveira, R. L., Pollard, B. C., Dominick, G., Duman, R., et al. (2018).** Characterization and engineering of a plastic-degrading aromatic polyesterase. *Proc Natl Acad Sci U S A*, 115(19), E4350-E4357. <https://doi.org/10.1073/pnas.1718804115>
- Avilan, L., Lichtenstein, B. R., Konig, G., Zahn, M., Allen, M. D., Oliveira, L., Clark, M., Bemmer, V., Graham, R., et al. (2023).** Concentration-dependent inhibition of

- mesophilic PETases on poly(ethylene terephthalate) can be eliminated by enzyme engineering. *ChemSusChem*, 16(8), e202202277. <https://doi.org/10.1002/cssc.202202277>
- Avio, C. G., Gorbi, S., & Regoli, F.** (2017). Plastics and microplastics in the oceans: From emerging pollutants to emerged threat. *Mar Environ Res*, 128, 2-11. <https://doi.org/10.1016/j.marenvres.2016.05.012>
- Baath, J. A., Borch, K., Jensen, K., Brask, J., & Westh, P.** (2021). Comparative biochemistry of four polyester (PET) hydrolases\*. *Chembiochem*, 22(9), 1627-1637. <https://doi.org/10.1002/cbic.202000793>
- Baker, P. J., Poultney, C., Liu, Z., Gross, R., & Montclare, J. K.** (2012). Identification and comparison of cutinases for synthetic polyester degradation. *Appl Microbiol Biotechnol*, 93(1), 229-240. <https://doi.org/10.1007/s00253-011-3402-4>
- Barnard, E., Rubio Arias, J. J., & Thielemans, W.** (2021). Chemolytic depolymerisation of PET: a review. *Green Chemistry*, 23(11), 3765-3789. <https://doi.org/10.1039/d1gc00887k>
- Barth, M., Oeser, T., Wei, R., Then, J., Schmidt, J., & Zimmermann, W.** (2015). Effect of hydrolysis products on the enzymatic degradation of polyethylene terephthalate nanoparticles by a polyester hydrolase from *Thermobifida fusca*. *Biochemical Engineering Journal*, 93, 222-228. <https://doi.org/10.1016/j.bej.2014.10.012>
- Beck, A., Borchert, E., Delaigue, L., Deng, F., Gueroun, S., Hamm, T., Jacob, O., Kaandorp, M. L. A., Molitor, R., et al.** (2021). *NAPTRAM - North Atlantic plastic transport mechanisms, sinks, and interactions with biota*. GEOMAR. Kiel.
- Bergmann, M., Gutow, L., & Klages, M.** (2015). *Marine Anthropogenic Litter* (M. Bergmann, L. Gutow, & M. Klages, Eds.). <https://doi.org/10.1007/978-3-319-16510-3>
- Bisswanger, H.** (2014). Enzyme assays. *Perspectives in Science*, 1(1-6), 41-55. <https://doi.org/10.1016/j.pisc.2014.02.005>
- Blasiak, R., Jouffray, J. B., Amon, D. J., Claudet, J., Dunshirn, P., Sogaard Jorgensen, P., Pranindita, A., Wabnitz, C. C. C., Zhivkoplias, E., et al.** (2023). Making marine biotechnology work for people and nature. *Nat Ecol Evol*, 7(4), 482-485. <https://doi.org/10.1038/s41559-022-01976-9>



- Bollinger, A., Molitor, R., Thies, S., Koch, R., Coscolin, C., Ferrer, M., & Jaeger, K. E.** (2020a). Organic-solvent-tolerant carboxylic ester hydrolases for organic synthesis. *Appl Environ Microbiol*, 86(9). <https://doi.org/10.1128/AEM.00106-20>
- Bollinger, A., Thies, S., Katzke, N., & Jaeger, K. E.** (2020b). The biotechnological potential of marine bacteria in the novel lineage of *Pseudomonas pertucinogena*. *Microb Biotechnol*, 13(1), 19-31. <https://doi.org/10.1111/1751-7915.13288>
- Bollinger, A., Thies, S., Knieps-Grunhagen, E., Gertzen, C., Kobus, S., Hoppner, A., Ferrer, M., Gohlke, H., Smits, S. H. J., et al.** (2020c). A novel polyester hydrolase from the marine bacterium *Pseudomonas aestusnigri* - structural and functional insights. *Front Microbiol*, 11, 114. <https://doi.org/10.3389/fmicb.2020.00114>
- Bräse, S., Bülle, J., & Hüttermann, A.** (2008). *Organische und bioorganische Chemie: Das Basiswissen für Master- und Diplomprüfungen*. Wiley.
- Brott, S., Pfaff, L., Schuricht, J., Schwarz, J. N., Bottcher, D., Badenhorst, C. P. S., Wei, R., & Bornscheuer, U. T.** (2022). Engineering and evaluation of thermostable IsPETase variants for PET degradation. *Eng Life Sci*, 22(3-4), 192-203. <https://doi.org/10.1002/elsc.202100105>
- Buchholz, P. C. F., Feuerriegel, G., Zhang, H., Perez-Garcia, P., Nover, L. L., Chow, J., Streit, W. R., & Pleiss, J.** (2022). Plastics degradation by hydrolytic enzymes: The plastics-active enzymes database-PAZy. *Proteins*, 90(7), 1443-1456. <https://doi.org/10.1002/prot.26325>
- Butterworth, A., & Sayer, S.** (2017). The welfare impact on pinnipeds of marine debris and fisheries. In A. Butterworth (Ed.), *Marine Mammal Welfare* (pp. 215-239). Springer International Publishing. [https://doi.org/10.1007/978-3-319-46994-2\\_13](https://doi.org/10.1007/978-3-319-46994-2_13)
- Caldwell, A., Seavey, J., & Craig, E.** (2019). Foraging strategy impacts plastic ingestion risk in seabirds. *Limnology and Oceanography Letters*, 5(1), 163-168. <https://doi.org/10.1002/lol2.10126>
- Camacho, C., Boratyn, G. M., Joukov, V., Vera Alvarez, R., & Madden, T. L.** (2023). ElasticBLAST: accelerating sequence search via cloud computing. *BMC Bioinformatics*, 24(1), 117. <https://doi.org/10.1186/s12859-023-05245-9>
- Carniel, A., Gomes, A. D. C., Coelho, M. A. Z., & de Castro, A. M.** (2021). Process strategies to improve biocatalytic depolymerization of post-consumer PET packages in bioreactors,

- and investigation on consumables cost reduction. *Bioprocess Biosyst Eng*, 44(3), 507-516. <https://doi.org/10.1007/s00449-020-02461-y>
- Charupanit, K., Tipmanee, V., Sutthibutpong, T., & Limsakul, P.** (2022). *In silico* identification of potential sites for a plastic-degrading enzyme by a reverse screening through the protein sequence space and molecular dynamics simulations. *Molecules*, 27(10). <https://doi.org/10.3390/molecules27103353>
- Chen, Z., Wang, Y., Cheng, Y., Wang, X., Tong, S., Yang, H., & Wang, Z.** (2020). Efficient biodegradation of highly crystallized polyethylene terephthalate through cell surface display of bacterial PETase. *Sci Total Environ*, 709, 136138. <https://doi.org/10.1016/j.scitotenv.2019.136138>
- Costigan, E., Collins, A., Hatinoglu, M. D., Bhagat, K., MacRae, J., Perreault, F., & Apul, O.** (2022). Adsorption of organic pollutants by microplastics: Overview of a dissonant literature. *Journal of Hazardous Materials Advances*, 6, 100091. <https://doi.org/10.1016/j.hazadv.2022.100091>
- Cowley, P. R.** (1985). The experience curve and history of the cellophane business. *Long Range Planning*, 18(6), 84-90. [https://doi.org/10.1016/0024-6301\(85\)90068-8](https://doi.org/10.1016/0024-6301(85)90068-8)
- Cozar, A., Echevarria, F., Gonzalez-Gordillo, J. I., Irigoien, X., Ubeda, B., Hernandez-Leon, S., Palma, A. T., Navarro, S., Garcia-de-Lomas, J., et al.** (2014). Plastic debris in the open ocean. *Proc Natl Acad Sci U S A*, 111(28), 10239-10244. <https://doi.org/10.1073/pnas.1314705111>
- Crowe, J., Dobeli, H., Gentz, R., Hochuli, E., Stuber, D., & Henco, K.** (1994). 6xHis-Ni-NTA chromatography as a superior technique in recombinant protein expression/purification. In A. J. Harwood (Ed.), *Protocols for gene analysis* (Vol. 31, pp. 371-387). Humana Press. <https://doi.org/10.1385/0-89603-258-2:371>
- Cui, Y., Chen, Y., Liu, X., Dong, S., Tian, Y. e., Qiao, Y., Mitra, R., Han, J., Li, C., et al.** (2021). Computational redesign of a PETase for plastic biodegradation under ambient condition by the GRAPE Strategy. *ACS Catalysis*, 11(3), 1340-1350. <https://doi.org/10.1021/acscatal.0c05126>
- Cui, Z., Lai, Q., Dong, C., & Shao, Z.** (2008). Biodiversity of polycyclic aromatic hydrocarbon-degrading bacteria from deep sea sediments of the Middle Atlantic Ridge. *Environ Microbiol*, 10(8), 2138-2149. <https://doi.org/10.1111/j.1462-2920.2008.01637.x>

- da Silva, M. A., Cavalett, A., Spinner, A., Rosa, D. C., Jasper, R. B., Quecine, M. C., Bonatelli, M. L., Pizzirani-Kleiner, A., Corcao, G., *et al.* (2013). Phylogenetic identification of marine bacteria isolated from deep-sea sediments of the eastern South Atlantic Ocean. *Springerplus*, 2(1), 127. <https://doi.org/10.1186/2193-1801-2-127>
- Daniel, R. M., Danson, M. J., Eisenthal, R., Lee, C. K., & Peterson, M. E. (2008). The effect of temperature on enzyme activity: new insights and their implications. *Extremophiles*, 12(1), 51-59. <https://doi.org/10.1007/s00792-007-0089-7>
- Danso, D., Chow, J., & Streit, W. R. (2019). Plastics: environmental and biotechnological perspectives on microbial degradation. *Appl Environ Microbiol*, 85(19). <https://doi.org/10.1128/AEM.01095-19>
- Danso, D., Schmeisser, C., Chow, J., Zimmermann, W., Wei, R., Leggewie, C., Li, X., Hazen, T., & Streit, W. R. (2018). New insights into the function and global distribution of polyethylene terephthalate (PET)-degrading bacteria and enzymes in marine and terrestrial metagenomes. *Appl Environ Microbiol*, 84(8). <https://doi.org/10.1128/AEM.02773-17>
- de Witt, J., Molitor, R., Gatgens, J., Ortmann de Percin Northumberland, C., Kruse, L., Polen, T., Wynands, B., van Goethem, K., Thies, S., *et al.* (2023). Biodegradation of poly(ester-urethane) coatings by *Halopseudomonas formosensis*. *Microb Biotechnol*. <https://doi.org/10.1111/1751-7915.14362>
- Duan, S., Zhang, N., Chao, T., Wu, Y., & Wang, M. (2023). The structural and molecular mechanisms of type II PETases: a mini review. *Biotechnol Lett*, 45(10), 1249-1263. <https://doi.org/10.1007/s10529-023-03418-3>
- Edelheit, O., Hanukoglu, A., & Hanukoglu, I. (2009). Simple and efficient site-directed mutagenesis using two single-primer reactions in parallel to generate mutants for protein structure-function studies. *BMC Biotechnol*, 9, 61. <https://doi.org/10.1186/1472-6750-9-61>
- Erickson, E., Shakespeare, T. J., Bratti, F., Buss, B. L., Graham, R., Hawkins, M. A., Konig, G., Michener, W. E., Miscall, J., *et al.* (2022). Comparative Performance of PETase as a Function of Reaction Conditions, Substrate Properties, and Product Accumulation. *ChemSusChem*, 15(1), e202101932. <https://doi.org/10.1002/cssc.202101932>
- Faber, A., & Fritz, G. (2024). Seek and you shall find-news on the quest for novel PET-degrading enzymes. *FEBS J*, 291(1), 57-60. <https://doi.org/10.1111/febs.16958>

- Fecker, T., Galaz-Davison, P., Engelberger, F., Narui, Y., Sotomayor, M., Parra, L. P., & Ramirez-Sarmiento, C. A. (2018). Active site flexibility as a hallmark for efficient PET degradation by *I. sakaiensis* PETase. *Biophys J*, 114(6), 1302-1312. <https://doi.org/10.1016/j.bpj.2018.02.005>
- Ferrer, M., Martinez-Abarca, F., & Golyshev, P. N. (2005). Mining genomes and 'metagenomes' for novel catalysts. *Curr Opin Biotechnol*, 16(6), 588-593. <https://doi.org/10.1016/j.copbio.2005.09.001>
- Fukushima, K., Coulembier, O., Lecuyer, J. M., Almegren, H. A., Alabdulrahman, A. M., Alsewaleem, F. D., McNeil, M. A., Dubois, P., Waymouth, R. M., *et al.* (2011). Organocatalytic depolymerization of poly(ethylene terephthalate). *Journal of Polymer Science Part A: Polymer Chemistry*, 49(5), 1273-1281. <https://doi.org/10.1002/pola.24551>
- Gasteiger, E., Gattiker, A., Hoogland, C., Ivanyi, I., Appel, R. D., & Bairoch, A. (2003). ExPASy: The proteomics server for in-depth protein knowledge and analysis. *Nucleic Acids Res*, 31(13), 3784-3788. <https://doi.org/10.1093/nar/gkg563>
- Georlette, D., Blaise, V., Collins, T., D'Amico, S., Gratia, E., Hoyoux, A., Marx, J. C., Sonan, G., Feller, G., *et al.* (2004). Some like it cold: biocatalysis at low temperatures. *FEMS Microbiol Rev*, 28(1), 25-42. <https://doi.org/10.1016/j.femsre.2003.07.003>
- Geyer, R., Jambeck, J. R., & Law, K. L. (2017). Production, use, and fate of all plastics ever made. *Sci Adv*, 3(7), e1700782. <https://doi.org/10.1126/sciadv.1700782>
- Gricajeva, A., Nadda, A. K., & Gudiukaite, R. (2021). Insights into polyester plastic biodegradation by carboxyl ester hydrolases. *Journal of Chemical Technology & Biotechnology*, 97(2), 359-380. <https://doi.org/10.1002/jctb.6745>
- Gubbels, E., Heitz, T., Yamamoto, M., Chilekar, V., Zarbakhsh, S., Gepraegs, M., Köpnick, H., Schmidt, M., Brüggling, W., *et al.* (2018). Polyesters. In *Ullmann's Encyclopedia of Industrial Chemistry* (pp. 1-30). [https://doi.org/10.1002/14356007.a21\\_227.pub2](https://doi.org/10.1002/14356007.a21_227.pub2)
- Guo, B., Vanga, S. R., Lopez-Lorenzo, X., Saenz-Mendez, P., Ericsson, S. R., Fang, Y., Ye, X., Schriever, K., Bäckström, E., *et al.* (2022). Conformational selection in biocatalytic plastic degradation by PETase. *ACS Catalysis*, 12(6), 3397-3409. <https://doi.org/10.1021/acscatal.1c05548>
- Haernvall, K., Zitzenbacher, S., Wallig, K., Yamamoto, M., Schick, M. B., Ribitsch, D., & Guebitz, G. M. (2017a). Hydrolysis of ionic phthalic acid based polyesters by wastewater

- microorganisms and their enzymes. *Environ Sci Technol*, 51(8), 4596-4605. <https://doi.org/10.1021/acs.est.7b00062>
- Haernvall, K., Zitzenbacher, S., Yamamoto, M., Schick, M. B., Ribitsch, D., & Guebitz, G. M.** (2017b). A new arylesterase from *Pseudomonas pseudoalcaligenes* can hydrolyze ionic phthalic polyesters. *J Biotechnol*, 257, 70-77. <https://doi.org/10.1016/j.jbiotec.2017.01.012>
- Hall, T.** (2011). BioEdit: An important software for molecular biology. *GERF Bulletin of Biosciences*, 2(1), 60-61.
- Hanahan, D.** (1983). Studies on transformation of *Escherichia coli* with plasmids. *J Mol Biol*, 166(4), 557-580. [https://doi.org/10.1016/s0022-2836\(83\)80284-8](https://doi.org/10.1016/s0022-2836(83)80284-8)
- Harris, P. T., Maes, T., Raubenheimer, K., & Walsh, J. P.** (2023). A marine plastic cloud - Global mass balance assessment of oceanic plastic pollution. *Continental Shelf Research*, 255, 104947. <https://doi.org/10.1016/j.csr.2023.104947>
- Hermabessiere, L., Dehaut, A., Paul-Pont, I., Lacroix, C., Jezequel, R., Soudant, P., & Duflos, G.** (2017). Occurrence and effects of plastic additives on marine environments and organisms: A review. *Chemosphere*, 182, 781-793. <https://doi.org/10.1016/j.chemosphere.2017.05.096>
- Hernandez-Milian, G., Tsangaris, C., Anestis, A., Fossi, M. C., Baini, M., Caliani, I., Panti, C., Bundone, L., & Panou, A.** (2023). Monk seal faeces as a non-invasive technique to monitor the incidence of ingested microplastics and potential presence of plastic additives. *Mar Pollut Bull*, 193, 115227. <https://doi.org/10.1016/j.marpolbul.2023.115227>
- Höppe, L.** (2020). *Functional expression of novel polyester hydrolases from marine bacteria* [Bachelor thesis, Heinrich Heine University Düsseldorf]. Düsseldorf.
- Horbach, T.** (2023). *Aktivitäts- und sequenzbasiertes Screening nach Polyesterabbauenden Enzymen aus Tiefseesediment* [Master thesis, Heinrich Heine University Düsseldorf]. Düsseldorf.
- Hwang, C. Y., Zhang, G. I., Kang, S. H., Kim, H. J., & Cho, B. C.** (2009). *Pseudomonas pelagia* sp. nov., isolated from a culture of the Antarctic green alga *Pyramimonas gelidicola*. *Int J Syst Evol Microbiol*, 59(Pt 12), 3019-3024. <https://doi.org/10.1099/ij.s.0.008102-0>

- Islam, S., Apitius, L., Jakob, F., & Schwaneberg, U.** (2019). Targeting microplastic particles in the void of diluted suspensions. *Environ Int*, 123, 428-435. <https://doi.org/10.1016/j.envint.2018.12.029>
- Janes, L. E., Löwendahl, A. C., & Kazlauskas, R. J.** (1998). Quantitative screening of hydrolase libraries using pH indicators: Identifying active and enantioselective hydrolases. *Chemistry - A European Journal*, 4(11), 2324-2331. [https://doi.org/10.1002/\(sici\)1521-3765\(19981102\)4:11<2324::Aid-chem2324>3.0.Co;2-i](https://doi.org/10.1002/(sici)1521-3765(19981102)4:11<2324::Aid-chem2324>3.0.Co;2-i)
- Jeong, J. Y., Yim, H. S., Ryu, J. Y., Lee, H. S., Lee, J. H., Seen, D. S., & Kang, S. G.** (2012). One-step sequence- and ligation-independent cloning as a rapid and versatile cloning method for functional genomics studies. *Appl Environ Microbiol*, 78(15), 5440-5443. <https://doi.org/10.1128/AEM.00844-12>
- Jiang, L. Q., Carter, B. R., Feely, R. A., Lauvset, S. K., & Olsen, A.** (2019). Surface ocean pH and buffer capacity: past, present and future. *Sci Rep*, 9(1), 18624. <https://doi.org/10.1038/s41598-019-55039-4>
- Joho, Y., Vongsouthi, V., Spence, M. A., Ton, J., Gomez, C., Tan, L. L., Kaczmariski, J. A., Caputo, A. T., Royan, S., et al.** (2023). Ancestral sequence reconstruction identifies structural changes underlying the evolution of *Ideonella sakaiensis* PETase and Variants with improved stability and activity. *Biochemistry*, 62(2), 437-450. <https://doi.org/10.1021/acs.biochem.2c00323>
- Joint, I., Muhling, M., & Querellou, J.** (2010). Culturing marine bacteria - an essential prerequisite for biodiscovery. *Microb Biotechnol*, 3(5), 564-575. <https://doi.org/10.1111/j.1751-7915.2010.00188.x>
- Joo, S., Cho, I. J., Seo, H., Son, H. F., Sagong, H. Y., Shin, T. J., Choi, S. Y., Lee, S. Y., & Kim, K. J.** (2018). Structural insight into molecular mechanism of poly(ethylene terephthalate) degradation. *Nat Commun*, 9(1), 382. <https://doi.org/10.1038/s41467-018-02881-1>
- Kaandorp, M. L. A., Lobelle, D., Kehl, C., Dijkstra, H. A., & van Sebille, E.** (2023). Global mass of buoyant marine plastics dominated by large long-lived debris. *Nature Geoscience*, 16(8), 689-694. <https://doi.org/10.1038/s41561-023-01216-0>
- Kaiser, D., Kowalski, N., & Waniek, J. J.** (2017). Effects of biofouling on the sinking behavior of microplastics. *Environmental Research Letters*, 12(12), 124003. <https://doi.org/10.1088/1748-9326/aa8e8b>

- Kaul, P., & Asano, Y. (2012). Strategies for discovery and improvement of enzyme function: state of the art and opportunities. *Microb Biotechnol*, 5(1), 18-33. <https://doi.org/10.1111/j.1751-7915.2011.00280.x>
- Khambhaty, Y. (2023). Marine enzymes: exploiting bacterial resource for blue biotechnology. In M. N. Gupta (Ed.), *Some Key Topics in Chemistry and Biochemistry for Biotechnologists* (1st Edition ed., pp. 117-151). CRC Press. <https://doi.org/https://doi.org/10.1201/9781003287599>
- Kim, K. H., Roh, S. W., Chang, H. W., Nam, Y. D., Yoon, J. H., Jeon, C. O., Oh, H. M., & Bae, J. W. (2009). *Pseudomonas sabulinigri* sp. nov., isolated from black beach sand. *Int J Syst Evol Microbiol*, 59(Pt 1), 38-41. <https://doi.org/10.1099/ijs.0.65866-0>
- Knott, B. C., Erickson, E., Allen, M. D., Gado, J. E., Graham, R., Kearns, F. L., Pardo, I., Topuzlu, E., Anderson, J. J., et al. (2020). Characterization and engineering of a two-enzyme system for plastics depolymerization. *Proc Natl Acad Sci U S A*, 117(41), 25476-25485. <https://doi.org/10.1073/pnas.2006753117>
- Koelmans, A. A., Besseling, E., & Foekema, E. M. (2014). Leaching of plastic additives to marine organisms. *Environ Pollut*, 187, 49-54. <https://doi.org/10.1016/j.envpol.2013.12.013>
- Kolattukudy, P. E. (1980). Biopolyester membranes of plants: cutin and suberin. *Science*, 208(4447), 990-1000. <https://doi.org/10.1126/science.208.4447.990>
- Königshausen, N. (2022). *Bedeutung der Aminosäureposition 265 einer Polyesterhydrolase aus Pseudomonas oceani für deren biochemische Eigenschaften* [Bachelor thesis, Heinrich Heine University Düsseldorf]. Düsseldorf.
- Laemmli, U. K. (1970). Cleavage of structural proteins during the assembly of the head of bacteriophage T4. *Nature*, 227(5259), 680-685. <https://doi.org/10.1038/227680a0>
- Li, A., Sheng, Y., Cui, H., Wang, M., Wu, L., Song, Y., Yang, R., Li, X., & Huang, H. (2023). Discovery and mechanism-guided engineering of BHET hydrolases for improved PET recycling and upcycling. *Nat Commun*, 14(1), 4169. <https://doi.org/10.1038/s41467-023-39929-w>
- Li, H., Aguirre-Villegas, H. A., Allen, R. D., Bai, X., Benson, C. H., Beckham, G. T., Bradshaw, S. L., Brown, J. L., Brown, R. C., et al. (2022). Expanding plastics recycling technologies: chemical aspects, technology status and challenges. *Green Chemistry*, 24(23), 8899-9002. <https://doi.org/10.1039/d2gc02588d>

- Liu, Y., Liu, C., Liu, H., Zeng, Q., Tian, X., Long, L., & Yang, J. (2022).** Catalytic features and thermal adaptation mechanisms of a deep sea bacterial cutinase-type poly(ethylene terephthalate) hydrolase. *Front Bioeng Biotechnol*, 10, 865787. <https://doi.org/10.3389/fbioe.2022.865787>
- Lodhi, A. F., Zhang, Y., Adil, M., & Deng, Y. (2023).** Design and application of a novel culturing chip (cChip) for culturing the uncultured aquatic microorganisms. *Arch Microbiol*, 205(8), 285. <https://doi.org/10.1007/s00203-023-03613-w>
- Lorenz, P., & Eck, J. (2005).** Metagenomics and industrial applications. *Nat Rev Microbiol*, 3(6), 510-516. <https://doi.org/10.1038/nrmicro1161>
- Lynch, J. M., Knauer, K., & Shaw, K. R. (2022).** Plastic additives in the ocean. In A. L. Andrady (Ed.), *Plastics and the Ocean: Origin, Characterization, Fate, and Impacts* (pp. 43-76). <https://doi.org/10.1002/9781119768432.ch2>
- Madeira, F., Pearce, M., Tivey, A. R. N., Basutkar, P., Lee, J., Edbali, O., Madhusoodanan, N., Kolesnikov, A., & Lopez, R. (2022).** Search and sequence analysis tools services from EMBL-EBI in 2022. *Nucleic Acids Res*, 50(W1), W276-W279. <https://doi.org/10.1093/nar/gkac240>
- Madhuri, R. J., Saraswathi, M., Gowthami, K., Bhargavi, M., Divya, Y., & Deepika, V. (2019).** Recent approaches in the production of novel enzymes from environmental samples by enrichment culture and metagenomic approach. In V. Buddolla (Ed.), *Recent Developments in Applied Microbiology and Biochemistry* (pp. 251-262). Academic Press. <https://doi.org/10.1016/b978-0-12-816328-3.00019-2>
- Martin, C., Young, C. A., Valluzzi, L., & Duarte, C. M. (2022).** Ocean sediments as the global sink for marine micro- and mesoplastics. *Limnology and Oceanography Letters*, 7(3), 235-243. <https://doi.org/10.1002/lol2.10257>
- Materic, D., Hietbrink, S. t., Holzinger, R., & Niemann, H. (2023).** High nanoplastic concentrations across the North Atlantic [Preprint]. *ResearchSquare*. <https://doi.org/10.21203/rs.3.rs-3376869/v1>
- Mato, Y., Isobe, T., Takada, H., Kanehiro, H., Ohtake, C., & Kaminuma, T. (2001).** Plastic resin pellets as a transport medium for toxic chemicals in the marine environment. *Environ Sci Technol*, 35(2), 318-324. <https://doi.org/10.1021/es0010498>
- Mican, J., Jaradat, D. s. M. M., Liu, W., Weber, G., Mazurenko, S., Bornscheuer, U. T., Damborsky, J., Wei, R., & Bednar, D. (2024).** Exploring new galaxies: Perspectives on



- the discovery of novel PET-degrading enzymes. *Applied Catalysis B: Environmental*, 342, 123404. <https://doi.org/10.1016/j.apcatb.2023.123404>
- Miroux, B., & Walker, J. E.** (1996). Over-production of proteins in *Escherichia coli*: mutant hosts that allow synthesis of some membrane proteins and globular proteins at high levels. *J Mol Biol*, 260(3), 289-298. <https://doi.org/10.1006/jmbi.1996.0399>
- Miyakawa, T., Mizushima, H., Ohtsuka, J., Oda, M., Kawai, F., & Tanokura, M.** (2015). Structural basis for the Ca<sub>(2+)</sub>-enhanced thermostability and activity of PET-degrading cutinase-like enzyme from *Saccharomonospora viridis* AHK190. *Appl Microbiol Biotechnol*, 99(10), 4297-4307. <https://doi.org/10.1007/s00253-014-6272-8>
- Moharir, R. V., & Kumar, S.** (2019). Challenges associated with plastic waste disposal and allied microbial routes for its effective degradation: A comprehensive review. *Journal of Cleaner Production*, 208, 65-76. <https://doi.org/10.1016/j.jclepro.2018.10.059>
- Molitor, R., Bollinger, A., Kubicki, S., Loeschcke, A., Jaeger, K. E., & Thies, S.** (2020). Agar plate-based screening methods for the identification of polyester hydrolysis by *Pseudomonas* species. *Microb Biotechnol*, 13(1), 274-284. <https://doi.org/10.1111/1751-7915.13418>
- Mukai, K., Yamada, K., & Doi, Y.** (1993). Kinetics and mechanism of heterogeneous hydrolysis of poly[(R)-3-hydroxybutyrate] film by PHA depolymerases. *Int J Biol Macromol*, 15(6), 361-366. [https://doi.org/10.1016/0141-8130\(93\)90054-p](https://doi.org/10.1016/0141-8130(93)90054-p)
- Nawrath, C., & Poirier, Y.** (2008). Pathways for the synthesis of polyesters in plants: cutin, suberin, and polyhydroxyalkanoates. In H. J. Bohnert, H. Nguyen, & N. G. Lewis (Eds.), *Bioengineering and Molecular Biology of Plant Pathways* (Vol. 1, pp. 201-239). [https://doi.org/10.1016/s1755-0408\(07\)01008-9](https://doi.org/10.1016/s1755-0408(07)01008-9)
- Nikolaivits, E., Kanelli, M., Dimarogona, M., & Topakas, E.** (2018). A middle-aged enzyme still in its prime: recent advances in the field of cutinases. *Catalysts*, 8(12), 612. <https://doi.org/10.3390/catal8120612>
- Nisticò, R.** (2020). Polyethylene terephthalate (PET) in the packaging industry. *Polymer Testing*, 90, 106707. <https://doi.org/10.1016/j.polymertesting.2020.106707>
- Nolasco-Soria, H., Moyano-Lopez, F., Vega-Villasante, F., Del Monte-Martinez, A., Espinosa-Chaurand, D., Gisbert, E., & Nolasco-Alzaga, H. R.** (2018). Lipase and phospholipase activity methods for marine organisms. *Methods Mol Biol*, 1835, 139-167. [https://doi.org/10.1007/978-1-4939-8672-9\\_7](https://doi.org/10.1007/978-1-4939-8672-9_7)

- Numoto, N., Kamiya, N., Bekker, G. J., Yamagami, Y., Inaba, S., Ishii, K., Uchiyama, S., Kawai, F., Ito, N., *et al.* (2018). Structural Dynamics Of The PET-Degrading cutinase-like enzyme from *Saccharomonospora viridis* AHK190 in substrate-bound states elucidates the  $\text{Ca}_{(2+)}$ -driven catalytic cycle. *Biochemistry*, 57(36), 5289-5300. <https://doi.org/10.1021/acs.biochem.8b00624>
- Park, K. (1966). Deep-Sea pH. *Science*, 154(3756), 1540-1542. <https://doi.org/10.1126/science.154.3756.1540>
- Peix, A., Ramirez-Bahena, M. H., & Velazquez, E. (2018). The current status on the taxonomy of *Pseudomonas* revisited: An update. *Infect Genet Evol*, 57, 106-116. <https://doi.org/10.1016/j.meegid.2017.10.026>
- Pena-Garcia, C., Martinez-Martinez, M., Reyes-Duarte, D., & Ferrer, M. (2016). High throughput screening of esterases, lipases and phospholipases in mutant and metagenomic libraries: a review. *Comb Chem High Throughput Screen*, 19(8), 605-615. <https://doi.org/10.2174/1386207319666151110123927>
- Penczek, P., Czub, P., & Pielichowski, J. (2005). Unsaturated polyester resins: chemistry and technology. In *Crosslinking in Materials Science* (pp. 1-95). Springer Berlin Heidelberg. <https://doi.org/10.1007/b136243>
- Perez-Garcia, P., Chow, J., Costanzi, E., Gurschke, M., Dittrich, J., Dierkes, R. F., Molitor, R., Applegate, V., Feuerriegel, G., *et al.* (2023). An archaeal lid-containing feruloyl esterase degrades polyethylene terephthalate. *Commun Chem*, 6(1), 193. <https://doi.org/10.1038/s42004-023-00998-z>
- Pettersen, E. F., Goddard, T. D., Huang, C. C., Meng, E. C., Couch, G. S., Croll, T. I., Morris, J. H., & Ferrin, T. E. (2021). UCSF ChimeraX: Structure visualization for researchers, educators, and developers. *Protein Sci*, 30(1), 70-82. <https://doi.org/10.1002/pro.3943>
- Ravindranath, K., & Mashelkar, R. A. (1986). Polyethylene terephthalate—I. Chemistry, thermodynamics and transport properties. *Chemical Engineering Science*, 41(9), 2197-2214. [https://doi.org/10.1016/0009-2509\(86\)85070-9](https://doi.org/10.1016/0009-2509(86)85070-9)
- Richter, P. K., Blazquez-Sanchez, P., Zhao, Z., Engelberger, F., Wiebeler, C., Kunze, G., Frank, R., Krinke, D., Frezzotti, E., *et al.* (2023). Structure and function of the metagenomic plastic-degrading polyester hydrolase PHL7 bound to its product. *Nat Commun*, 14(1), 1905. <https://doi.org/10.1038/s41467-023-37415-x>

- Roda, S., Fernandez-Lopez, L., Benedens, M., Bollinger, A., Thies, S., Schumacher, J., Coscolin, C., Kazemi, M., Santiago, G., *et al.* (2022). A plurizyme with transaminase and hydrolase activity catalyzes cascade reactions. *Angew Chem Int Ed Engl*, 61(37), e202207344. <https://doi.org/10.1002/anie.202207344>
- Rodrigues, M. O., Abrantes, N., Goncalves, F. J. M., Nogueira, H., Marques, J. C., & Goncalves, A. M. M. (2019). Impacts of plastic products used in daily life on the environment and human health: What is known? *Environ Toxicol Pharmacol*, 72, 103239. <https://doi.org/10.1016/j.etap.2019.103239>
- Routti, H., Atwood, T. C., Bechshoft, T., Boltunov, A., Ciesielski, T. M., Desforges, J. P., Dietz, R., Gabrielsen, G. W., Jenssen, B. M., *et al.* (2019). State of knowledge on current exposure, fate and potential health effects of contaminants in polar bears from the circumpolar Arctic. *Sci Total Environ*, 664, 1063-1083. <https://doi.org/10.1016/j.scitotenv.2019.02.030>
- Rudra, B., & Gupta, R. S. (2021). Phylogenomic and comparative genomic analyses of species of the family *Pseudomonadaceae*: Proposals for the genera *Halopseudomonas* *gen. nov.* and *Atopomonas* *gen. nov.*, merger of the genus *Oblitimonas* with the genus *Thiopseudomonas*, and transfer of some misclassified species of the genus *Pseudomonas* into other genera. *Int J Syst Evol Microbiol*, 71(9). <https://doi.org/10.1099/ijsem.0.005011>
- Sanchez, D., Mulet, M., Rodriguez, A. C., David, Z., Lalucat, J., & Garcia-Valdes, E. (2014). *Pseudomonas aestusnigri* *sp. nov.*, isolated from crude oil-contaminated intertidal sand samples after the Prestige oil spill. *Syst Appl Microbiol*, 37(2), 89-94. <https://doi.org/10.1016/j.syapm.2013.09.004>
- Sanluis-Verdes, A., Colomer-Vidal, P., Rodriguez-Ventura, F., Bello-Villarino, M., Spinola-Amilibia, M., Ruiz-Lopez, E., Illanes-Vicioso, R., Castroviejo, P., Aiese Cigliano, R., *et al.* (2022). Wax worm saliva and the enzymes therein are the key to polyethylene degradation by *Galleria mellonella*. *Nat Commun*, 13(1), 5568. <https://doi.org/10.1038/s41467-022-33127-w>
- Santiago, G., Martinez-Martinez, M., Alonso, S., Bargiela, R., Coscolin, C., Golyshin, P. N., Guallar, V., & Ferrer, M. (2018). Rational engineering of multiple active sites in an ester hydrolase. *Biochemistry*, 57(15), 2245-2255. <https://doi.org/10.1021/acs.biochem.8b00274>

- Sayers, E. W., Bolton, E. E., Brister, J. R., Canese, K., Chan, J., Comeau, D. C., Connor, R., Funk, K., Kelly, C., *et al.* (2022). Database resources of the national center for biotechnology information. *Nucleic Acids Res*, 50(D1), D20-D26. <https://doi.org/10.1093/nar/gkab1112>
- Scandola, M., Focarete, M. L., & Frisoni, G. (1998). Simple kinetic model for the heterogeneous enzymatic hydrolysis of natural poly(3-hydroxybutyrate). *Macromolecules*, 31(12), 3846-3851. <https://doi.org/10.1021/ma980137y>
- Sevilla, M. E., Garcia, M. D., Perez-Castillo, Y., Armijos-Jaramillo, V., Casado, S., Vizuite, K., Debut, A., & Cerda-Mejia, L. (2023). Degradation of PET bottles by an engineered *Ideonella sakaiensis* PETase. *Polymers (Basel)*, 15(7). <https://doi.org/10.3390/polym15071779>
- Sheel, A., & Pant, D. (2019). Chemical depolymerization of PET bottles via glycolysis. In S. Thomas, A. Rane, K. Kanny, A. V.K., & M. G. Thomas (Eds.), *Recycling of Polyethylene Terephthalate Bottles* (pp. 61-84). William Andrew Publishing. <https://doi.org/10.1016/b978-0-12-811361-5.00004-3>
- Sin, L. T., & Tueen, B. S. (2023). Eco-profile of plastics. In L. T. Sin & B. S. Tueen (Eds.), *Plastics and Sustainability* (pp. 45-89). Elsevier. <https://doi.org/10.1016/b978-0-12-824489-0.00010-6>
- Sinha, V., Patel, M. R., & Patel, J. V. (2008). PET waste management by chemical recycling: a review. *Journal of Polymers and the Environment*, 18(1), 8-25. <https://doi.org/10.1007/s10924-008-0106-7>
- Smith, C., & Ferrer-Gonzalez, F. (2018). *Artificial Seawater Medium*. Retrieved 18.12.2023 from <https://www.protocols.io/view/artificial-seawater-medium-yxmvmmzz5g3pe/v1>
- Sobecky, P. A., & Hazen, T. H. (2009). Horizontal gene transfer and mobile genetic elements in marine systems. In M. B. Gogarten, J. P. Gogarten, & L. C. Olendzenski (Eds.), *Horizontal Gene Transfer: Genomes in Flux* (pp. 435-453). Humana Press. [https://doi.org/10.1007/978-1-60327-853-9\\_25](https://doi.org/10.1007/978-1-60327-853-9_25)
- Sogin, M. L., Morrison, H. G., Huber, J. A., Mark Welch, D., Huse, S. M., Neal, P. R., Arrieta, J. M., & Herndl, G. J. (2006). Microbial diversity in the deep sea and the underexplored "rare biosphere". *Proc Natl Acad Sci U S A*, 103(32), 12115-12120. <https://doi.org/10.1073/pnas.0605127103>

- Sonke, J. E., Koenig, A. M., Yakovenko, N., Hagelskjær, O., Margenat, H., Hansson, S. V., De Vleeschouwer, F., Magand, O., Le Roux, G., et al.** (2022). A mass budget and box model of global plastics cycling, degradation and dispersal in the land-ocean-atmosphere system. *Microplastics and Nanoplastics*, 2(1). <https://doi.org/10.1186/s43591-022-00048-w>
- Stewart, E. J.** (2012). Growing unculturable bacteria. *J Bacteriol*, 194(16), 4151-4160. <https://doi.org/10.1128/JB.00345-12>
- Studier, F. W.** (2005). Protein production by auto-induction in high density shaking cultures. *Protein Expr Purif*, 41(1), 207-234. <https://doi.org/10.1016/j.pep.2005.01.016>
- Tamura, K., Stecher, G., & Kumar, S.** (2021). MEGA11: molecular evolutionary genetics analysis version 11. *Mol Biol Evol*, 38(7), 3022-3027. <https://doi.org/10.1093/molbev/msab120>
- Tarazona, N. A., Wei, R., Brott, S., Pfaff, L., Bornscheuer, U. T., Lendlein, A., & Machatschek, R.** (2022). Rapid depolymerization of poly(ethylene terephthalate) thin films by a dual-enzyme system and its impact on material properties. *Chem Catal*, 2(12), 3573-3589. <https://doi.org/10.1016/j.checat.2022.11.004>
- Thapa, S., Li, H., J, O. H., Bhatti, S., Chen, F. C., Nasr, K. A., Johnson, T., & Zhou, S.** (2019). Biochemical characteristics of microbial enzymes and their significance from industrial perspectives. *Mol Biotechnol*, 61(8), 579-601. <https://doi.org/10.1007/s12033-019-00187-1>
- Thompson, R. C., Olsen, Y., Mitchell, R. P., Davis, A., Rowland, S. J., John, A. W., McGonigle, D., & Russell, A. E.** (2004). Lost at sea: where is all the plastic? *Science*, 304(5672), 838. <https://doi.org/10.1126/science.1094559>
- Thomsen, T. B., Almdal, K., & Meyer, A. S.** (2023). Significance of poly(ethylene terephthalate) (PET) substrate crystallinity on enzymatic degradation. *New Biotechnol*, 78, 162-172. <https://doi.org/10.1016/j.nbt.2023.11.001>
- Thomsen, T. B., Hunt, C. J., & Meyer, A. S.** (2022). Influence of substrate crystallinity and glass transition temperature on enzymatic degradation of polyethylene terephthalate (PET). *New Biotechnol*, 69, 28-35. <https://doi.org/10.1016/j.nbt.2022.02.006>
- Tijsskens, L. M., Greiner, R., Biekman, E. S., & Konietzny, U.** (2001). Modeling the effect of temperature and pH on activity of enzymes: the case of phytases. *Biotechnol Bioeng*,

- 72(3), 323-330. [https://doi.org/10.1002/1097-0290\(20010205\)72:3<323::aid-bit9>3.0.co;2-i](https://doi.org/10.1002/1097-0290(20010205)72:3<323::aid-bit9>3.0.co;2-i)
- Tournier, V., Duquesne, S., Guillamot, F., Cramail, H., Taton, D., Marty, A., & Andre, I.** (2023). Enzymes' power for plastics degradation. *Chem Rev*, 123(9), 5612-5701. <https://doi.org/10.1021/acs.chemrev.2c00644>
- Tournier, V., Topham, C. M., Gilles, A., David, B., Folgoas, C., Moya-Leclair, E., Kamionka, E., Desrousseaux, M. L., Texier, H., et al.** (2020). An engineered PET depolymerase to break down and recycle plastic bottles. *Nature*, 580(7802), 216-219. <https://doi.org/10.1038/s41586-020-2149-4>
- Urbanek, A. K., Kosiorowska, K. E., & Mironczuk, A. M.** (2021). Current knowledge on polyethylene terephthalate degradation by genetically modified microorganisms. *Front Bioeng Biotechnol*, 9, 771133. <https://doi.org/10.3389/fbioe.2021.771133>
- Valvason, L.** (2020). *Klonierung, Expression und Reinigung von Polyesterasen aus verschiedenen Bakterien der Gattung Pseudomonas* [Bachelor thesis, Heinrich Heine University Düsseldorf]. Düsseldorf.
- Van Rossum G, D. F.** (2009). *Python 3 Reference Manual*. CreateSpace.
- van Seville, E., Aliani, S., Law, K. L., Maximenko, N., Alsina, J. M., Bagaev, A., Bergmann, M., Chapron, B., Chubarenko, I., et al.** (2020). The physical oceanography of the transport of floating marine debris. *Environmental Research Letters*, 15(2), 023003. <https://doi.org/10.1088/1748-9326/ab6d7d>
- van Seville, E., Wilcox, C., Lebreton, L., Maximenko, N., Hardesty, B. D., van Franeker, J. A., Eriksen, M., Siegel, D., Galgani, F., et al.** (2015). A global inventory of small floating plastic debris. *Environmental Research Letters*, 10(12), 124006. <https://doi.org/10.1088/1748-9326/10/12/124006>
- Wackett, L. P.** (2004). Novel biocatalysis by database mining. *Curr Opin Biotechnol*, 15(4), 280-284. <https://doi.org/10.1016/j.copbio.2004.05.003>
- Wang, M. Q., & Sun, L.** (2016). *Pseudomonas oceani* sp. nov., isolated from deep seawater. *Int J Syst Evol Microbiol*, 66(10), 4250-4255. <https://doi.org/10.1099/ijsem.0.001343>
- Wei, R., Oeser, T., Barth, M., Weigl, N., Lübs, A., Schulz-Siegmund, M., Hacker, M. C., & Zimmermann, W.** (2014). Turbidimetric analysis of the enzymatic hydrolysis of polyethylene terephthalate nanoparticles. *Journal of Molecular Catalysis B: Enzymatic*, 103, 72-78. <https://doi.org/10.1016/j.molcatb.2013.08.010>

- Wei, R., Oeser, T., Schmidt, J., Meier, R., Barth, M., Then, J., & Zimmermann, W.** (2016). Engineered bacterial polyester hydrolases efficiently degrade polyethylene terephthalate due to relieved product inhibition. *Biotechnol Bioeng*, 113(8), 1658-1665. <https://doi.org/10.1002/bit.25941>
- Wei, R., von Haugwitz, G., Pfaff, L., Mican, J., Badenhorst, C. P. S., Liu, W., Weber, G., Austin, H. P., Bednar, D., et al.** (2022). Mechanism-based design of efficient PET hydrolases. *ACS Catal*, 12(6), 3382-3396. <https://doi.org/10.1021/acscatal.1c05856>
- Werner, A. Z., Clare, R., Mand, T. D., Pardo, I., Ramirez, K. J., Haugen, S. J., Bratti, F., Dexter, G. N., Elmore, J. R., et al.** (2021). Tandem chemical deconstruction and biological upcycling of poly(ethylene terephthalate) to beta-ketoadipic acid by *Pseudomonas putida* KT2440. *Metab Eng*, 67, 250-261. <https://doi.org/10.1016/j.ymben.2021.07.005>
- Wilcox, C., Puckridge, M., Schuyler, Q. A., Townsend, K., & Hardesty, B. D.** (2018). A quantitative analysis linking sea turtle mortality and plastic debris ingestion. *Sci Rep*, 8(1), 12536. <https://doi.org/10.1038/s41598-018-30038-z>
- Winkler, U. K., & Stuckmann, M.** (1979). Glycogen, hyaluronate, and some other polysaccharides greatly enhance the formation of exolipase by *Serratia marcescens*. *J Bacteriol*, 138(3), 663-670. <https://doi.org/10.1128/jb.138.3.663-670.1979>
- Woodall, L. C., Sanchez-Vidal, A., Canals, M., Paterson, G. L., Coppock, R., Sleight, V., Calafat, A., Rogers, A. D., Narayanaswamy, B. E., et al.** (2014). The deep sea is a major sink for microplastic debris. *R Soc Open Sci*, 1(4), 140317. <https://doi.org/10.1098/rsos.140317>
- Xin, J., Zhang, Q., Huang, J., Huang, R., Jaffery, Q. Z., Yan, D., Zhou, Q., Xu, J., & Lu, X.** (2021). Progress in the catalytic glycolysis of polyethylene terephthalate. *J Environ Manage*, 296, 113267. <https://doi.org/10.1016/j.jenvman.2021.113267>
- Yoshida, S., Hiraga, K., Takehana, T., Taniguchi, I., Yamaji, H., Maeda, Y., Toyohara, K., Miyamoto, K., Kimura, Y., et al.** (2016). A bacterium that degrades and assimilates poly(ethylene terephthalate). *Science*, 351(6278), 1196-1199. <https://doi.org/10.1126/science.aad6359>
- Yoshida, S., Hiraga, K., Taniguchi, I., & Oda, K.** (2021). *Ideonella sakaiensis*, PETase, and MHETase: From identification of microbial PET degradation to enzyme characterization. *Methods Enzymol*, 648, 187-205. <https://doi.org/10.1016/bs.mie.2020.12.007>

---

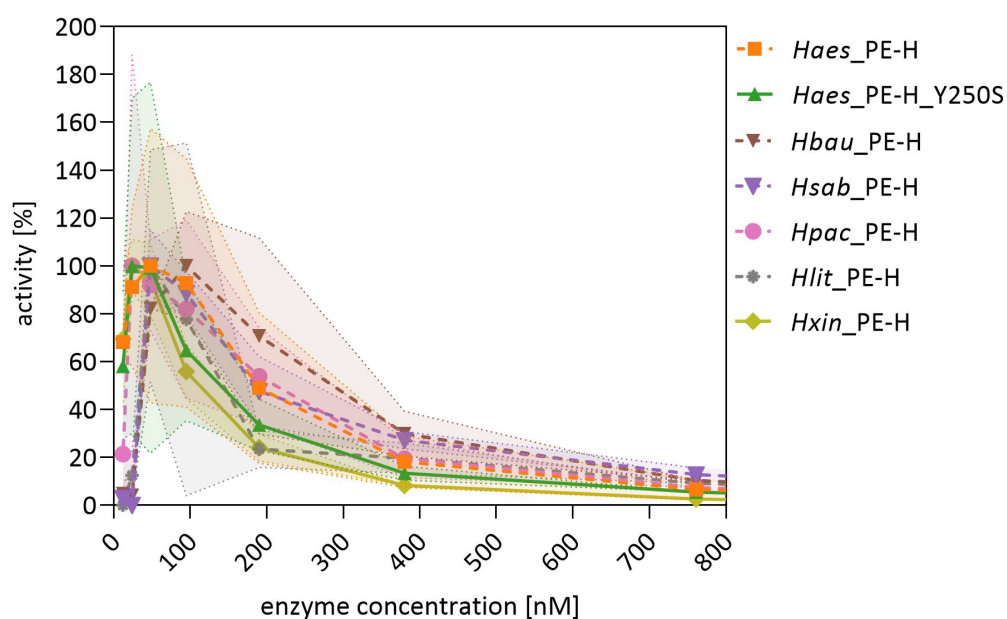
Zinger, L., Amaral-Zettler, L. A., Fuhrman, J. A., Horner-Devine, M. C., Huse, S. M., Welch, D. B., Martiny, J. B., Sogin, M., Boetius, A., *et al.* (2011). Global patterns of bacterial beta-diversity in seafloor and seawater ecosystems. *PLoS One*, 6(9), e24570. <https://doi.org/10.1371/journal.pone.0024570>



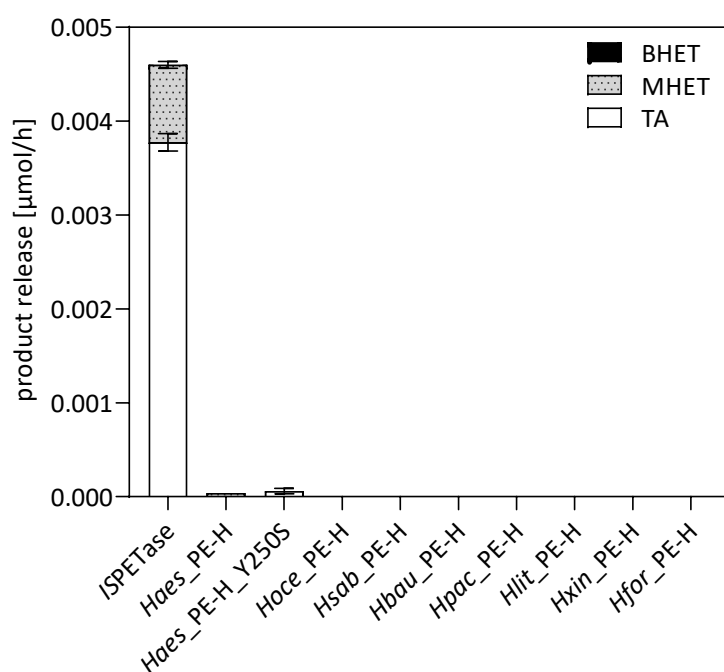
## Appendix

**Table 9: List of all used primers in this work.**

Primer name	sequence 5' to 3'	Donor organism/plasmid	Use
RM_NZ_FOGN-FW_Slic	TTTAAGAAGGAGATATACATATGATCAATAAAATCTATC	<i>Halopseudomonas bauzanensis</i>	Preparation of expression plasmid
RM_NZ_FOGN-RV_Slic	TGGTGGTGGTGGTCTCGAGGTAAGGGCAGTTGCCGCGGTAC	<i>Halopseudomonas bauzanensis</i>	Preparation of expression plasmid
RM_NZ_PPSK-FW_Ndel	CATATGTACCCAACAACAAAAACAC	<i>Halopseudomonas oceani</i>	Preparation of expression plasmid
RM_NZ_PPSK-RV_XhoI	CTCGAGGTACGGGCAGTTGCCGCGATAAC	<i>Halopseudomonas oceani</i>	Preparation of expression plasmid
RM_NZ_LT62-FW_Ndel	CATATGATCAATAAGAACTTACCCAG	<i>Halopseudomonas litoralis</i>	Preparation of expression plasmid
RM_NZ_LT62-RV_XhoI	CTCGAGGTACGGGCAATTGCCACGGTATTC	<i>Halopseudomonas litoralis</i>	Preparation of expression plasmid
RM_Psab_NdeI_FW	ATATAT CATATG ATCAACAATAAGCAGAAAAAG	<i>Halopseudomonas sabulinigri</i>	Preparation of expression plasmid
RM_Psab_XhoI_RV	ATATAT CTCGAG GTAGACGCAGTTACCACGGTAC	<i>Halopseudomonas sabulinigri</i>	Preparation of expression plasmid
RM_Pxin_NdeI_FW	ATATAT CATATG AATAACAACTATTCCCGAAG	<i>Halopseudomonas xinjiangensis</i>	Preparation of expression plasmid
RM_Pxin_XhoI_RV	ATATAT CTCGAG GTACGGGCAGTTACCACGGTAC	<i>Halopseudomonas xinjiangensis</i>	Preparation of expression plasmid
PE-HPpa_FW_Ndel	AGA GAG CAT ATG ATG CCA TTT AAC AAG AAA AG	<i>Halopseudomonas pachastrellae</i>	Preparation of expression plasmid
PE-HPpa_RV_XhoI	ATA TAT CTC GAG GTA CGG GCA GTT ACC GCG ATA G	<i>Halopseudomonas pachastrellae</i>	Preparation of expression plasmid
RM_Pfor_PE-H_Ndel_fw	ATATATCATATGATCAATAACATCTTCCCGAAATC	<i>Halopseudomonas formosensis</i>	Preparation of expression plasmid
RM_Pfor_PE-H_XhoI_rv	ATATATCTCGAGAGTACGGGCAATTGCCCGCGG	<i>Halopseudomonas formosensis</i>	Preparation of expression plasmid
AB_PEH_D129H_fw	CACCGGCTTTCATCACGCCGCCAGCCGCTG	pET22b_Haes_PE-H	Mutagenesis of Haes_PE-H
AB_PEH_D129H_rv	CACGGCTCGGCGGCTGATGAAAGCCGCTG	pET22b_Haes_PE-H	Mutagenesis of Haes_PE-H
AB_PEH_D238S_fw	TCGCCTCCAGCATCTCCAAGGCTTTGTGG	pET22b_Haes_PE-H	Mutagenesis of Haes_PE-H
AB_PEH_D238S_rv	CCACAAAGGCTTGGAGATGCTGGAAGGCAG	pET22b_Haes_PE-H	Mutagenesis of Haes_PE-H
AB_PEH_Q137E_fw	CCGAGCCGTGCGGTGAGATCAACAACGCACTG	pET22b_Haes_PE-H	Mutagenesis of Haes_PE-H
AB_PEH_Q137E_rv	CAGTGGCTTGTGATCTCACGCGCAGGGCTCGG	pET22b_Haes_PE-H	Mutagenesis of Haes_PE-H
AB_PEH_T124L_fw	GTCATGACCATTGACCTGAACACCGGCTTTG	pET22b_Haes_PE-H	Mutagenesis of Haes_PE-H
AB_PEH_T124L_rv2	GCCGGTGTTCAGGTCAATGGTCATGAC	pET22b_Haes_PE-H	Mutagenesis of Haes_PE-H
AB_PEH_W269D_fw	CGGTTCCGGGTGTCCGATATGAAACTGCATCTG	pET22b_Haes_PE-H	Mutagenesis of Haes_PE-H
AB_PEH_W269D_rv	CAGATGCAGTTTCATATCGGACACCCCGAACCG	pET22b_Haes_PE-H	Mutagenesis of Haes_PE-H
RM_4_K187E_FW	CAGTGAAGGTCGTATCGAA GCAGCCATTCCGCTG	pET22b_Haes_PE-H	Mutagenesis of Haes_PE-H
RM_4_K187E_RV	CAGCGGAATGGCTGCTTCGATACGACCTCACTG	pET22b_Haes_PE-H	Mutagenesis of Haes_PE-H
RM_1_Y81H_FW	GCGGCACCATTTACCAT CCGACAGGCACAACC	pET22b_Haes_PE-H	Mutagenesis of Haes_PE-H
RM_1_Y81H_RV	GGTTGTGCTGTGCGATGGTAAATGTGCGCGC	pET22b_Haes_PE-H	Mutagenesis of Haes_PE-H
RM_4_D161S_R164H_FW	GTTCGCGGCATGATCTCC ACCAATCAT CTGGGCGTCATTGGC	pET22b_Haes_PE-H	Mutagenesis of Haes_PE-H
RM_4_D161S_R164H_RV	GCCAATGACGCCAGATGATTGGTGAGATCATGCCGCGAAC	pET22b_Haes_PE-H	Mutagenesis of Haes_PE-H
RM_123_P155S_FW	CAGCCGCAGCTCCAGCTCC GTTCGCGGCATGATC	pET22b_Haes_PE-H	Mutagenesis of Haes_PE-H
RM_123_P155S_RV	GATCATGCCGCGAACGAGCTGGAGCTGCGGCTG	pET22b_Haes_PE-H	Mutagenesis of Haes_PE-H
RM_3_Y81H_T83D_FW	GGCGGCACCATTTACCAT CCGGAT GGCACAACCGGCACTATG	pET22b_Haes_PE-H	Mutagenesis of Haes_PE-H
RM_3_Y81H_T83D_RV	GCCAATGCCGTTGTGCCATCCGGATGGTAAATGGTGCCGCC	pET22b_Haes_PE-H	Mutagenesis of Haes_PE-H
RM_1_R63D_FW	GGTCAGTACAGCGTCGAT TCCAGCCGTGTCTCC	pET22b_Haes_PE-H	Mutagenesis of Haes_PE-H
RM_1_R63D_RV	GGAGACACGGCTGGAATCGACGCTGTACTGACC	pET22b_Haes_PE-H	Mutagenesis of Haes_PE-H
RM_2_Y81H_T83E_FW	GGCGGCACCATTTACCAT CCGGAA GGCACAACCGGCACTATG	pET22b_Haes_PE-H	Mutagenesis of Haes_PE-H
RM_2_Y81H_T83E_RV	CATAGTGCCTGTTGTGCTTCCGGATGGTAAATGGTGCCGCC	pET22b_Haes_PE-H	Mutagenesis of Haes_PE-H
RM_23_R63A_FW	GGTCAGTACAGCGTCGCG TCCAGCCGTGTCTCC	pET22b_Haes_PE-H	Mutagenesis of Haes_PE-H
RM_23_R63A_RV	GGAGACACGGCTGGACGCGACGCTGTACTGACC	pET22b_Haes_PE-H	Mutagenesis of Haes_PE-H
RM_1_Y81H_FW_NEU	GATCGCGGTGAGTACAGCGTCCAT CCGACAGGCAC	pET22b_Haes_PE-H	Mutagenesis of Haes_PE-H
RM_1_Y81H_RV_NEU	GTGCCTGTGCGGATGGACGCTGTACTGACCGGATC	pET22b_Haes_PE-H	Mutagenesis of Haes_PE-H
RM_123_P155S_FW_NEU	CAGAACACCGCAGCTCCAGCTCC GTTCGCGGC	pET22b_Haes_PE-H	Mutagenesis of Haes_PE-H
RM_123_P155S_RV_NEU	GCCGCGAACGAGCTGGAGCTGCGGCTGTTCTG	pET22b_Haes_PE-H	Mutagenesis of Haes_PE-H
RM_1_R63D_FW_NEU	GATCGCGGTGAGTACAGCGTCGAT TCCAGCCGTGTC	pET22b_Haes_PE-H	Mutagenesis of Haes_PE-H
RM_1_R63D_RV_NEU	GACACGGCTGGAATCGACGCTGTACTGACCGGATC	pET22b_Haes_PE-H	Mutagenesis of Haes_PE-H
RM_23_R63A_FW_NEU	GATCGCGGTGAGTACAGCGTCGCG TCCAGCCGTGTC	pET22b_Haes_PE-H	Mutagenesis of Haes_PE-H
RM_23_R63A_RV_NEU	GACACGGCTGGACGCGACGCTGTACTGACCGGATC	pET22b_Haes_PE-H	Mutagenesis of Haes_PE-H
RM_Poce_F265S_FW	GGTGGCAGCCACAGCTGTGCAATGGTGCC	pET22b_Hoce_PE-H	Mutagenesis of Hoce_PE-H
RM_Poce_F265S_RV	CCACCATTTGGCACAGCTGTGGTGCCACCG	pET22b_Hoce_PE-H	Mutagenesis of Hoce_PE-H
RM_Poce_F265A_FW	GGTGGCAGCCACGCGTGTGCCAATGGTGCC	pET22b_Hoce_PE-H	Mutagenesis of Hoce_PE-H
RM_Poce_F265A_RV	CCACCATTTGGCACACGCTGTGGTGCCACCG	pET22b_Hoce_PE-H	Mutagenesis of Hoce_PE-H
RM_Poce_F265I_FW	GGTGGCAGCCACATTTGTGCAATGGTGCC	pET22b_Hoce_PE-H	Mutagenesis of Hoce_PE-H
RM_Poce_F265I_RV	CCACCATTTGGCACAAATGTGGTGCCACCG	pET22b_Hoce_PE-H	Mutagenesis of Hoce_PE-H
RM_Pfor_PE-H_Y250S_FW	CGGCACACATTCTTGTGCAAAACG	pET21a_Hfor_PE-H	Mutagenesis of Hfor_PE-H
RM_Pfor_PE-H_Y250S_RV	CGTTTGCAACAAGATGTGTGCCG	pET21a_Hfor_PE-H	Mutagenesis of Hfor_PE-H
RM_Pfor_PE-H_Y250A_FW	CGGCACACATGCGTGTGCAAAACG	pET21a_Hfor_PE-H	Mutagenesis of Hfor_PE-H
RM_Pfor_PE-H_Y250A_RV	CGTTTGCAACACGATGTGTGCCG	pET21a_Hfor_PE-H	Mutagenesis of Hfor_PE-H
RM_Pfor_PE-H_Y250V_FW	CGGCACACATGTGTGTGCAAAACG	pET21a_Hfor_PE-H	Mutagenesis of Hfor_PE-H
RM_Pfor_PE-H_Y250V_RV	CGTTTGCAACACATGTGTGCCG	pET21a_Hfor_PE-H	Mutagenesis of Hfor_PE-H
RM_Pfor_PE-H_Y250F_FW	CGGCACACATTTTGTGCAAAACG	pET21a_Hfor_PE-H	Mutagenesis of Hfor_PE-H
RM_Pfor_PE-H_Y250F_RV	CGTTTGCACAAAATGTGTGCCG	pET21a_Hfor_PE-H	Mutagenesis of Hfor_PE-H



**Figure 38: Relationship of enzyme concentration and enzyme activity.** Activity of the characterized enzymes on the substrate *p*NPH at 30°C for 10 min with varying enzyme concentration. The enzyme activity is relative to the highest activity of every enzyme. The error bars are shown as shadows in the corresponding color.



**Figure 39: Enzymatic activity of 1500 nM enzyme solution on amorphous PET-film over 96 h of incubation at 30°C.** Samples were taken every 24 h and measured after filtration (MWCO 10,000) in an UPLC. The activity was measured as release of BHET, MHET or TA per hour in  $\mu\text{mol}$  [ $\mu\text{mol/h}$ ].

## Acknowledgments

Vielen Dank zunächst einmal an Herr Prof. Jäger und Herr Prof. Pietruszka für die Übernahme der Betreuung und des Mentoring. Herrn Jäger möchte ich noch einmal besonders für die aufmunternden Gespräche danken.

Des Weiteren möchte ich mich besonders bei Stephan Thies bedanken. Danke für deine stete Bereitschaft mir mit allen Problemen und Fragestellungen beiseitezustehen und dir alle meine Probleme mit einem Lächeln anzuhören. Dazu möchte ich auch besonders Alexander Bollinger für die großartigen Diskussionen und die stete Hilfe bei allen Belangen danken. Ohne euch beide hätte ich das nicht so hinbekommen.

Vielen Dank auch an die Studenten, die mir so tatkräftig bei meiner Arbeit geholfen haben. Danke an Tobias Horbach, Nadine Königshausen, Lisa Höppe und Laura Valvason. Vielen Dank auch allen aus dem IMET. Die großartige Zusammenarbeit, viele Hilfe und netten Gespräche, besonders zu Zeiten Coronas, haben immer sehr geholfen.

Vielen Dank auch Pablo Perez-Garcia, Jenny Chow und Robert Dierkes sowie Wolfgang Streit von der Universität Hamburg für die großartige Zusammenarbeit und Hilfe bei allen Belangen.

Vielen Dank auch an die Projektpartner Sander Smits und Holger Gohlke und deren Teams von der Universität Düsseldorf für die gute und sehr produktive Zusammenarbeit.

A big thank you also to Jo-Anne Verschoor from the University of Leiden. Thank you so much for providing the MHET standard and for being a great conversation partner to share ideas with.

Thanks also to the team of the SO279 Sonne expedition for great evenings in the sun of the Azores and great nights while processing samples and watching TV shows. You made this an amazing unforgettable adventure. In this regard also special thanks to Gabriella Panto for helping me process my sediment sampling and for having great talks over amazing food. Looking forward to meeting up again soon for some more great evenings.

Danke an meine Familie die mich immer unterstützt hat. Besonders zu Zeiten von Corona wart ihr ein großer Rückhalt und Zufluchtsort. Danke Mama, Papa und Saskia. Vielen Dank auch an meine Freunde, die in schweren Zeiten immer für Aufmunterung gesorgt haben.

Finally, the biggest thanks to my sediment sieving buddy Mikael Kaandorp. Thanks to the bottom of the Atlantic that gave us enough time to get to know each other. Looking forward to a lifetime of fun adventures with you.

## **Erklärung**

### **Eidesstattliche Erklärung**

Ich versichere an Eides Statt, dass die Dissertation von mir selbständig und ohne unzulässige fremde Hilfe unter Beachtung der „Grundsätze zur Sicherung guter wissenschaftlicher Praxis an der Heinrich-Heine-Universität Düsseldorf“ erstellt worden ist.

Ort, Datum,

---

Name